ASPECTS OF TAPERED OPTICAL FIBRE POLARIZERS

by

Marcel Lefrançois

B.A.Sc., The University of British Columbia, 1985

A THESIS SUBMITTED IN PARTIAL FULFILLMENT OF
THE REQUIREMENTS OF THE DEGREE OF
MASTER OF APPLIED SCIENCE
in
THE FACULTY OF GRADUATE STUDIES
DEPARTMENT OF PHYSICS

We accept this thesis as conforming
to the required standard.

THE UNIVERSITY OF BRITISH COLUMBIA
September, 1987

In presenting this thesis in partial fulfilment of the requirements for an advanced degree at the University of British Columbia, I agree that the Library shall make it freely available for reference and study. I further agree that permission for extensive copying of this thesis for scholarly purposes may be granted by the head of my department or by his or her representatives. It is understood that copying or publication of this thesis for financial gain shall not be allowed without my written permission.

Department of PHYSICS

The University of British Columbia
1956 Main Mall
Vancouver, Canada
V6T 1Y3

Date SEPT 23/87

ABSTRACT

This thesis prooves that it is possible in principle to make in line optical fibre polarizers from tapered optical fibres surrounded by a quartz cladding. The theory of light propagation and polarization in fibres was reviewed as background information and several fabrication processes were evaluated and tried experimentally. The best results are obtained by heating a quartz tube in an oxy-propane flame, so that it collapses onto the fibre. Unfortunately, due to residues remaining between fibre and quartz tube, and due to large differences in melting points the results are quite irreproducible, and routine fabrication of polarizers with predictable properties is not yet feasible by the methods described in this thesis.

TABLE OF CONTENTS

LIST OF TABLES

LIST OF FIGURES

ACKNOWLEDGEMENTS

I would like to thank Gordon Frank for suggesting the project, giving guidance, and for making the facilities and resources of B.C. Hydro available to carry out the research. Andrew Labun's contribution of the design of the electromagnet used in the beat length measurement experiment must also be recognized. I would also like to thank Dr. B. Ahlborn for suggested revisions to this thesis. Lastly, I would like to thank Dr. F. Curzon for supervising and supporting the project and for many helpful discussions.

CHAPTER 1–INTRODUCTION

Optical fibres started gathering attention as a possible medium for light wave communications in the early 60's. This goal was not realized until 1976 when Bell Labs installed the first optical fibre communications link in Atlanta, Georgia [1] [2]. Many firms followed suit, by 1978 there were over 70 optical communications systems worldwide [3]. Since then the number of systems has exploded; fibre communications links are now common place in aircraft, ships, and telecommunications networks.

A similar explosion is expected in the fibre optic transducer industry. The industry is expected to grow by 30% per year into the 1990's, reaching a market of $100 million U.S. by 1991 [4]. High growth is anticipated for two reasons. First, optical fibre transducers offer many advantages over conventional devices. The advantages are:

1. compactness,
2. light weight,
3. high noise immunity, and
4. strong resistance to corrosion.

The second reason for a high growth rate is the diversity of products yet to be introduced. Currently only a few optical fibre transducers are commercially available, such as temperature, pressure and flow sensors [5], yet there are over 60 different types being developed [6]. Some optical fibre devices under development are PH sensors, smoke detectors, gyroscopes, dosimeters, and current transducers.

To demonstrate the advantages consider a current transducer for use on high voltage transmission lines. Such a device must provide accurate information on alternating currents of a few hundred amperes at potentials up to 500 kV. At present the information is supplied by a unit consisting of a primary coil, which is the transmission line, and a secondary, or sensing, coil both wrapped around a ferrite core which is immersed in an insulating oil and surrounded by a ceramic bushing [7]. This device suffers from three problems:

1. the bushing, used for electrical insulation from the outside world, is costly [8],
2. in high current applications the ferrite core suffers from hysteresis causing inaccurate waveform recording [9], and
3. the oil used for electrical insulation between parts may catch fire if there is a short.

These problems are not experienced when an optical fibre current transducer is utilized [10]. The transducer itself is a birefringent optical fibre wrapped around the conductor, as shown in figure 1–1. Since the transducer is composed of glass and transmits light rather than electricity, electrical insulation problems are nonexistent, thus the oil and the bushing are unnecessary. Further, since there is no ferrite core the device will not exhibit hysteresis.

The principle of operation is very simple. Linearly polarized light is launched into one end of the fibre. This light undergoes Faraday rotation [11] as it interacts with the magnetic field surrounding the conductor. The light then travels out the other end of the fibre where the rotation of the polarization state is analyzed. The rotation is directly proportional to the magnetic field, which in turn is proportional to the current. Therefore, the electric current can be found from the rotation of the polarization state. The polarization state may be found using bulk components, such as a Glan-Thompson prism, but not without component alignment problems and high attenuation of the optical signals. Both problems may be alleviated by using the fibre itself to seperate the polarization components. This is done by

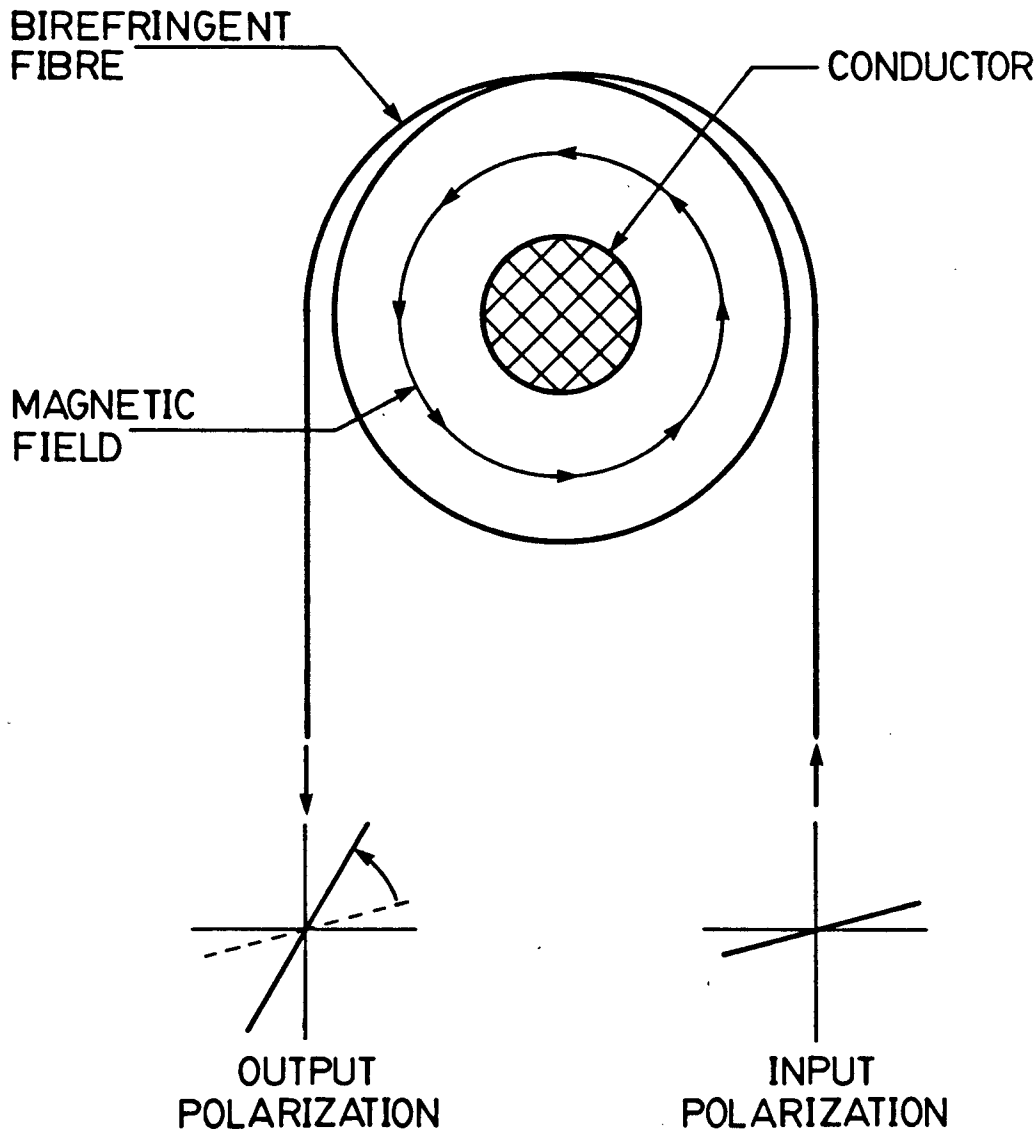

FIGURE 1-1. OPTICAL FIBRE CURRENT TRANSDUCER
The polarization state is Faraday rotated by the magnetic field around the conductor.

forming a biconical taper in a highly birefringent fibre [12] as shown in figure 1-2. The taper forces one polarization component to radiate away while the other continues along the fibre.

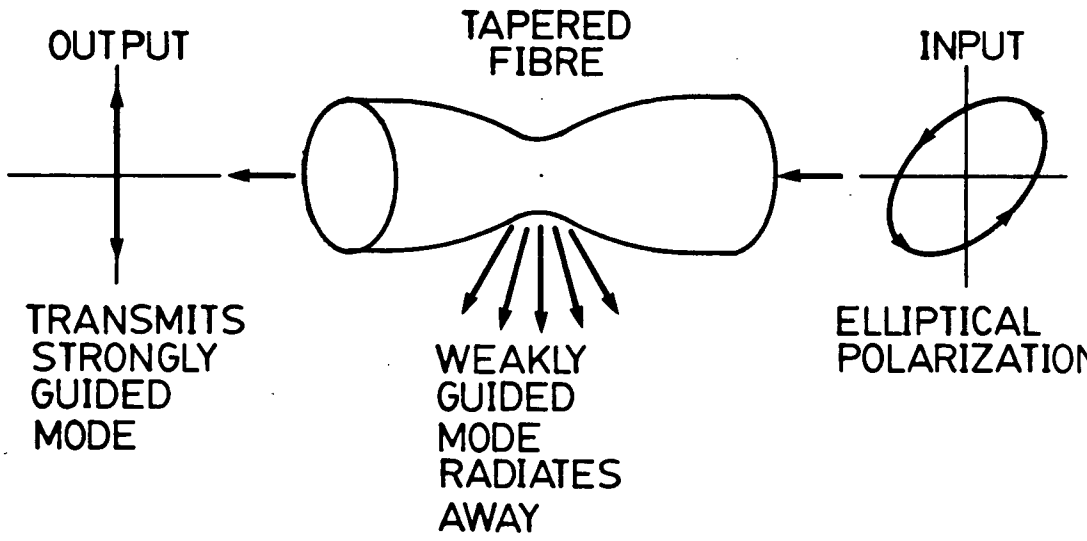

FIGURE 1–2. TAPERED OPTICAL FIBRE POLARIZER

The taper attenuates one polarization mode more than the other causing the light to become polarized.

This is a report on tapered polarizer fabrication for use in an optical current transducer being developed by B.C. Hydro.

This thesis contains the theory, fabrication process, and performance results of tapered optical fibre polarizers (see chapter 8). The first few sections are an introduction to optical fibres. The construction of various fibres is covered and the theory of light propagation is reviewed. The following chapter, "Representations," presents a convenient representation for understanding the behavior of complex optical systems, along with the formulations used to quantify energy and polarization. The following chapter, "Birefringence Measurement," describes a simple optical fibre experiment which has been included because such an experiment was performed and because it brings together the concepts contained in the previous chapters. This makes the remaining few chapters easier to read. These chapters cover tapered polarizer theory, construction, and the polarization performance of the tapered fibres

themselves. The conclusion summarizes the results and discusses the significance of the author's study of tapered birefringent fibre polarizer manufacture.

REFERENCES

[1] Jacobs, Ira. "Lightwave Communications Passes its First Test," *Bell Laboratories Record*, **54**, (1976), p.290–297.

[2] Miller, Stewart E., and Alan G. Chynoweth. *Optical Fiber Telecommunications*, (New York: Academic Press, 1979), p.10.

[3] Kapron, Felix P., John C. Dyment, Jan Conradi, and Carl W. Anderson. *Fiber Optic Communications*, (Bell Northern Research, 1979), chapter 6, p.43–57.

[4] McMahon, Donald H., Arthur R. Nelson, and William B. Spillman Jr. "Fiber-Optic Transducers," *IEEE Spectrum*, **18**, (Dec. 1981), p.24–29.

[5] Giallorenzi, Thomas G., Joseph A. Bucaro, Anthony Dandridge, and James H. Cole. "Optical-Fiber Sensors Challenge the Competition," *IEEE Spectrum*, **23**, (Sept. 1986), p.44–49.

[6] Giallorenzi, Thomas G., Joseph A. Bucaro, Anthony Dandridge, James H. Cole, Scott C. Rashleigh, and Richard G. Priest. "Optical Fiber Sensor Technology," *IEEE Journal of Quantum Electronics*, **18**, (1982), p.626–665.

[7] Bowdler, G.W. *Measurements In High-voltage Test Circuits*, (New York: Pergamon Press Inc., 1973), p.151–154.

[8] Saito, S., Y. Fujii, K. Yokoyama, J. Hamasaki, and Y. Ohno. "The Laser Current Transformer for EHV Power Transmission Lines," *IEEE Journal of Quantum Electronics*, **2**, (1966), p.255–259.

[9] ibid.

[10] Saito, Shigebumi, Joji Hamasaki, Yoichi Fujii, Koji Yokoyama, and Yutaka Ohno. "Development of the Laser Current Transformer for Extra-High-Volt-

age Power Transmission Lines," *IEEE Journal of Quantum Electronics*, **3**, (1967), p.589–597.

[11] Jordan, Edward C., and Keith G. Balmain. *Electromagnetic Waves and Radiating Systems*, (New Jersey:Prentice-Hall Inc., 1968), p.693.

[12] Villarruel, Carl A., M. Abebe, William K. Burns, and R.P. Moeller. "In-Line Birefringent Fiber Polarizer," *Proceedings of the Optical Fiber Conference*, New Orleans, (January 23–25, 1984), p.14.

CHAPTER 2–OPTICAL FIBRE STRUCTURE

Optical fibres are thin strands of glass used to transport optical energy. The simplest and most widely used are communications fibres. Through simple modifications these fibres may be converted to many other types of optical fibres. For instance, doping the fibre with rare earth elements produces a fibre laser [1]. A much more common modification is the addition of stress lobes to produce birefringent fibres. Birefringent fibres are of current interest because they are used in many devices being developed, including gyroscopes, current sensors, and tapered polarizers. The structure of such fibres is discussed in detail, following considerations of communications fibres. Communications fibres are considered first since they are the simplest and also because they form the basis for birefringent fibres.

2.1 COMMUNICATIONS FIBRE

The typical optical fibre is a long thin glass cylinder with a cross section as shown in figure 2–1. The fibre consists of a *core* directly surrounded by a *cladding* which in turn is surrounded by a *coating*. The core size ranges from 5 to 100 μm with the cladding diameter being 125 to 140 μm [2]. The coating, having a diameter of approximatly 300 μm, is a plastic polymer which protects the fibre from damage and strengthens the structure so it does not shatter when bent. The core and cladding confine and guide light. Light is bound around the core by the cladding's refractive index, n_{cl}, being less than 1% lower than the core's, n_{co}. The core index

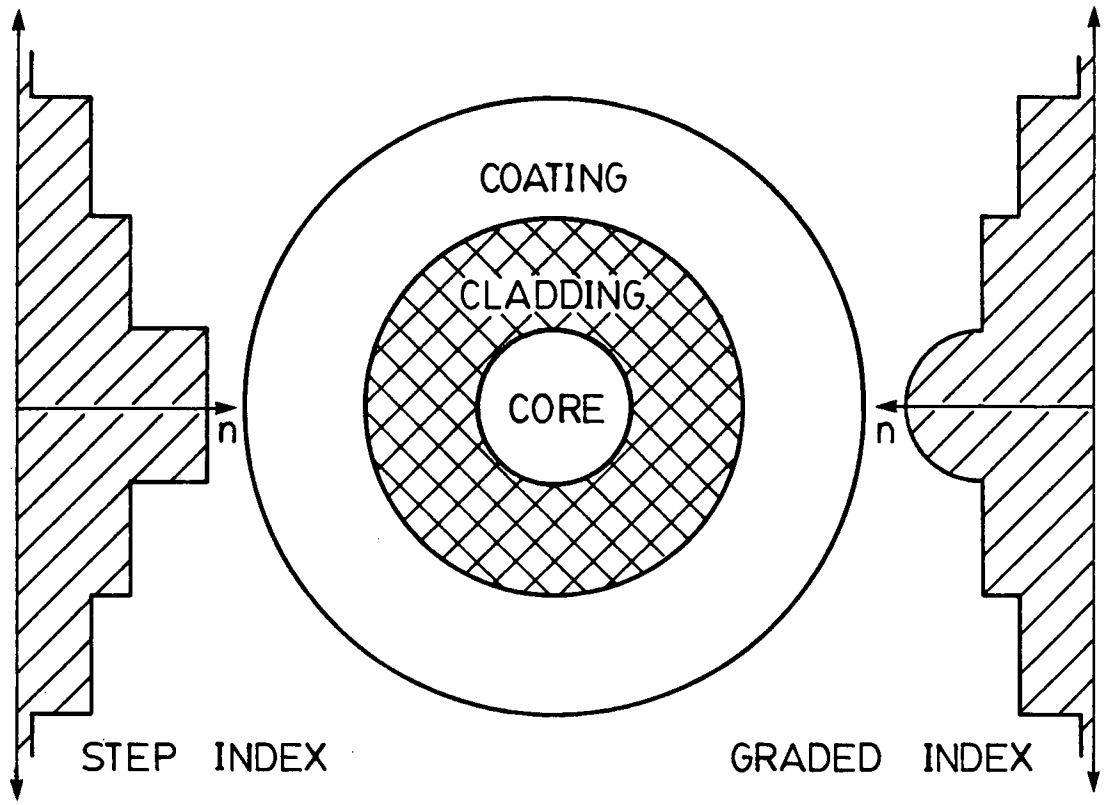

FIGURE 2–1. TYPICAL OPTICAL FIBRE CROSS SECTION

is uniform in *step index fibres*, and varies in *graded index fibres*, as indicated in figure 2–1.

Graded index fibres were first announced in 1969 jointly by Nippon Electric Company and Nippon Sheet Glass Company [3]. This fibre, known as *SELFOC*, has transmission losses of 600 dB/km. Due to such high losses SELFOC fibres are impractical for long distance transmission; they are, however, useful in 3–6 mm lengths as lens. A SELFOC lens has flat ends and the focal point is on the surface, making it easy to attach an optical fibre to it [4].

The high loss experienced in the early SELFOC fibres was most likely due to impurities in the glass. Fortunately, the semi-conductor industry has developed the high purity silicates necessary for producing low loss fibres. Fused quartz has the lowest attenuation of any material [5], below 3 dB/km. This makes fused quartz fibres attractive despite very high working temperatures (softening temperatures are 1700 C). Often, fibres are made with a pure quartz core surrounded by a B_2O_3 doped cladding. The boron doping lowers the refractive index of the silica (n=1.4585) while preserving the similarity between core and cladding with respect to thermal expansion, working temperature, viscosity, and optical properties [6]. Alternatively, fibres are also made with pure fused quartz claddings. In such a case, the core index is raised by introducing small amounts of GeO_2.

Besides GeO_2 and B_2O_3, other dopants are often added to adjust thermal expansion, working temeratures, and/or refractive index [7]. Today most fibres consist of doped quartz, some exhibiting losses as low as 1.1 dB/km [8].

2.2 BIREFRINGENT FIBRE

Many optical fibre devices being developed, including current transducers and polarizing tapers, depend on the fibre's ability to maintain or suppress polarization states [9]. Communications fibres cannot be used for such applications even though they are slightly birefringent. The birefringence arises from very small strains in the fibre (about 10 psi) and/or slightly elliptical cores [10], but it is not enough to overcome the perturbations in the birefringence due to small external pressures and slight bends.

Unlike communications fibres, birefringent fibres maintain birefringence above perturbation levels, either through employing a highly elliptical core [11], and/or through introducing internal stress. Kaminow and Ramaswamy [12], have pointed out that even though a highly elliptical core raises the birefringence [13] it is not as high as stress induced birefringence.

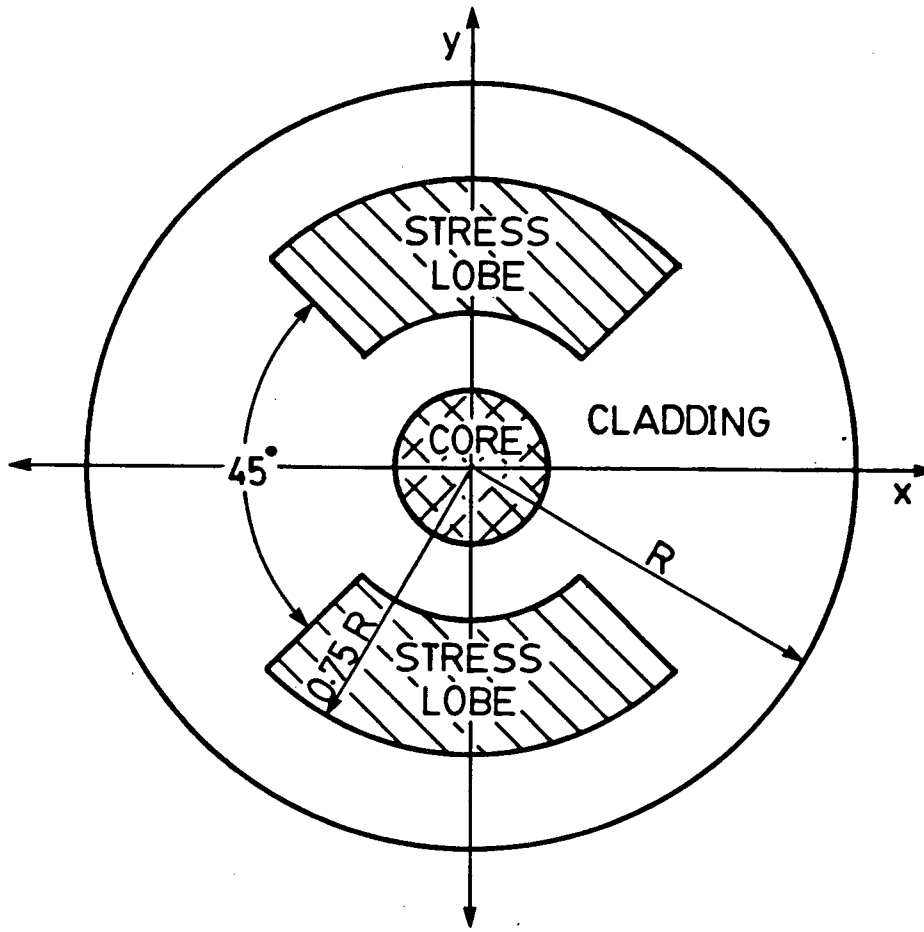

FIGURE 2–2. BIREFRINGENT FIBRE CROSS SECTION

In the later case a strain is applied to the core region by introducing stress lobes in the cladding [14], as shown in figure 2–2. The stress producing regions are doped with B_2O_3 to raise their thermal expansion coefficient above the rest of the cladding. Therefore, the regions do not contract uniformly as the fibre cools after being formed, resulting in a permanent stress on the core. A tension exists along the line joining the stress lobes (y axis). The index of refraction of glass is proportional to the applied stress [15], therefore, the refractive index for the y polarization is lower than that for the x polarization, making the fibre birefringent. In order to achieve

the largest birefringence possible the stress producing regions should be arranged around the core as shown in figure 2–2 with the stress producing regions reaching out to 0.75 of the fibre radius [16]. A further increase in birefringence could be achieved by bringing the stress regions into the core, but since a low loss cladding is required the region is limited to coming within one core diameter of fibre centre.

This fibre is often referred to as *bow-tie fibre* and is used in the tapered polarizer.

REFERENCES

[1] Payne, D.N., S.B. Poole, M.P. Varnham, and R.D. Birch. "Characterization of Specialty Fibres and Components," *Technical Digest: Symposium On Optical Fiber Measurements*, Boulder Colorado, (Sept. 9–10, 1986), p.107–113.

[2] Hentschel, Christian. *Fiber Optics Handbook* , (Federal Republic of Germany: Hewlett Packard, 1983), p.58–61.

[3] Uchida, T., M. Furukawa, I. Kitano, K. Kuizumi, and H. Matsumara. "A Light-Focusing Fiber Guide," *IEEE Journal of Quantum Electronics*, (1969), p.331.

[4] [2], p.125-126.

[5] Rich, T.C., and D.A. Pinnow. "Total Optical Attenuation in Bulk Fused Silica," *Applied Physics Letters*, **20**, (1972), p.264–266.

[6] Van Uitert, L.G., D.A. Pinnow, J.C. Williams, T.C. Rich, R.E. Jaeger, and W.H. Grodkiewicz. "Borosilicate Glasses for Optical Waveguides," *Material Research Bulletin*, **8**, (1973), p.469–476.

[7] Rigterink, M.D. "Materials Systems and Fiber Fabrication Processes in the U.S.A.," *Topical Meeting on Optical Fiber Transmission*, (January 7–9, 1975), Williamsburg, Virginia.

[8] Tasker, G. William, and William G. French. "Low-Loss Optical Waveguides with Pure Fused SiO_2 Cores," *Proceedings of the IEEE*, (1974), p.1281–1282.

[9] Kaminow, Ivan P. "Polarization in Optical Fibers," *IEEE Journal of Quantum Electronics*, **17**, (1981), p.15–22.

[10] Kapron, Felix P., Nicholas F. Borrelli, and Donald B. Keck. "Birefringence in Dielectric Optical Waveguides," *IEEE Journal of Quantum Electronics*, **8**, (1972), p.222–225.

[11] Katsuyama, T., H. Matsumara, and T. Suganuma. "Low-Loss Single Polarisation Fibres," *Electronics Letters*, **17**, (1981), p.473.

[12] Kaminow, I.P., and V. Ramaswamy. "Single-Polarization Optical Fibers: Slab Model," *Applied Physics Letters*, **34**, (1979), p.268–270.

[13] Kumar, A., R.K. Varshney, and K. Thyagarajan. "Birefringence Calculations in Elliptical-Core Optical Fibres," *Electronics Letters*, **20**, (1984), p.112–113.

[14] Birch, R.D., D.N. Payne, and M.P. Varnham. "Fabrication of Polarisation-Maintaining Fibres Using Gas-Phase Etching," *Electronics Letters*, **18**, (1982), p.1036–1038.

[15] McLellan, George W., and Errol B. Shand, eds. *Glass Engineering Handbook*, (New York: McGraw-Hill Book Company, 1984), p.(2-29)–(2-31).

[16] Varnham, Malcolm P., David N. Payne, Arthur J. Barlow, and Robin D. Birch. " Analytic Solution for the Birefringence Produced by Thermal Stress in Polarization-Maintaining Optical Fibers," *Journal of Lightwave Technology*, **1**, (1983), p.332–339.

CHAPTER 3–OPTICAL FIBRE THEORY

It was briefly mentioned in the previous chapter that light is confined to a fibre's core because the cladding's refractive index, n_{cl}, is lower than the core's, n_{co}. While this describes the physical situation, it does not give any insight into how fibres transmit light. To this end, a full explanation of how light propagates in a fibre, along with power flow and electromagnetic field calculations are presented in this chapter.

The discussions and calculations assume straight ideal fibres with circular symmetry. Non-ideal and bent fibres are covered in later chapters. For the most part, step index fibres are dealt with since they are mathematically simpler than graded index fibres. A further simplification is the assumption that the fibres are not lossy. This assumption is valid since fibres exhibit attenuations less than 5 dB/km.

The physics of light transmission by a fibre is discussed first, followed by a complete and accurate solution of Maxwell's equations. The solution yields expressions for the energy flow in the fibre, the cut-off conditions, and the field amplitudes. These are needed for predicting how bends and tapers affect power transmission.

3.1 BASIC PRINCIPLE OF LIGHT GUIDANCE

When a ray meets the core–cladding interface, as shown in figure 3–1, the ray is either refracted or undergoes total internal reflection as described by Snell's law,

$$n_{co} \cos \theta_{co} = n_{cl} \cos \theta_{cl}. \qquad (3-1)$$

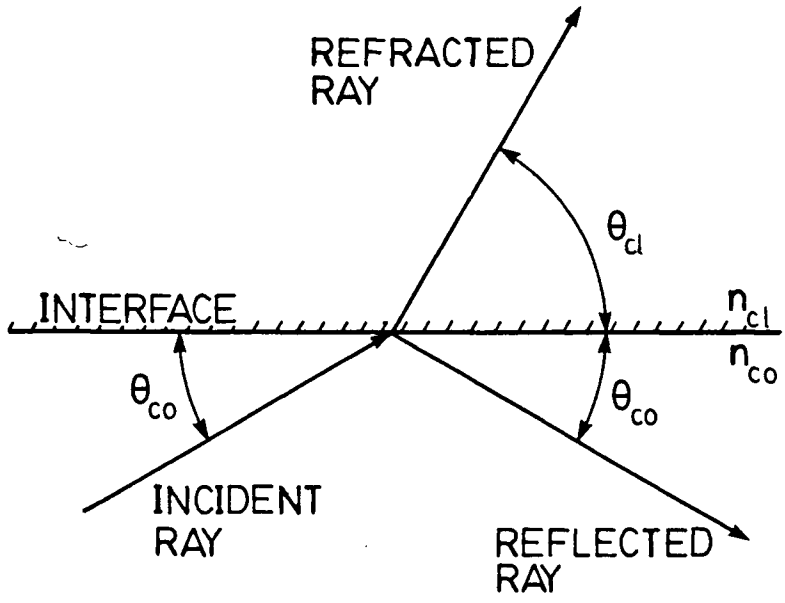

FIGURE 3–1. RAY BEHAVIOR AT AN INTERFACE

The incident and reflected rays are at θ_{co} and the refracted ray is at angle θ_{cl}. The critical angle is given by $\cos\theta_c = n_{cl}/n_{co}$.

Rays introduced above the critical angle, θ_c, will refract at the interface while those introduced below will be reflected. The reflected rays undergo many subsequent reflections as they travel down the fibre. The light, therefore, remains in the core and is guided by the fibre.

3.2 REFLECTION AND POWER PROPAGATION

Even though ray optics describes the light guidance mechanism it does not accurately portray how light travels in a fibre. This becomes evident on examination of the electric fields at the boundary.

These fields are found by solving the wave equation,

$$\left(\nabla^2 - \frac{n^2}{c^2}\frac{\partial^2}{\partial t^2}\right)\vec{\mathrm{E}} = 0, \tag{3–2}$$

where:

$\vec{\mathrm{E}}$ is the electric field,

n is the index of refraction, and

c is the speed of light in vacuum.

For an electric field parallel to the interface and perpendicular to the direction of travel the incident field which satisfies the wave equation is

$$\vec{\mathrm{E}_i} = E_i \hat{j} \exp[-i(\omega t - n_{co}k(z\cos\theta_{co} + x\sin\theta_{co}))], \tag{3–3}$$

where:

θ_{co} is the angle the incident ray makes with the boundary,

ω is the angular frequency of the light wave, and

k is the wave number in free space.

Similarly, the reflected wave is

$$\vec{\mathrm{E}_r} = E_r \hat{j} \exp[-i(\omega t - n_{co}k(z\cos\theta_{co} - x\sin\theta_{co}))]. \tag{3–4}$$

So that power flow is constant along the fibre (no loss) the transmitted wave is assumed to travel parallel to the interface. Therefore, the cladding field is evanescent and decays to zero at $x = \infty$. Using these assumptions the transmitted wave is found to be

$$\vec{\mathrm{E}_t} = E_t \hat{j} e^{-\gamma x} \exp[-i(\omega t - \beta z)], \tag{3–5}$$

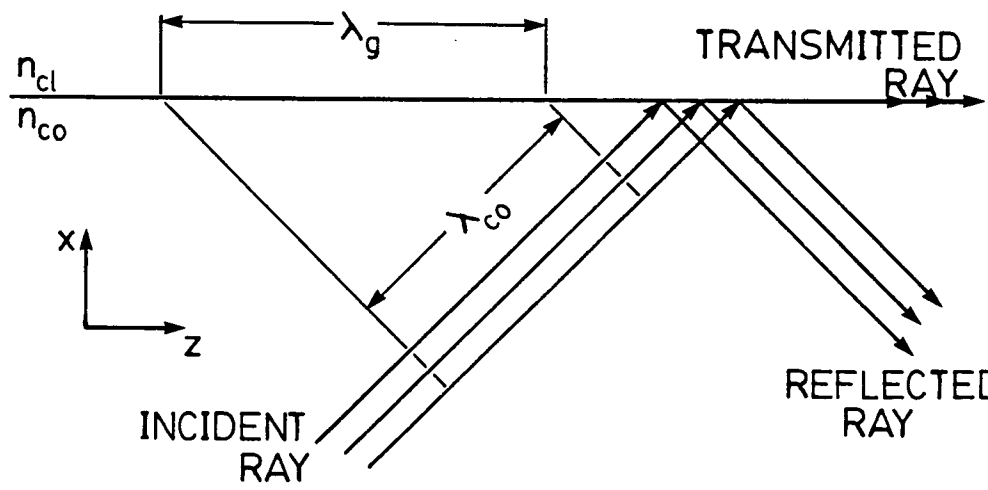

FIGURE 3–2. TOTAL INTERNAL REFLECTION

where γ is the attenuation coefficient in the cladding and β is the propagation constant, or angular spatial frequency, in the cladding.

By realizing the electric field tangent to the boundary is continuous γ and β can be found. Since the field is continuous across the boundary the cladding and core fields possess the same maxima and minima along the interface. Hence, given that the maxima are one wavelength apart in the core, ($\lambda_{co} = 2\pi/n_{co}k$), and at angle θ_{co}, the wavefronts define a length between maxima at the interface, known as the *guide wavelength*, as shown in figure 3–2. The guide wavelength is found through geometry to be

$$\lambda_g = \frac{2\pi}{n_{co}k\cos\theta_{co}}. \tag{3–6}$$

This is then used to find the angular spatial frequency, which is

$$\beta = \frac{2\pi}{\lambda_g} = n_{co} k \cos\theta_{co}. \tag{3–7}$$

Substituting the above into equation (3–5),and then substituting into the wave equation yields the relation

$$\gamma^2 - (n_{co} k \cos\theta_{co})^2 - \frac{n^2}{c^2}\omega^2 = 0. \tag{3–8}$$

Knowing $k = \omega/c$ and using the relation for the critical angle given by Snell's law,

$$\cos\theta_c = \frac{n_{cl}}{n_{co}}, \tag{3–9}$$

equation (3–8) becomes

$$\gamma = n_{co} k \sqrt{\sin^2\theta_c - \sin^2\theta}. \tag{3–10}$$

The cladding field can now be specified by equations (3–5), (3–7), (3–9) and (3–10).

Since the field is continuous across the boundary the field amplitudes obey the relation

$$E_i + E_r = E_t. \tag{3–11}$$

Further, since the magnetic field component tangent to the boundary must also be continuous the derivative of this equation with respect to x is also continuous†.

---

† Continuity can also be demonstrated using the wave equation. If the first derivative of E is discontinuous then the ∇^2 operator in the wave equation would produce a derivative of a delta function. In such a case the equation would hold true only if the refractive index also contains a derivative of a delta function. This condition is never satisfied since the refractive index profile contains at most one singularity (step index fibre). The first derivative is therefore continuous.

Performing the differentiation using (3–3) through (3–5) and then substituting in for E_t from the original equation one obtains

$$E_r = E_i\left(\frac{n_{co}k\sin\theta - i\gamma}{n_{co}k\sin\theta_{co} + i\gamma}\right). \tag{3–12}$$

The term in parentheses in the above equation has real and imaginary parts, therefore a phase shift exists between the incident and reflected waves. Realizing this and defining the phase shift to be Φ the shift is found to be

$$\Phi(\theta_{co}) = -2\arctan\left(\frac{\sqrt{\sin^2\theta_c - \sin^2\theta_{co}}}{\sin\theta_{co}}\right). \tag{3–13}$$

In a similar manner, for the other polarization, with the magnetic field parallel to the interface, one finds

$$\Phi(\theta_{co}) = -2\arctan\left(\frac{n_{co}^2}{n_{cl}^2}\frac{\sqrt{\sin^2\theta_c - \sin^2\theta_{co}}}{\sin\theta_{co}}\right). \tag{3–14}$$

For most fibres $n_{co} \cong n_{cl}$ (within 1%) so the above two equations are approximately equal. Therefore it is reasonable to assume the phase shift equals (3–13) and is independent of polarization.

In truth, what has been referred to as a phase shift is in fact a displacement of the reflected beam as shown in figure 3–3. This was first demonstrated by F. Goos and H. Hänchen [1].

The above analysis assumes planar wave fronts thus the power flow, given by the Poynting vector, is uniform in the direction of propagation. This makes the displacment the same everywhere so the linear shift is considered a phase shift.

To prove that the beam is in fact displaced consider a gaussian beam incident on the interface as shown in figure 3–3. As previously shown for planar waves an

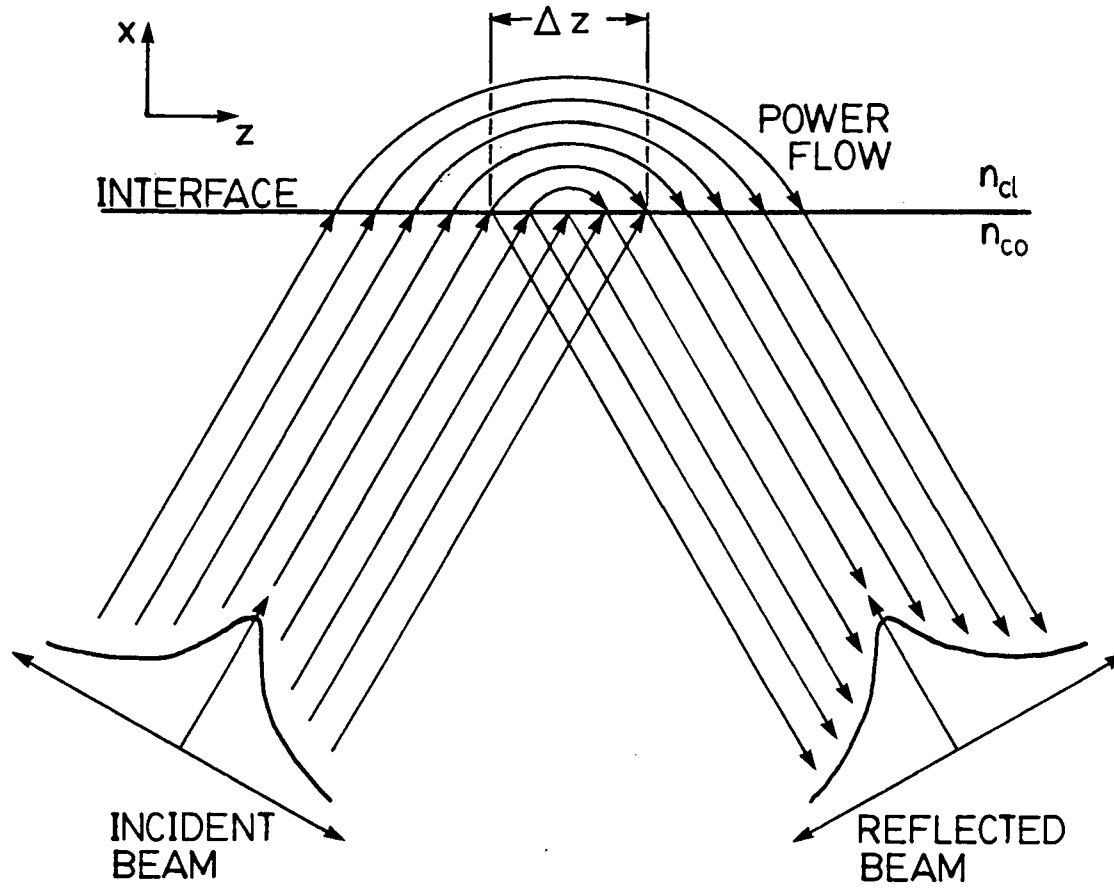

FIGURE 3–3. GOOS-HÄNCHEN SHIFT

The beam enters the medium before being reflected back. (The light waves must realize the existence of the reflecting medium so it must penetrate the reflecting medium before being reflected.)

evanescent electric field propagates in the cladding transporting power along the fibre. In a similar manner, for a gaussian beam, some power is transported by an evanescent field along a short section of the fibre. It is this power transport which displaces the beam. Unlike planar wavefronts, the amplitude of a gaussian beam's electric field varies with position. The amplitude approaches zero at $z = \infty$,

and is maximum at the center of the beam. This field distribution is the same at the interface and, since the electric field is continuous across the boundary the evanescent field also follows the same distribution. The evanescent field variations cause power flow in the cladding to change with position along the fibre. Power flow is proportional to E^2, so the power flow falls to 0 at $z = \infty$ and is maximum where the center of the beam meets the interface. This power flow variation means that power must cross the boundary otherwise energy would not be conserved. So on one side of the beam power flows into the cladding, increasing power flow from zero to a maximum at beam center, and on the other side power flows from the cladding to the core, thus reducing the cladding power flow back to zero. In the region where power flows from core to cladding the reflected light intensity is reduced, and conversely, where the power goes from cladding to core the reflected intensity is increased. These changes in reflected intensity cause the center of the beam to shift over, thus the beam is displaced on reflection.

This displacement is known as the *Goos-Hänchen shift* [2] [3] [4]. An approximate solution for the displacement can be found from the phase change of a beam of light on reflection. The expression for a ray which undergoes one reflection is

$$E_r = C\, e^{i\beta z + i\Phi}. \tag{3–15}$$

Assuming the light beam to consist of a set of rays travelling at angles close to θ_{co}, the phase shift can be expressed as a first order Taylor expansion about $\sin\theta_{co}$,

$$\Phi(\sin\theta) \cong \Phi(\sin\theta_{co}) + (\sin\theta - \sin\theta_{co})\frac{\partial\phi(\sin\theta_{co})}{\partial\sin\theta}. \tag{3–16}$$

Substituting this into (3–15) the reflected field is found to be of the form

$$E_r = C\exp\left(i\beta z + i\sin\theta\frac{\partial\Phi(\sin\theta_{co})}{\partial\sin\theta}\right), \tag{3–17}$$

where C has absorbed the part of the exponent containing the constant phase terms of Φ. As mentioned, the phase shift on reflection is actually a linear displacement, hence, the second term in the exponent should be of the form $\beta\delta z$. Therefore, the linear displacement of the beam is given by

$$\delta z = \frac{\sin\theta}{\beta}\,\frac{\partial\Phi(\sin\theta_{co})}{\partial\sin\theta}.$$

Substituting in for Φ from (3–13) yields the displacement,

$$\delta z = \frac{2\cot\theta_{co}}{n_{co}k\sqrt{\sin^2\theta_c - \sin^2\theta_{co}}}. \qquad (3\text{–}18)$$

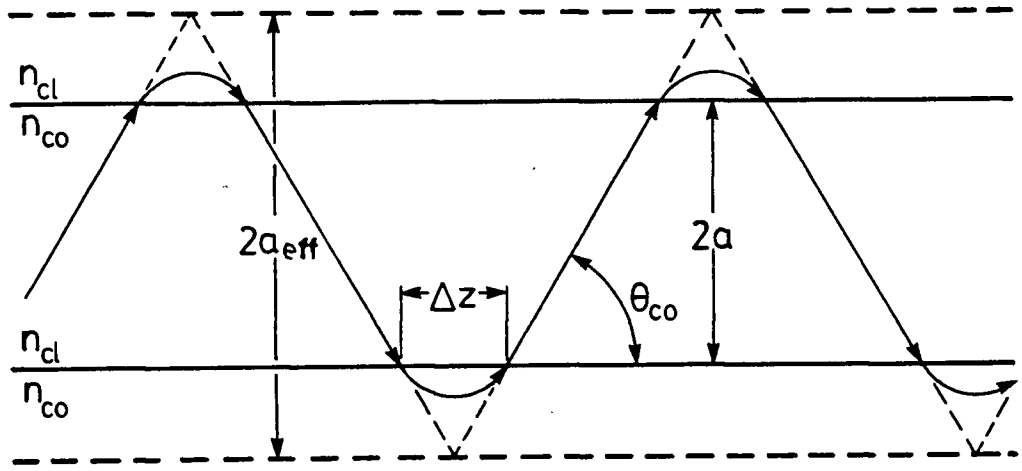

FIGURE 3–4. RAY PATHS AND EFFECTIVE CORE SIZE

Due to the nature of this shift, the ray path can be interpreted as a zigzag path which penetrates into the cladding as shown in figure 3–4. Using this newly defined path an effective core size can be found through geometry to be

$$a_{\text{eff}} = a + \frac{\delta z}{2}\tan\theta = a + \frac{1}{n_{co}k\sqrt{\sin^2\theta_c - \sin^2\theta_{co}}}. \qquad (3-19)$$

This implies that as the ray angle increases the effective core size increases, thus the power penetrates deeper into the cladding.

The power in the cladding indicates that reflection takes place not at the boundary as ray optics suggests, but inside the cladding, near the interface. This reflection mechanism is responsible for introducing power into the cladding, and for keeping all the power bound in the vicinity of the core. The power in the cladding does not travel solely in the cladding but is constantly flowing into and out of the core giving the appearance of a continuous flow in the cladding.

3.3 DIFFRACTION AND COHERENCE

Even though a fibre can bind light to the core there is no guarantee it will effectively transmit optical energy. One effect which limits a fibre's effectiveness is diffraction.

The diffraction of a beam by a fibre is very similar to that experienced by collimated light passing through a pin-hole. The similarity lies in the fibre core being very small and the critical angle of the guided light being very shallow (typically less than 4°). The low angle produces nearly collimated light and the core acts as the pin-hole†. For a gaussian beam of the form $\exp[-(r/a)^2]$ falling on a pin-hole

† The pin-hole could also be the beam size, but as a demonstration of the concepts it is more convenient to choose the core size.

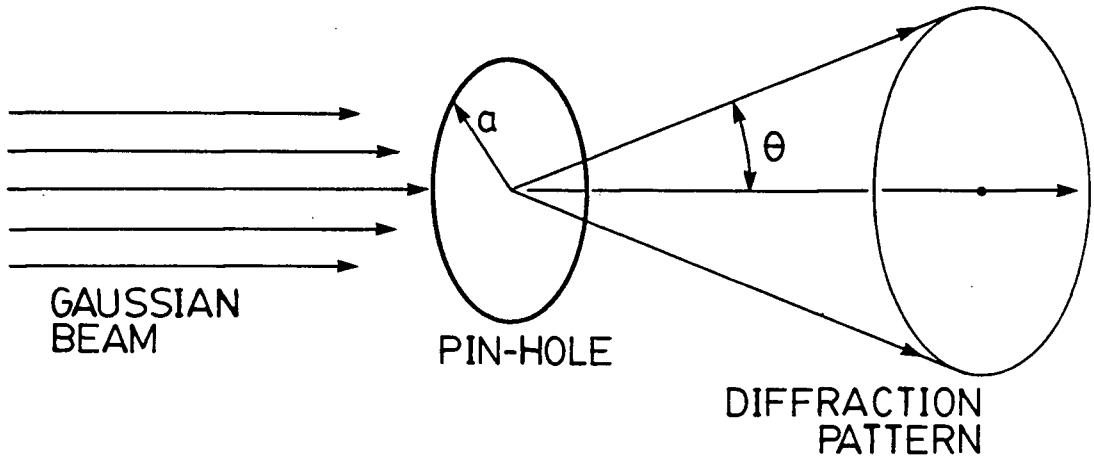

FIGURE 3–5. DIFFRACTION OF A GAUSSIAN BEAM

of radius a, as shown in figure 3–5, the far field intensity pattern is

$$I(\theta) = \exp\left[-\frac{1}{2}\left(\frac{2\pi a n_{co}}{\lambda}\right)^2 \sin^2\theta\right]. \qquad (3-20)$$

The exponent in the above equation can be expressed in terms of the *fibre parameter*, or *V-value*, which is defined as

$$V = \frac{2\pi a}{\lambda}\sqrt{(n_{co}^2 - n_{cl}^2)} = \frac{2\pi a n_{co}}{\lambda}\sin\theta_c. \qquad (3-21)$$

This important value indicates the propagation properties of the fibre, as shown later. The V value is also indicative of the order of diffraction. The higher the V value the larger the number of 'rings' which appear in the diffraction pattern. This is much like diffraction from a slit: the number of fringes a specific fringe is away

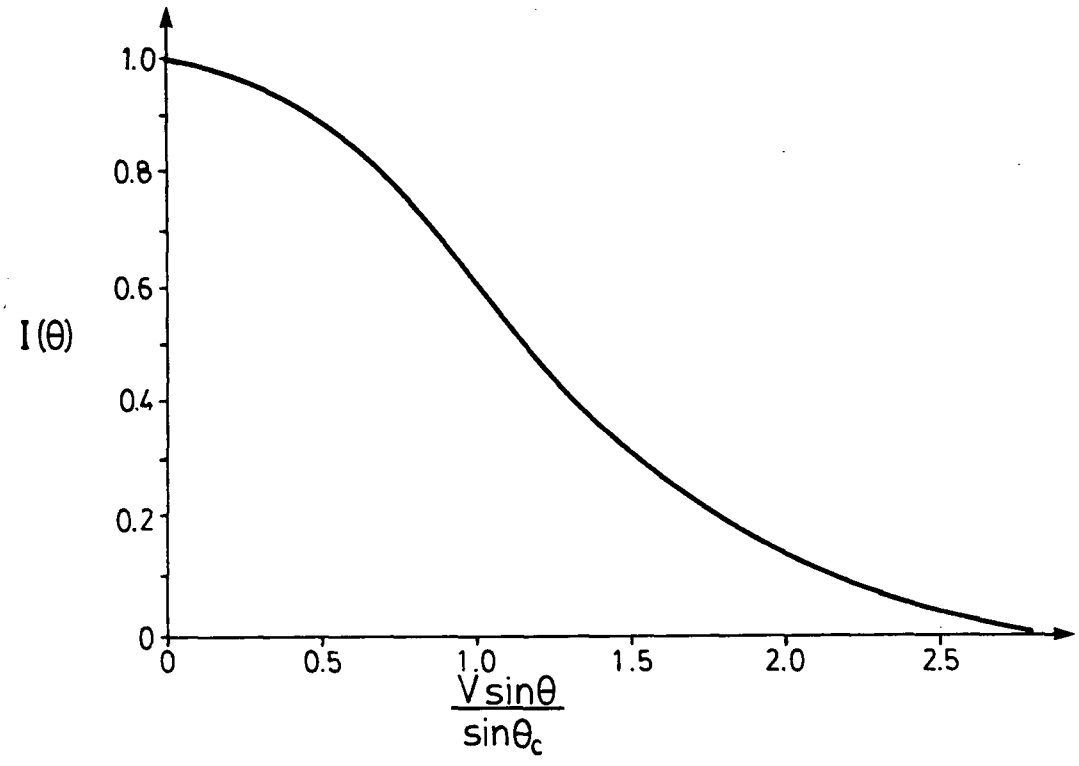

FIGURE 3–6. FAR FIELD DIFFRACTION PATTERN

from the central fringe is its order of diffraction. equation (3–20) using V yields

$$I(\theta) = \exp\left(-\frac{V^2 \sin^2\theta}{2\sin^2\theta_c}\right), \qquad (3-22)$$

which is plotted in figure 3–6. As can be seen in the diagram, the spreading goes up as either V or θ decreases†.

† Note that a decrease in core size, a, or an increase in wavelength, λ, decreases the value of V.

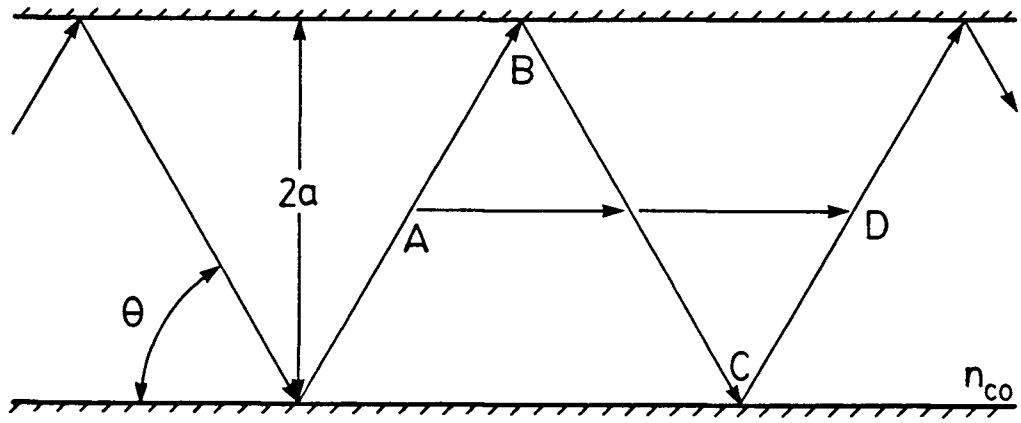

FIGURE 3–7. LIGHT PATH COHERENCE

The spreading of the light trajectories sends light in other directions some of which propagate in the fibre and others which do not. Consider the situation depicted in figure 3–7. The phase change between points A and D of the light following the zigzag path shown is $4kan_{co}/\sin\theta$, due to path length, plus 2Φ, due to reflections. For the z–directed component the phase change is $4kan_{co}\cos^2\theta/\sin\theta$. The phase difference between the two must be a multiple of 2π, otherwise the waves are not translationally invariant (each period of the wave is the same). If the two waves were not a multiple of 2π out of phase the superposition would decrease the power flow in that ray trajectory. Therefore the equation describing the angles for good power transmission is

$$\frac{4kan_{co}}{\sin\theta} + 2\Phi = \frac{4kan_{co}\cos^2\theta}{\sin\theta} + 2m\pi, \qquad (3-23)$$

where m is an integer. Subtituting in for Φ, and using the relation for V, one finds the preferred ray directions, besides $\theta = 0°$, are given by

$$\tan\left(\frac{V \sin\theta}{\sin\theta_c}\right) = \frac{\sqrt{\sin^2\theta_c - \sin^2\theta}}{\sin\theta}. \qquad (3\text{–}24)$$

For $V \leq \pi/2$ only one solution for θ exists [5], in which case the fibre is single moded.

So the effectiveness of a fibre depends on launching light into these preferred modes. This is accomplished both through launching light into the fibre along the preferred ray directions and through diffraction of the beam. The beams continually diffract as they travel along the fibre causing energy loss through rays introduced above the critical angle and forcing energy into the preferred ray directions.

3.4 ELECTROMAGNETIC THEORY

The preceding sections presented the physics of light guidance. The concepts were developed using physical arguments and simple mathematical analysis. The expressions produced are not accurate enough for evaluating bending and tapering effects. More precise solutions are obtained by solving Maxwell's equations on a straight fibre with an infinite cladding, as shown in figure 3–8. The infinite cladding assumption is reasonable since the core of any actual fibre is much smaller than the cladding. As already discussed, most of the optical energy is bound around the core and does not penetrate far into the cladding, therefore the cladding can be considered infinite.

Precise field solutions are found by solving Maxwell's equations,

$$\nabla \times \vec{E} = -\mu_0 \frac{\partial \vec{H}}{\partial t} \quad \text{and} \quad \nabla \times \vec{H} = \frac{\partial \vec{D}}{\partial t}, \qquad (3\text{–}25)$$

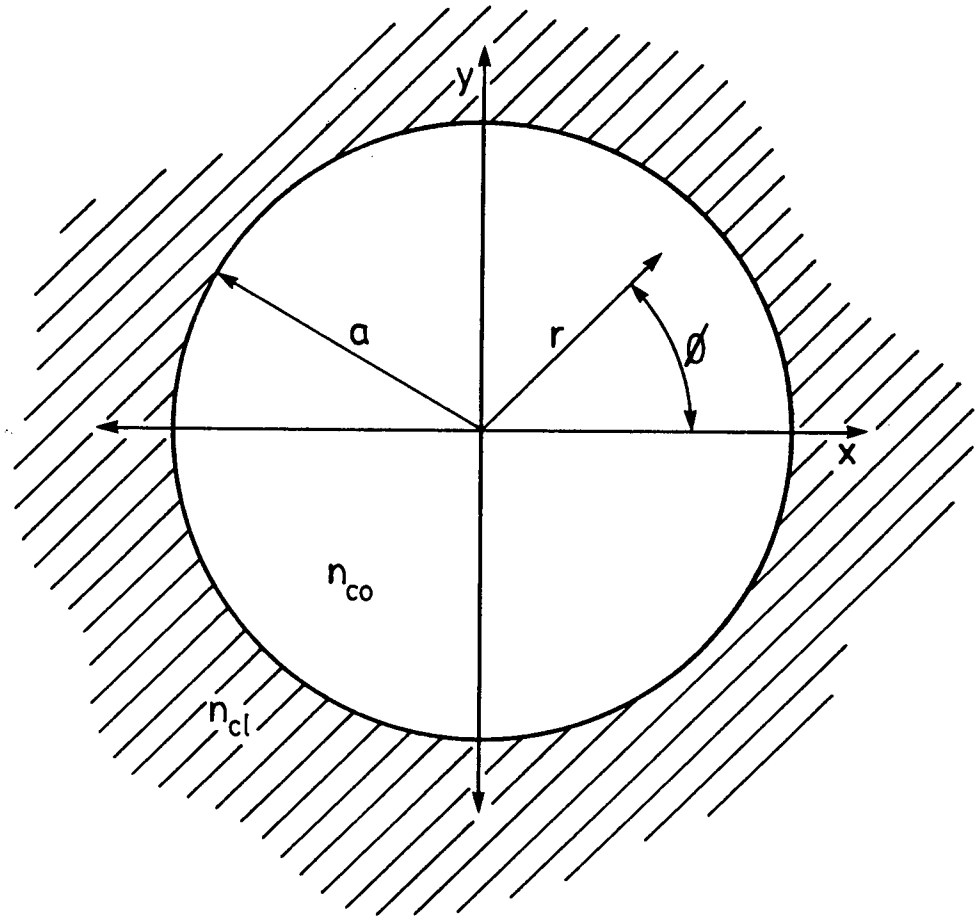

FIGURE 3–8. FIBRE COORDINATES

where $\vec{H}$ is the magnetic field, $\vec{E}$ is the electric field, and $\vec{D}$ is the dielectric field†. Taking the curl of the first equation and the derivative of the second equation then

† It is important to use the dielectric field rather than the electric field since the permittivity, ϵ, can be different along each axis, such as in birefringent fibres.

combining to eliminate $\vec{H}$ yields the wave equation

$$\nabla^2\vec{E} - \mu_0\frac{\partial^2\vec{D}}{\partial t^2} = 0. \tag{3-26}$$

Using this, one finds that both field components (polarizations) satisfy the equation

$$\left(\nabla^2 - \mu_0\epsilon\frac{\partial^2}{\partial t^2}\right)\psi = 0, \tag{3-27}$$

where ϵ is the value of the permittivity for the electric field component ψ. The field is assumed to vary with angular frequencies ω in time and β in the direction of travel, z. Further, the solution must be continuous around the core (in the ϕ direction), therefore the solution undergoes an integral number of periods around the core, ν. The field solution will then be of the form

$$\psi = F(r)\, e^{-i(\omega t - \beta z - \nu\phi)} \tag{3-28}$$

where $F(r)$ is a function of radius r. Substituting this into equation (3-27) yields Bessel's equation [6].

$$\frac{\partial^2 F}{\partial r^2} + \frac{1}{r}\frac{\partial F}{\partial r} + \left(n^2k^2 - \beta^2 - \frac{\nu^2}{r^2}\right)F = 0 \tag{3-29}$$

where n is n_{co} in the core, and is n_{cl} in the cladding. Since ν is an integer the solutions to the above equation are Bessel functions, J_ν, or modified Bessel functions, K_ν, of integer order ν. The solution must be finite at fibre center, $r = 0$, and 0 at $r = \infty$, therefore the solutions are of the form

$$F_{co}(r) = C_{co}J_\nu(Ur/a), \quad \text{and} \quad F_{cl}(r) = C_{cl}K_\nu(Wr/a), \tag{3-30}$$

where the C's are constants, and

$$U^2 = a^2(n_{co}^2 k^2 - \beta^2), \quad \text{and} \quad W^2 = a^2(\beta^2 - n_{cl}^2 k^2). \tag{3–31}$$

Since both U^2 and W^2 are positive for bound modes a condition for light propagation is

$$n_{cl}k \leq \beta \leq n_{co}k. \tag{3–32}$$

This could have been predicted earlier from figure 3–2 using ray optics. The minimum guide wavelength equals the wavelength of light in the core, hence $\beta \leq n_{co}k$. For guide wavelengths longer than the wavelength in the cladding, $\beta \leq n_{cl}k$, the mode is unbound since some light must travel away from the core. Alternatively, knowing $\beta = n_{co}k\cos\theta_{co}$ and the critical angle the same expression can be found. So some power is lost when $\beta \leq n_{cl}k$. At the onset of this condition one finds

$$W^2 = 0, \quad \text{and} \quad U^2 = a^2k^2(n_{co}^2 - n_{cl}^2)$$

The value of U at cutoff is the waveguide parameter, seen earlier,

$$V = \sqrt{U^2 + W^2} = ak\sqrt{n_{co}^2 - n_{cl}^2} \tag{3–33}$$

These parameters describe the cutoff conditions providing the value of V at cutoff is known. The cutoff value is found by examining the continuity of the electric field. As already pointed out the electric field tangent to the boundary is continuous, thus

$$F_{co}(a) = F_{cl}(a). \tag{3–34}$$

From this one obtains

$$F_{co}(r) = C\,\frac{J_\nu(Ur/a)}{J_\nu(U)} \quad \text{and} \quad F_{cl}(r) = C\,\frac{K_\nu(Wr/a)}{K_\nu(W)}. \tag{3–35}$$

TABLE III–I ROOTS OF THE EIGENVALUE EQUATION AT CUTOFF

The order of the mode is ν and its rank is l. ($l = 1$ is the first root of the eigenvalue equation for mode ν, $l = 2$ is the second and so on.)

ν	V		
	$l = 1$	$l = 2$	$l = 3$
0	0.000	3.831	7.016
1	2.405	5.520	8.653
2	3.832	7.016	10.173
3	5.136	8.417	11.620
4	6.380	9.761	13.015
5	7.588	11.065	14.373

Assuming the electric field is in the x direction, and using Maxwell's equations along with (3–28) the fields are found to be:

$$E_x = F(r)e^{-i(\omega t-\beta z-\nu\phi)}, \tag{3–36}$$

$$H_y = \frac{\beta}{\omega\mu_0}F(r)e^{-i(\omega t-\beta z-\nu\phi)}, \tag{3–37}$$

and

$$H_z = \frac{1}{i\omega\mu_0}\left(\frac{dF}{dr}\frac{\partial r}{\partial y} + i\nu\frac{\partial\phi}{\partial y}F\right)e^{-i(\omega t-\beta z-\nu\phi)}. \tag{3–38}$$

The tangential component of $\vec{\mathrm{H}}$, i.e. H_z, must also be continuous at the boundary. According to equation (3–34) F is continuous. The partial derivatives of r and ϕ are also continuous and ν is a constant for the mode, therefore H_z is continuous if

$$\left.\frac{dF_{co}(r)}{dr}\right|_{r=a} = \left.\frac{dF_{cl}(r)}{dr}\right|_{r=a}.$$

This is not surprising since in the previous section the derivative of the field was shown to be continuous. After substitution for the F's from (3–30) the above equation becomes the *eigenvalue equation* for the fibre,

$$\frac{UJ_{\nu+1}(U)}{J_\nu(U)} = \frac{WK_{\nu+1}(W)}{K_\nu(W)}. \qquad (3-39)$$

This equation gives the cutoff values for V. As mentioned, close to cutoff U approaches V, and W approaches 0. For small values of W the modified bessel functions are [7]

$$K_\nu(W) \sim \frac{1}{2}\Gamma(\nu)\left(\frac{2}{W}\right)^\nu \quad \text{for} \quad \nu > 0.$$

and

$$K_0(W) \sim -\ln(W) \quad \text{for} \quad \nu = 0.$$

Using the above approximations, and $U = V$, the eigenvalue equation at cutoff becomes

$$VJ_1(V) = 0 \quad \text{for} \quad \nu = 0, \quad \text{and} \quad J_{\nu-1}(V) = 0 \quad \text{for} \quad \nu > 0. \qquad (3-40)$$

The roots to the above equations give the minimum values of V for transmission of a mode, the results of which are given in table III–I [8]. For a given order, ν, there are multiple roots possible (numbered from $l = 1$ onward). For each of the roots less than or equal to the fibre parameter there exists a unique solution of the eigenvalue equation and, hence, also a unique solution to Maxwell's equations. A mode, therefore, is defined as a unique solution to Maxwell's equations (different set of values, W, U, and ν, for each). Notice that if V is chosen below 2.405 only

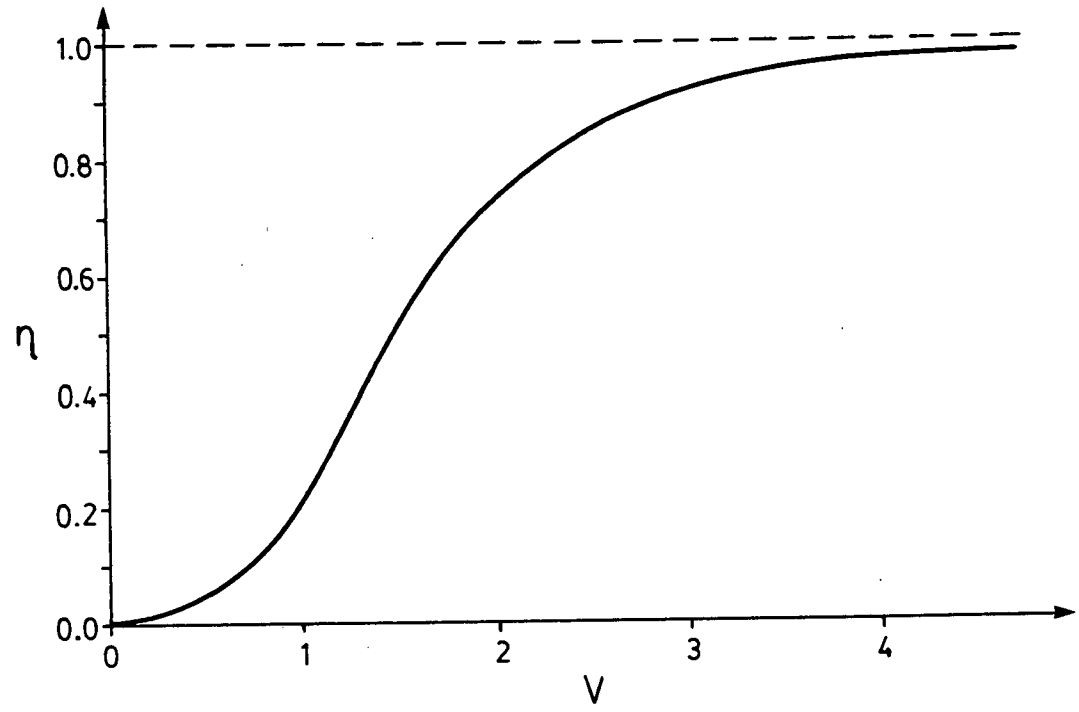

FIGURE 3–9. POWER RATIO IN THE CORE

one mode will propagate hence, the fibre is type *single mode*†. Above this number, two or more modes may propagate hence, the fibre type is *multimode*.

Attention is now turned to power flow along a single mode fibre. The power flow is found by using the Poynting vector,

$$\vec{S} = \frac{1}{2}\int_A (\vec{E} \times \vec{H}^*) dA, \qquad (3-41)$$

† In actual fact a single mode fibre allows two different modes to propagate. The two modes are the two orthogonal polarization modes of order 0.

where A is the cross sectional area of the fibre and $*$ indicates complex conjugation. Defining the *power ratio*, η, as the power flow in the core over the total power flow, and using (3–36) through (3–38) and the Poynting vector one finds

$$\eta = \frac{U^2}{V^2}\left(\frac{W^2}{U^2} + \frac{K_0^2(W)}{K_1^2(W)}\right). \qquad (3-42)$$

The results of this equation are plotted in figure 3–9†. As V decreases, the power carried by the core also decreases thus forcing the cladding to transmit more of the power. When most of the power is in the cladding the light becomes bound by the cladding–jacket interface instead of the core–cladding interface.

3.5 SUMMARY

This chapter presented the physics of light transmission in optical fibres.

Total internal reflection was shown to be responsible for introducing power into the cladding and keeping all of the optical energy bound about the core. Transmission is also affected by diffraction channelling power into modes which remain coherent along the fibre and thus will propagate. Finally, expressions were found for the cutoff conditions, the field amlpitudes, and for the power flow.

All of this is necessary for understanding later chapters.

---

† The values are found by choosing a value for V, then using $V^2 = U^2 + W^2$ and the eigenvalue equation to find the values for U and W. The power ratio can then be found by straight substitution [9].

REFERENCES

[1] Goos, Von F., and H. Hänchen. "Ein neuer und fundamentaler Versuch zur Totalreflexion," *Annalen der Physik*, **1**, (1947), p.333–346.

[2] Lotsch, Helmut K.V. "Reflection and Refraction of a Beam of Light at a Plane Interface," *Journal of the Optical Society of America*, **58**, (1968), p.551–561.

[3] Snyder, Allen W., and John D. Love. "Goos-Hänchen Shift," *Applied Optics*, **15**, (1976), p.236–238.

[4] Snyder, Allen W., and John D. Love. *Optical Waveguide Theory*, (New York: Chapman and Hall, 1983), p.194–198.

[5] ibid., p. 200-201.

[6] Abramowitz, Milton, and Irene A. Stegun. *Handbook of Mathematical Functions*, (New York: Dover Publications Inc., 1964), p.358.

[7] ibid., p.360, 375.

[8] ibid., p.409.

[9] [4], p.314–315.

CHAPTER 4–MODAL ANALYSIS

The previous chapter contains a detailed account of the bound modes in a fibre. Taking a combination of these modes and superimposing them on a set of radiation modes yields the total field in a fibre. As these modes propagate along the fibre they couple and exchange energy, thus affecting fibre performance. Evaluating fibre performance requires an understanding of the properties of modes as well as an understanding of how the modes interact.

This chapter discusses some of the properties and provides mode coupling and power equations.

4.1 MODES

Before proceeding an explanation of fibre modes is in order.

A *mode* is a single electromagnetic wave which satisfies Maxwell's equations†. There are three types of modes in a fibre:

1. bound,
2. radiation, and
3. leaky modes.

---

† A mode can also be identified as a ray, or beam, of radiation travelling in a fixed direction. A radiation field, therefore, is a superposition of many rays.

Bound modes are guided by the fibre while *radiation modes* are not. Between bound and radiation modes exist the weakly guided radiation modes, called *leaky modes*.

All modes are of the form

$$E_x = F(r)e^{-i(\omega t-\beta z-\nu\phi)}, \tag{4–1}$$

where the radial function, $F(r)$, is different for each mode. The radial functions for bound modes were presented in the previous chapter. The leaky and radiation mode functions are described below.

Both leaky and radiation modes lose power as they propagate along a fibre. This is accounted for through the propagation constant gaining an imaginary component,

$$\beta = \beta^r + i\beta^i. \tag{4–2}$$

In order for power loss to occur there must be an outward travelling wave, hence,

$$\beta^r \leq n_{cl}k, \tag{4–3}$$

as found in the previous chapter. Under this condition the solution to the wave equation (equation (3–29))in the core is unchanged from (equation (3–30)),

$$F_{co}(r) = C_{co}J_\nu(Ur/a), \tag{4–4}$$

however, the cladding solution is modified yielding,

$$F_{cl}(r) = C_{cl\ 1}J_\nu(Qr/a) + C_{cl\ 2}H_\nu^{(1)}(Qr/a), \tag{4–5}$$

where,

$$Q = iW = a\sqrt{n_{cl}^2k^2 - \beta^2}. \tag{4–6}$$

The Bessel function, J_ν, in equation (4–5) is the outgoing wave [1] (it is essentially the core field modified by propagation in the cladding). The evanescent field is given by the Hankel function of the first kind, $H_\nu^{(1)}$. As with bound modes, both the derivative of the tangential electric field and its amplitude are continuous across the boundary, giving

$$C_{co}J_\nu(U) = C_{cl\ 1}J_\nu(Q) + C_{cl\ 2}H_\nu^{(1)}(U) \tag{4–7}$$

and

$$C_{co}UJ_{\nu+1}(U) = C_{cl\ 1}QJ_{\nu+1}(Q) + C_{cl\ 2}QH_{\nu+1}^{(1)}(U). \tag{4–8}$$

Given the amplitude in the core, C_{co}, there are still 3 unknowns in the above two equations: $C_{cl\ 1}$, $C_{cl\ 2}$, and β. Therefore, there is no eigenvalue equation for radiation modes.

Consider the set of radiation modes just below cut off (β^r approaches $n_{cl}k$ from below $n_{cl}k$). These modes are expected to be similar to the bound modes of the fibre with the exception that they experience a low level attenuation. Just below cut off the cladding parameter is almost pure imaginary with its value close to zero, hence Q is small and real. For small values of Q the Bessel and Hankel functions are approximated by [2]

$$J_\nu(Q) \sim \frac{1}{\nu!}\left(\frac{z}{2}\right)^\nu,$$

$$J_0(Q) \sim 1 - \frac{Q^2}{4},$$

$$H_\nu^{(1)}(Q) \sim \frac{-i(\nu-1)!}{\pi}\left(\frac{2}{Q}\right)^\nu,$$

and

$$H_0^{(1)}(Q) \sim -\left(\frac{2i}{\pi}\right) \ln Q.$$

It is readily seen from the above equations that as Q approaches zero the Bessel functions become negligible when compared to the Hankel functions. Therefore, just below cut off equations (4–7) and (4–8) combine to form the eigenvalue equation for leaky modes [3],

$$\frac{UJ_{\nu+1}(U)}{J_\nu(U)} = \frac{QH_{\nu+1}^{(1)}(Q)}{H_\nu^{(1)}(Q)}. \tag{4–9}$$

Note that using $W = -iQ$ in the eigenvalue equation for bound modes (equation (3–39)) and the relation [4]

$$K_\nu(-iQ) = \frac{\pi}{2} i^{\nu+1} H_\nu^{(1)}(Q) \tag{4–10}$$

yields the same relation as (4–9). So these modes are similar to bound modes except that they slowly leak away, hence, they are called leaky modes.

Both leaky and bound modes are strongly guided by the fibre, possessing similar core fields and each giving rise to evanescent cladding fields. Fitting these two fields to the boundary conditions yields an eigenvalue equation for the propagation constant for each mode. In the case of bound modes the solution is exact but for leaky modes the solution is a close approximation to the actual propagation constant. The solution is an approximation since there also exists a set of outward propagating waves whose contribution is very small compared to the evanescent field, and so is ignored. Increasing the contribution of the outward travelling wave leaves an arbitrary choice in propagation constant when solving the boundary conditions, yielding a continuum of radiation modes.

4.2 ORTHOGONAL MODES

The total field in a fibre is a superposition of bound, leaky, and radiation modes. In an ideal fibre the modes propagate independent of each other, hence, no coupling should exist between the modes as explained below†.

In order to prove that the modes are orthogonal consider the function

$$\vec{G} = \vec{\mathrm{E}}_j \times \vec{\mathrm{H}}_l^* + \vec{\mathrm{E}}_l^* \times \vec{\mathrm{H}}_j, \tag{4–11}$$

where '$*$' denotes complex conjugation and 'j' and 'l' denote different solutions of Maxwell's equations. Taking the divergence of $\vec{G}$ and using the identity

$$\nabla \cdot (\vec{A} \times \vec{B}) = \vec{B} \cdot (\nabla \times \vec{A}) - \vec{A} \cdot (\nabla \times \vec{B})$$

yields

$$\nabla \cdot \vec{G} = \vec{\mathrm{H}}_l^* \cdot (\nabla \times \vec{\mathrm{E}}_j) - \vec{\mathrm{E}}_j \cdot (\nabla \times \vec{\mathrm{H}}_l^*) + \vec{\mathrm{H}}_j \cdot (\nabla \times \vec{\mathrm{E}}_l^*) - \vec{\mathrm{E}}_l^* \cdot (\nabla \times \vec{\mathrm{H}}_j). \tag{4–12}$$

Using Maxwell's equations in a current source free media (equation (3–25)) to reduce the '$\nabla\times$' terms changes this equation to

$$\nabla \cdot \vec{G} = -ik\sqrt{\frac{\epsilon_0}{\mu_0}}\left((n_l^*)^2 - n_j^2\right)\vec{\mathrm{E}}_j \cdot \vec{\mathrm{E}}_l^*, \tag{4–13}$$

where the values of n may be mode dependent.

---

† This proof of orthonormality parallels that of Love and Snyder [5]. It is included here because of its use in later calculations.

Integrating this over the cross sectional area of the waveguide out to infinity, A_∞, and using the divergence theorem yields

$$\int_{A_\infty} \nabla \cdot \vec{G}\, dA = \frac{\partial}{\partial z} \int_{A_\infty} \vec{G} \cdot \hat{z}\, dA + \oint_{\partial A} \vec{G} \cdot \hat{\mathrm{n}}\, d\ell, \tag{4–14}$$

where ℓ is distance along the boundary of A. The portion of $\vec{G}$ directed along the outward normal, $\hat{\mathrm{n}}$, depends on the field components parallel to the closed path ∂A. Since the fields are continuous across even a discontinuous boundary $\vec{G}$ has no singularities inside the bound region, therefore the integral along the closed path is zero. So equation (4–14) becomes

$$\int_{A_\infty} \nabla \cdot \vec{G}\, dA = \frac{\partial}{\partial z} \int_{A_\infty} \vec{G} \cdot \hat{z}\, dA. \tag{4–15}$$

Assuming lossless media ($n_2^* = n_1$) $\nabla \cdot \vec{G} = 0$ by equation (4–13), therefore, the above equation becomes

$$\frac{\partial}{\partial z} \int_{A_\infty} \vec{G} \cdot \hat{z}\, dA = 0. \tag{4–16}$$

Using modal fields of the form $\vec{\mathrm{E}} = \vec{e} \exp(i\beta z)$ to form $\vec{G}$ the above equation becomes

$$(\beta_j - \beta_k) \int_{A_\infty} (\vec{e_j} \times \vec{h}_k^* + \vec{e}_k^* \times \vec{h_j}) \cdot \hat{z}\, dA = 0, \tag{4–17}$$

for forward propagating modes. If the k^{th} mode travels backwards,

$$\vec{\mathrm{E}}_\mathrm{k} = \vec{e_k} \exp(-i\beta_k z),$$

then (4–16) becomes

$$(\beta_j + \beta_k) \int_{A_\infty} (\vec{e_j} \times \vec{h}_k^* - \vec{e}_k^* \times \vec{h_j}) \cdot \hat{z}\, dA = 0. \tag{4–18}$$

By comparing the above two equations it is obvious that

$$\int_{A_\infty} (\vec{e}_j \times \vec{h}_k^*) \cdot \hat{z}\, dA = \int_{A_\infty} (\vec{e}_k^* \times \vec{h}_j) \cdot \hat{z}\, dA = 0 \quad \text{for } j \neq k$$
$$= 2\mathcal{N}_j \quad \text{for } j = k, \tag{4–19}$$

where $\mathcal{N}_j$ is a constant. This is an important property of modes—*the modes are orthogonal to one another.*

Modal calculations can be greatly simplified by using *normalized modes*:

$$\hat{e}_j = \frac{\vec{e}_j}{\sqrt{\mathcal{N}_j}} \quad \text{and} \quad \hat{h}_j = \frac{\vec{h}_j}{\sqrt{\mathcal{N}_j}}. \tag{4–20}$$

These normalized modes will be used throughout the rest of this chapter.

4.3 MODE POWERS

By conservation of energy the total power contained in the bound, radiation, and leaky modes is constant along a fibre. The power in each mode varies along the fibre due to mode coupling and phase changes.

The amplitude and phase of a mode at point z is given by [6]

$$b_j(z) = a_j(z) \exp\left(i \int_0^z \beta_j(z) dz \right), \tag{4–21}$$

where:

a_j is the amplitude,

β_j is the propagation constant of the j^{th} mode, and

the exponent gives the phase of the mode at point z.

Using this, the total fields in the fibre are

$$\vec{\mathrm{E}} = \sum_j b_j \hat{e}_j \quad \text{and} \quad \vec{\mathrm{H}} = \sum_j b_j \hat{h}_j. \tag{4–22}$$

These expressions are substituted into the Poynting vector,

$$\vec{S} = \frac{1}{2}\mathrm{Re}\left(\int_{A_\infty} (\vec{E} \times \vec{H}^*) dA\right),$$

giving the power flow as

$$\vec{S} = \frac{1}{2}\mathrm{Re}\left[\int_{A_\infty} \left(\sum_j b_j \hat{e}_j\right) \times \left(\sum_k b_k^* \hat{h}_k^*\right) dA\right]. \qquad (4\text{–}23)$$

This is simplified by applying the orthogonality condition, (4–19), yielding

$$\vec{S} = \sum_j b_j b_j^*. \qquad (4\text{–}24)$$

Therefore, the power carried by each individual mode is $b_j b_j^*$.

The value of b_j is a function of β_j. For bound modes the eigenvalue equation fixes β_j, hence b_j is fixed, but for radiation modes β_j varies between 0 and kn_{cl}. So for a given mode b_j takes on a continuum of values. Therefore the power in a mode is an integral over β_j. Since β_j may be complex it is easier to choose b_j to be a function of Q, which is always real for radiation modes. The power in a radiation mode is therefore

$$S_j = \int_0^{akn_{cl}} |b_j(Q)|^2 dQ. \qquad (4\text{–}25)$$

4.4 MODE COUPLING EQUATIONS

The electric field at a point in a slowly varying waveguide is a superposition of the local modes. At each point along the fibre the superposition changes, therefore the fields must couple to exchange power.

In order to find the coupling coefficients†. consider the total electric field in a waveguide,

$$\vec{\mathrm{E}} = \vec{\mathrm{E}}_T + E_z\hat{z} \quad \text{and} \quad \vec{\mathrm{H}} = \vec{\mathrm{H}}_T + H_z\hat{z}, \tag{4–26}$$

where 'T' denotes the transverse component. Substituting this into the source free Maxwell's equations,

$$\nabla \times \vec{E} = ik\sqrt{\frac{\mu_0}{\epsilon_0}}\vec{H}$$

and

$$\nabla \times \vec{H} = -ikn^2\sqrt{\frac{\epsilon_0}{\mu_0}}\vec{E},$$

along with ∇ in the form

$$\nabla = \nabla_T + \frac{\partial}{\partial z}\hat{z},$$

yields the relationships for the transverse components as

$$ik\sqrt{\frac{\mu_0}{\epsilon_0}}\vec{H}_T = \nabla_T \times E_z\hat{z} + \hat{z} \times \frac{\partial \vec{E}_T}{\partial z} \tag{4–27}$$

and

$$-ikn^2\sqrt{\frac{\epsilon_0}{\mu_0}}\vec{E}_T = \nabla_T \times H_z\hat{z} + \hat{z} \times \frac{\partial \vec{H}_T}{\partial z}, \tag{4–28}$$

---

† This derivation follows that of Love and Snyder [7] It is included here because of its applicability to tapered fibres and to present its limitations and assumptions.

and for the $\hat{z}$ directed components,

$$ik\sqrt{\frac{\mu_0}{\epsilon_0}}\vec{H}_z\hat{z} = \nabla_T \times \vec{E}_T \tag{4-29}$$

and

$$-ikn^2\sqrt{\frac{\epsilon_0}{\mu_0}}\vec{E}_z\hat{z} = \nabla_T \times \vec{H}_T. \tag{4-30}$$

Replacing E_z and H_z in equations (4-27) and (4-28) using the above two equations gives

$$n^2k^2\vec{H}_T = \nabla_T \times (\nabla_T \times \vec{H}_T) - ikn^2\sqrt{\frac{\epsilon_0}{\mu_0}}\hat{z} \times \frac{\partial \vec{E}_T}{\partial z} \tag{4-31}$$

and

$$n^2k^2\vec{E}_T = \nabla_T \times (\nabla_T \times \vec{E}_T) + ik\sqrt{\frac{\mu_0}{\epsilon_0}}\hat{z} \times \frac{\partial \vec{H}_T}{\partial z}. \tag{4-32}$$

The total transverse fields for forward and backward propagating components are†

$$\vec{\mathrm{E}}_T = \sum_j (b_j + b_{-j})\hat{e}_{Tj} \quad \text{and} \quad \vec{\mathrm{H}}_T = \sum_j (b_j - b_{-j})\hat{h}_{Tj},$$

where b_j is as defined in equation (4-21). Each individual mode must satisfy equations (4-31) and (4-32), hence, assuming that the modal fields, $\hat{e}_{Tj}$ and $\hat{h}_{Tj}$, change

---

† The reason for the minus sign in front of b_{-j} in $\vec{H}_T$ is evident from examination of equations (3-36) and (3-37) where for a backward propagating mode β has been replaced by $-\beta$.

slowly with z one obtains

$$n^2k^2\hat{h}_{Tj} = \nabla_T \times (\nabla_T \times \hat{h}_{Tj}) + \beta_j kn^2\sqrt{\frac{\epsilon_0}{mu_0}}\hat{z} \times \hat{e}_{Tj} \tag{4–33}$$

and

$$n^2k^2\hat{e}_{Tj} = \nabla_T \times (\nabla_T \times \hat{e}_{Tj}) - \beta_j k\sqrt{\frac{mu_0}{\epsilon_0}}\hat{z} \times \hat{h}_{Tj}. \tag{4–34}$$

The total field must also satisfy equations (4–31) and (4–32), giving

$$\begin{aligned}\sum_j n^2k^2(b_j - b_{-j})\hat{h}_{Tj} = &\sum_j \nabla_T \times (\nabla_T \times (b_j - b_{-j})\hat{h}_{Tj}) \\ &- \sum_j kn^2\sqrt{\frac{\epsilon_0}{mu_0}}\hat{z} \times \frac{\partial}{\partial z}(b_j + b_{-j})\hat{e}_{Tj}\end{aligned} \tag{4–35}$$

and

$$\begin{aligned}\sum_j n^2k^2(b_j + b_{-j})\hat{e}_{Tj} = &\sum_j \nabla_T \times (\nabla_T \times (b_j + b_{-j})\hat{e}_{Tj}) \\ &+ \sum_j k\sqrt{\frac{mu_0}{\epsilon_0}}\hat{z} \times \frac{\partial}{\partial z}(b_j - b_{-j})\hat{h}_{Tj}.\end{aligned} \tag{4–36}$$

Substituting in for $n^2k^2\hat{e}_{Tj}$ and $n^2k^2\hat{h}_{Tj}$ from equations (4–33) and (4–34) into the left hand side of the above two equations yields

$$\sum_j \left[(b_j - b_{-j})\hat{z} \times \frac{\partial \hat{h}_{Tj}}{\partial z} - i\beta_j(b_j + b_{-j})\hat{z} \times \hat{h}_{Tj} + \left(\frac{db_j}{dz} - \frac{db_{-j}}{dz}\right)\hat{z} \times \hat{h}_{Tj}\right] = 0 \tag{4–37}$$

and

$$\sum_j \left[(b_j + b_{-j})\hat{z} \times \frac{\partial \hat{e}_{Tj}}{\partial z} - i\beta_j(b_j - b_{-j})\hat{z} \times \hat{e}_{Tj} + \left(\frac{db_j}{dz} + \frac{db_{-j}}{dz}\right)\hat{z} \times \hat{e}_{Tj}\right] = 0, \tag{4–38}$$

The above relations are simplified by taking dot products with $\hat{e}_l^*$ in the first equation, and $\hat{h}_l^*$ in the second, then integrating over the cross section (using the orthonormality condition of equation (4–19)). The waveguides are assumed to be nonabsorbing, hence $\hat{e}_l^* = \hat{e}_l$ and $\hat{h}_l^* = \hat{h}_l$ (recall that phase is contained in b_l), yielding the coupling equations [8]

$$\frac{db_j}{dz} - i\beta_j b_j = \sum_l (C_{jl} b_l + C_{j-l} b_{-l}) \tag{4–39}$$

and

$$\frac{db_{-j}}{dz} + i\beta_j b_{-j} = -\sum_l (C_{-jl} b_l + C_{-j-l} b_{-l}), \tag{4–40}$$

where the C_{jl}'s are the coupling coefficients,

$$C_{jl} = \frac{1}{4} \int_{A_\infty} \left(\hat{h}_j \times \frac{\partial \hat{e}_l}{\partial z} - \hat{e}_j \times \frac{\partial \hat{h}_l}{\partial z} \right) \cdot \hat{z}\, dA. \tag{4–41}$$

Note that the left hand side of equation (4–40) is the rate of change in the amplitude, b_j, along the fibre minus the rate of change due to the periodicity of the mode, the difference being the amplitude change due to coupling with other modes, as accounted for in the right hand side of the equation. Love and Snyder have demonstrated that this is equivalent to [9] [10]

$$C_{jl} = \frac{k}{4(\beta_j - \beta_l)} \sqrt{\frac{\epsilon_0}{\mu_0}} \int_{A_\infty} \hat{e}_j^* \cdot \hat{e}_l \frac{\partial n^2}{\partial z}\, dA. \tag{4–42}$$

According to the above equation, coupling strength depends on the behavior of the refractive index profile. The coupling effects therefore are dependent on guide geometry as will be discussed later.

4.5 SUMMARY

The total field in a fibre is a superposition of bound, radiation, and leaky modes. The propagation constants for both leaky and bound modes take on discrete values as described by an eigenvalue equation. For radiation modes the propagation constant is any value in the range $0 \leq \beta^r \leq n_{cl}k$. In an ideal, straight fibre these modes do not interact or exchange energy therefore, the modes are orthogonal and the total energy is the sum of the energies in each mode. However, when the fibre is bent, tapered or contains some other imperfection the modes couple and exchange energy.

REFERENCES

[1] Snyder, Allen W. "Continuous Mode Spectrum of a circular Dielectric Rod," *IEEE Transactions on Microwave Theory and Techniques*, **19**, (1971), p.720–727.

[2] Snyder, Allen W., and John D. Love, *Optical Waveguide Theory*, (New York: Chapman and Hall, 1983), p. 713.

[3] ibid., p.502.

[4] ibid., p.713.

[5] ibid., p.602–605.

[6] ibid., p.617.

[7] ibid., p.617–619.

[8] ibid., p.618.

[9] ibid., p.619.

[10] Snyder, Allen W. "Mode Propagation in a Nonuniform Cylindrical Medium," *IEEE Transactions on Microwave Theory and Techniques*, **19**, (1971), p.402–403.

CHAPTER 5–REPRESENTATIONS

This chapter defines the terms used in characterizing optical fibres. Expressions for power and attenuation are given along with terms for quantifying polarization properties. The Poincaré sphere, a useful representation for evaluating optical system performance, is also presented. These representations will be used throughout the rest of this work.

5.1 POWER AND ATTENUATION

Power is lost between the input and the output of any optical fibre. The ratio of output power to input is known as the *transmittance*,

$$T = \frac{\mathrm{P_{out}}}{\mathrm{P_{in}}}. \tag{5-1}$$

This quantity can also be expressed as attenuation in decibels [1],

$$\alpha_{\mathrm{dB}} = -10 \log\left(\frac{\mathrm{P_{out}}}{\mathrm{P_{in}}}\right). \tag{5-2}$$

The decibel scale is also used to express power. Decibel power is defined by [2]

$$\mathrm{dBm} = 10 \log\left(\frac{\mathrm{P}}{1\ \mathrm{mW}}\right) \tag{5-3}$$

for referencing against 1 mW. Similarly, the comparison to 1 μW is

$$\mathrm{dB}\mu = 10\log\left(\frac{\mathrm{P}}{1\ \mu\mathrm{W}}\right). \tag{5–4}$$

5.2 POLARIZING ABILITY

All polarization modes of a light beam passing through an isotropic media experience the same attenuation. In anisotropic media, such as a polaroid, one polarization mode experiences higher attenuation than the other. The greater the attenuation difference the higher the degree of polarization of the emerging light. The difference in attenuation is known as the *extinction ratio* [3], or *polarization ratio*,

$$\mathcal{E}_{\mathrm{dB}} = \left|(\alpha_{\mathrm{dB}})_x - (\alpha_{\mathrm{dB}})_y\right|. \tag{5–5}$$

Rather than use decibels, many authors express the extinction ratio as a fraction of power in the high power mode to that in the low power mode,

$$\mathcal{E} = \frac{\mathrm{P}_{\mathrm{max}}}{\mathrm{P}_{\mathrm{min}}}. \tag{5–6}$$

5.3 BEAT LENGTH

Polarization states are not only affected by polarizers, they are also affected by material birefringence.

The refractive index in a birefringent material is different for each polarization, hence the propagation constant, β, is also different. Since the speed of light varies with index the two polarizations, x and y, travel at different speeds causing their

relative phase to change along the fibre. The phase shift after travelling a distance z is $\phi = \beta z$, so the phase separation between the modes is

$$\delta\phi = \beta_x z - \beta_y z = \mathcal{B} z, \tag{5–7}$$

where $\mathcal{B}$ is the material birefringence. The *beat length*, L_p, is the distance travelled along the fibre for the relative phase to slip by 2π radians, hence [4],

$$L_p = \frac{2\pi}{\beta_x - \beta_y} = \frac{2\pi}{\mathcal{B}}. \tag{5–8}$$

The beat length is a trait of birefringent fibres, the shorter the beat length the greater the birefringence and hence, the greater the difference in refractive index experienced by the two polarizations. The refractive index is proportional to the internal stress. The higher the stress the more immune the refractive index profile is to perturbations caused by pressure on the fibre. Therefore, the shorter the beat length the greater the polarization holding ability of the fibre.

5.4 POINCARÉ SPHERE

As light propagates through an optical system the polarization state changes. Birefringent materials cause the polarization to vary cyclicly between linear and elliptical states while polarizers force the modes to progress towards linear states. The mathematical treatment of an optical system can be very complex. Analysis is greatly simplified by employing the Poincaré sphere representation.

A *Poincaré sphere* is a spherical surface which represents all possible polarization states. Polarization states are specified by two quantities:

1. the ellipticity, and
2. The orientation of the polarization ellipse.

Consider elliptically polarized light with the major axis of the polarization ellipse directed along the x' axis which has been rotated by an angle ϕ from the weakly

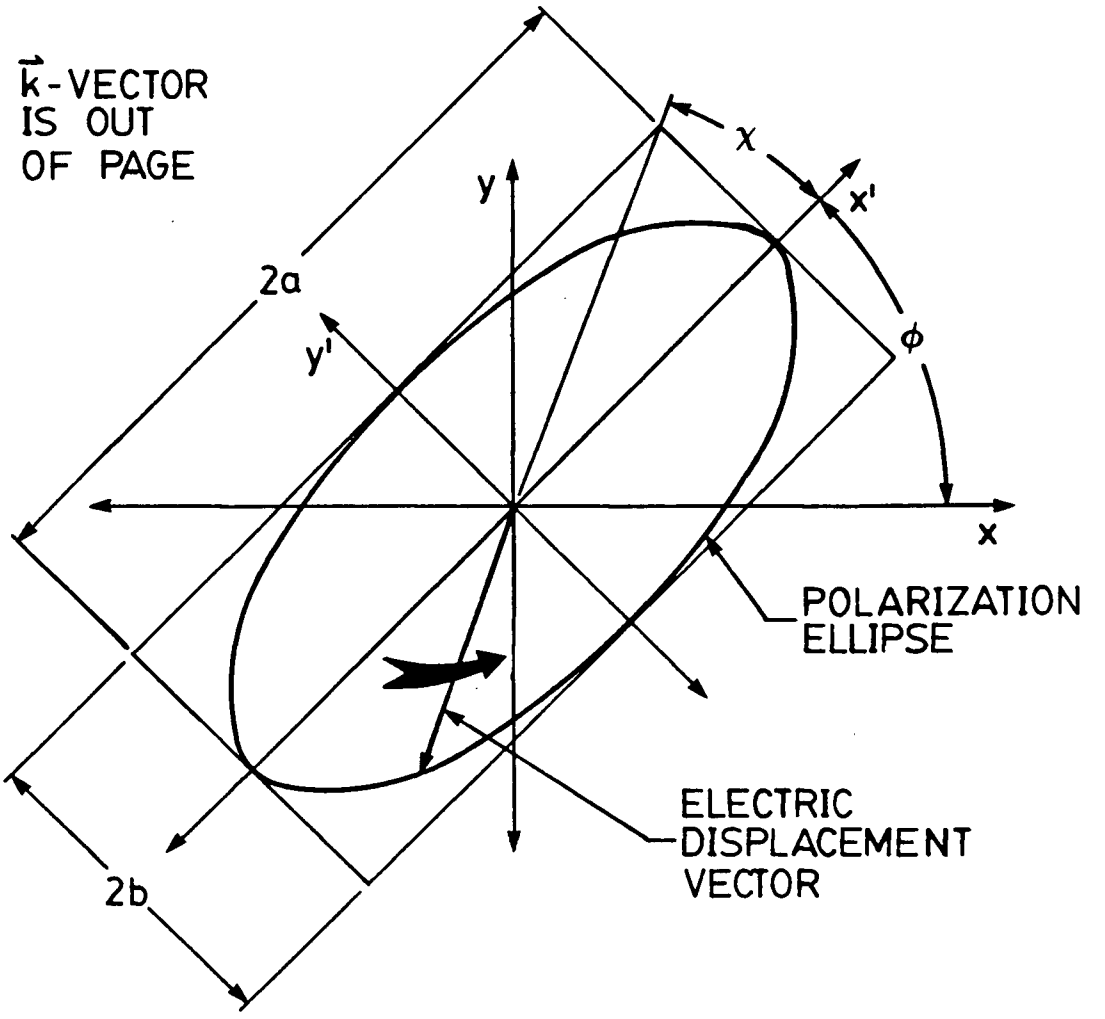

FIGURE 5–1. ELLIPTICAL POLARIZATION

The motion and amplitude of the electric displacement vector describes an ellipse with ellipticity χ and rotated from the reference axis, x, by ϕ. The x axis represents the fast polarization eigenstate and the y axis is the slow eigenstate.

guided polarization state, or fast axis (x), as shown in figure 5–1. The ellipticity can be quantified by using an enclosing rectangle. The angle between the x' axis

and the rectangle's corner is the ellipticity,

$$\chi = \pm \arctan\left(\frac{b}{a}\right). \tag{5–9}$$

The ellipticity is positive for right-handed polarizations (counterclockwise rotation of the electric displacement vector) and negative for left-handed polarizations. Rotating the ellipse about the origin introduces a phase shift, ϕ. Unique states are defined for:

$$0 \leq \phi < \pi \quad \text{and} \quad -\frac{\pi}{4} \leq \chi < \frac{\pi}{4}.$$

These angles do not cover an entire sphere, however 2χ and 2ϕ do, with each set of values defining a unique point on the sphere [5]. These angles describe the Poincaré sphere shown in figure 5–2. Any polarization state can be represented as a point on the surface. The equator is all possible linear polarization states, while the poles are the left and right handed circular states, all other points are elliptical states.

The polarization state is not stationary on the sphere. Birefringence, electro-magnetic fields, and polarizers move the state over the sphere's surface. Phase changes alter the angle 2ϕ and ellipticity changes alter the angle 2χ.

In a birefringent medium both the ellipticity and phase of the polarization state vary along the fibre. The resulting motion of the polarization state is a rotation on the sphere's surface about the axis through the two orthogonal polarization eigenstates of the medium [6] [7], as shown in figure 5–3. The polarization state rotates through an angle, ς, equal to the phase difference, equation (5–7), between the modes.

The action of an electro-magnetic field is the same as that of birefringence with the exception that the eigenstates are the poles, as shown in figure 5–4. When

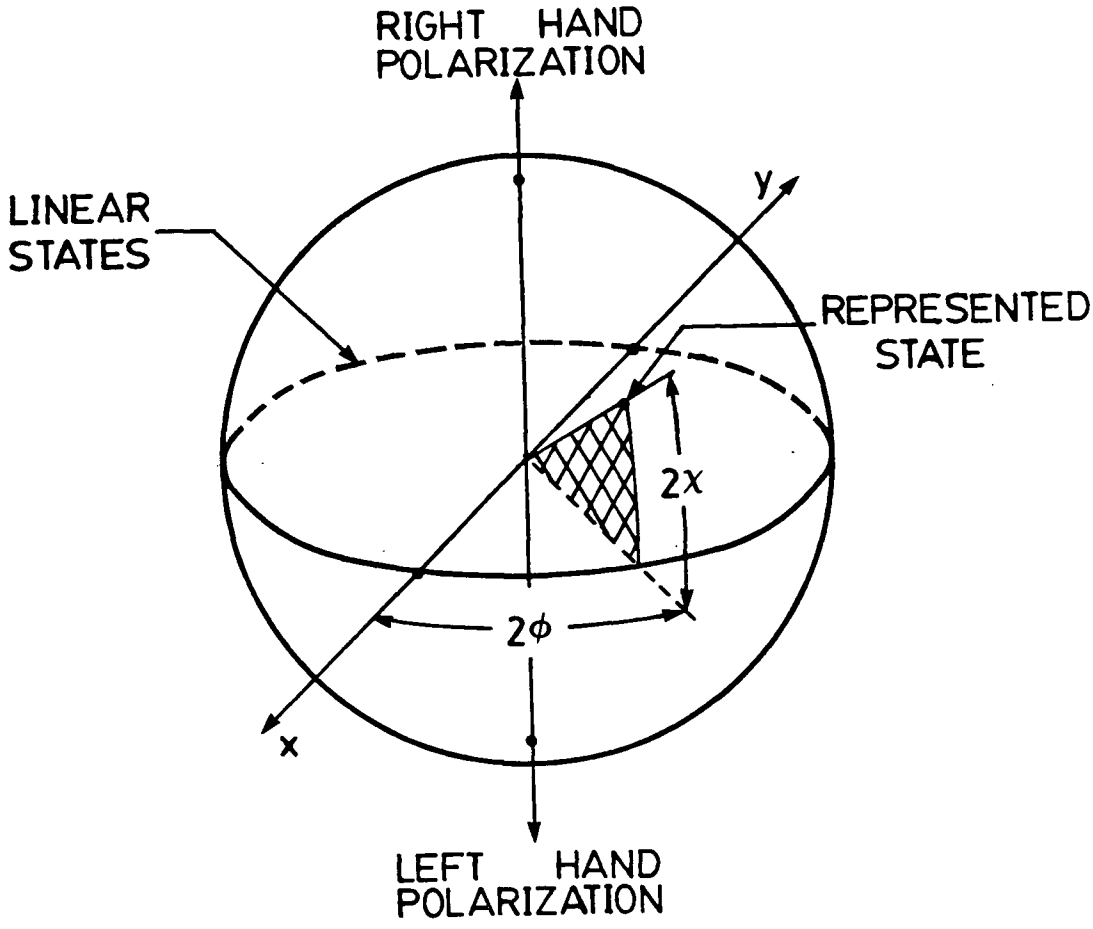

FIGURE 5–2. POINCARÉ SPHERE

A polarization state of phase ϕ and ellipticity χ is represented as a point on the Poincaré sphere's surface. Since the phase and ellipticity are represented by an angle twice their value, orthogonal polarization states are directly opposite each other on the sphere. In other words, the orthogonal polarization states and the centre of the sphere form a line.

a magnetic field is applied at an angle ϑ to the direction of propagation the polarization state is Faraday rotated [8] at a rate [9]

$$\frac{d\phi}{dz} = \frac{1}{2}\frac{d\varsigma}{dz} = \tilde{V} H \cos\vartheta, \qquad (5-10)$$

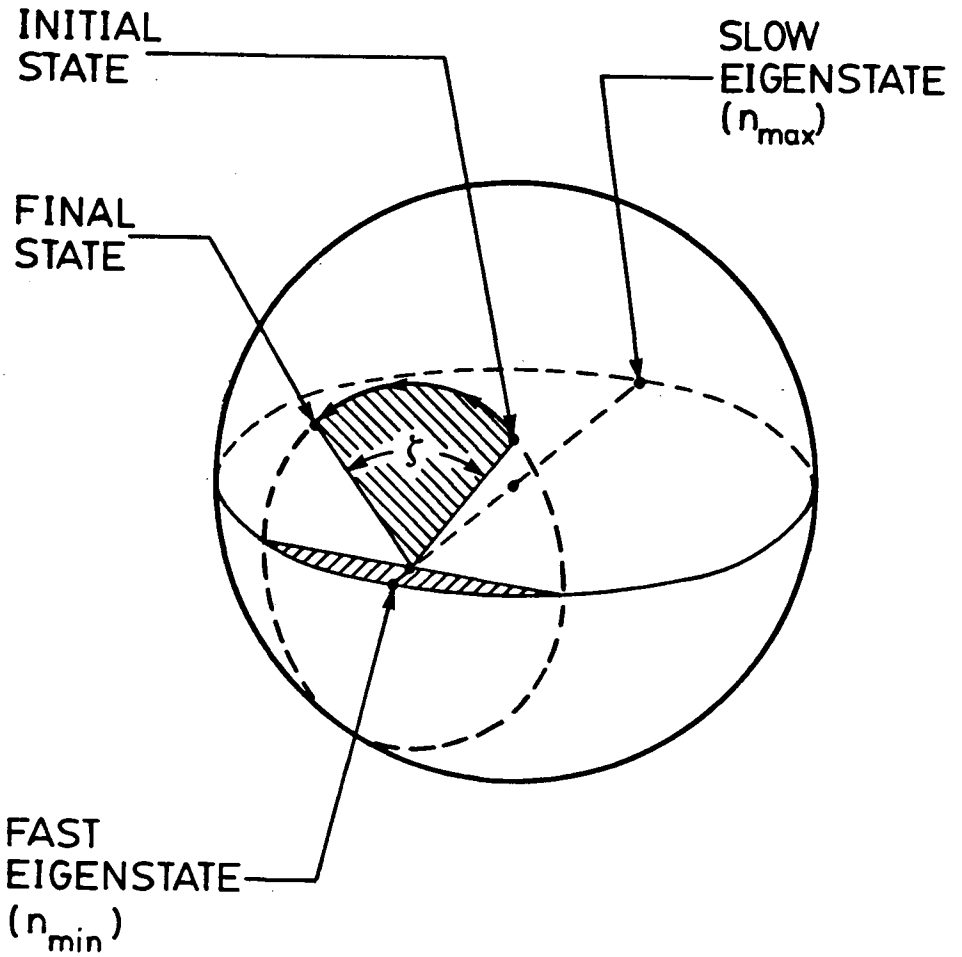

FIGURE 5–3. BIREFRINGENCE EFFECT ON POLARIZATION

The polarization state rotates about the axis containing the fast and slow eigenstates of the birefringent media.

where $\tilde{V}$ is the *Verdet constant*, ($\tilde{V}_{\text{silica}} = 4.5 \times 10^{-6}$ Rads/A) [10]. This rotation has the same sense for both forward and backward propagating modes since a reversal in the direction of travel also reverses the angle of the applied field.

When light interacts with a polaroid the polarization state does not rotate about an axis defined by eigenstates but instead takes the shortest path towards the unimpeded polarization state. The resulting path is a portion of the great circle

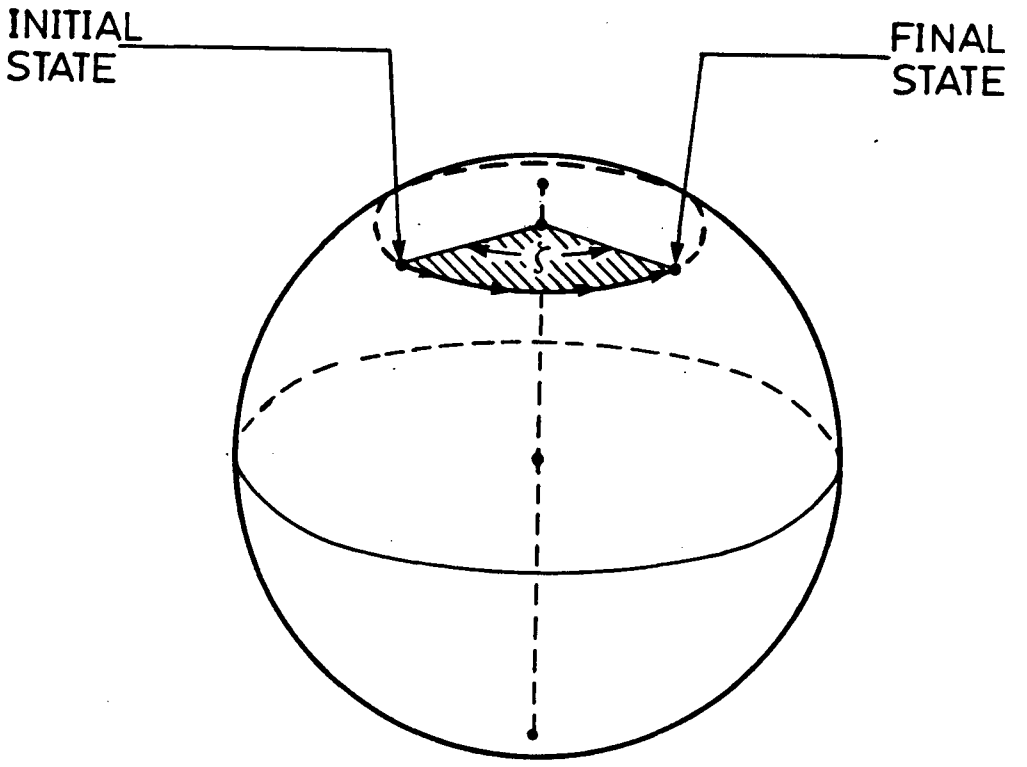

FIGURE 5–4. FARADAY ROTATION ON A POINCARÉ SPHERE
Only the polarization state's orientation (phase angle) changes, thus the state revolves around an axis through the poles.

containing the input state as well as the transmitted and attenuated polarizations, as shown in figure 5–5. The transmitted intensity is [11]

$$T = \cos^2\left(\frac{\varsigma}{2}\right) \tag{5–11}$$

where ς is the angle between the input and output states on the Poincaré sphere.

The use of this representation is demonstrated in the next chapter where it is applied to an experiment.

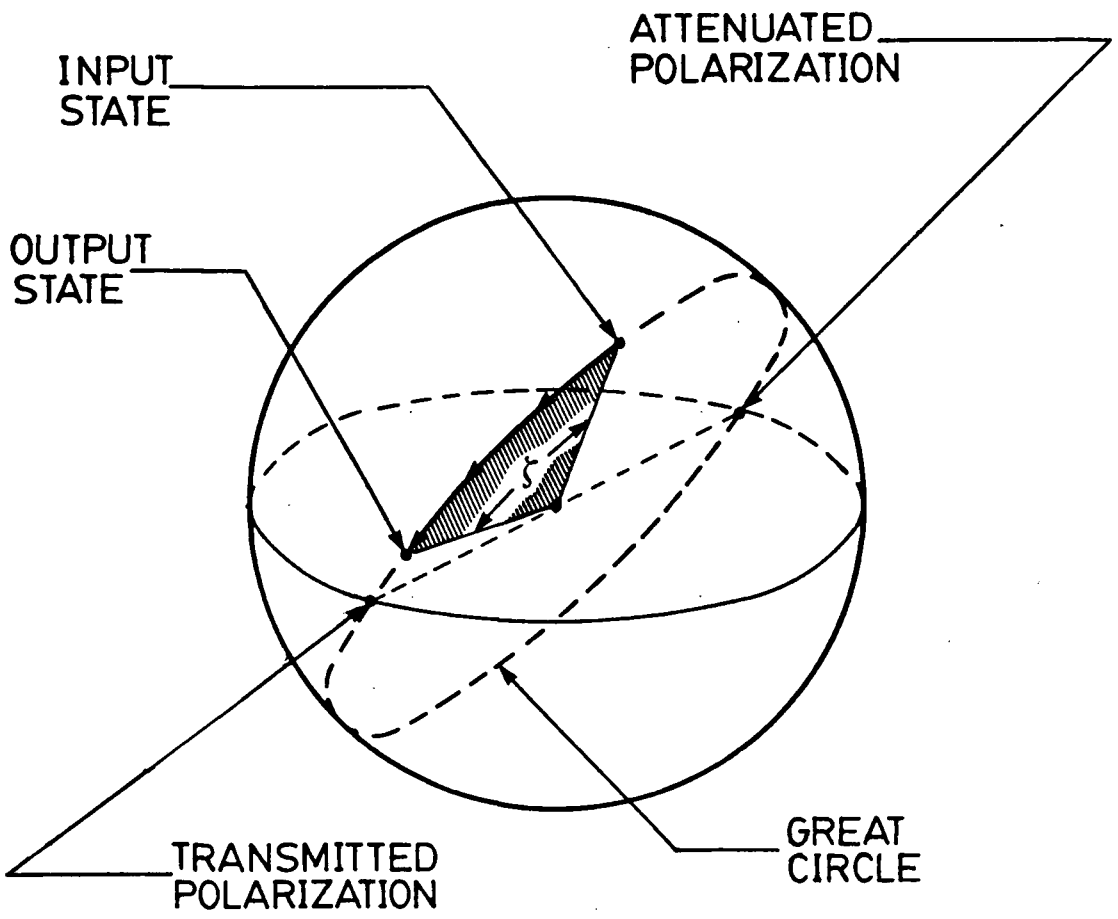

FIGURE 5–5. POLAROID ACTION ON A POINCARÉ SPHERE

The polarization state moves toward the transmitted state on a great circle. The great circle contains the input state along with the transmitted and attenuated polarizations.

5.5 SUMMARY

This chapter described Poincaré sphere mechanics and described terms for quantifying power, attenuation, polarization and birefringence. The usefulness of these various representations will become apparent in the next chapter where they are applied to a real system.

REFERENCES

[1] Hentschel, Christian. *Fiber Optics Handbook* , (Federal Republic of Germany: Hewlett Packard, 1983), p.28–30.

[2] ibid., p.52.

[3] ibid., p.55.

[4] Kaminow, Ivan P. "Polarization in Optical Fibers," *IEEE Journal of Quantum Electronics*, **17**, (1983), p.15–22.

[5] Rashleigh, Scott C. "Origins and Control of Polarization Effects in Single-Mode Fibers," *Journal of Lightwave Technology*, **1**, (1983), p.312–331.

[6] Johnson, Mark. "Poincaré Sphere Representation of Birefringent Networks," *Applied Optics*, **20**, (1981), p.2075–2080.

[7] Ramachandran, G.N., and S. Ramaseshan. *Handbuch der Physik XXV/1*, S. Flügge ed., (Berlin: Springer-Verlag, 1961), p.5–11.

[8] Baldwin, George C. *An Introduction to Nonlinear Optics*, (New York: Plenum Press, 1969), p.63–64.

[9] [7], p.198–199.

[10] Payne, David N., Arthur J. Barlow, and Jens J. Ramskov Hansen. "Development of Low- and High-Birefringence Optical Fibers," *IEEE Journal of Quantum Electronics*, **18**, 1982, p.477–487.

[11] [7] p.1–5.

CHAPTER 6–BEAT LENGTH MEASUREMENT

The beat length is a measure of both fibre birefringence as well as the ability to maintain a polarization state [1] [2].

Beat length measurements are useful for two reasons. First, the application wavelength may differ from that used by the fibre manufacturer for rating beat length. Since birefringence varies with wavelength [3] the beat length quoted by the manufacturer is not the application's beat length. Second, beat length measurements are useful as a tool for analyzing polarization state evolution along a fibre. The polarization state information can be used to evaluate the effects and performance of fibre devices and gives hints about the internal structure (internal stresses affect birefringence).

Because such data is valuable in tapered polarizer development an attempt was made to measure the beat length of the birefringent fibres by using Faraday rotation. The beat length experiment proved to be a good introduction to optical fibre techniques and the experimental setup. This chapter is a description of the beat length measurement experiments. This not only introduces the setup and the techniques, but it also demonstrates applications of the theory presented in the previous chapters.

6.1 THEORY

The measurement technique can be understood by considering polarized light propagating in a birefringent fibre. As light propagates along the fibre the birefringence causes the polarization state to rotate on the Poincaré sphere's surface, as discussed in the previous chapter. The rotation rate is proportional to the beat length hence, by sensing the rotation along the fibre the beat length can be found.

The simplest method to measure the rotation along the fibre is to measure the change in ellipticity of the output polarization state of two different lengths of the same fibre. Linearly polarized light is introduced into the fibre at $\phi = 45°$ to both polarization eigenstates and the ellipticity of the output polarization state is measured. The fibre is then shortened by cutting and polishing the output end, then the ellipticity is measured again, as shown in figure 6–1. The beat length is given by

$$L_p = \frac{\pi}{\chi_1 - \chi_2}(L_1 - L_2), \qquad (6-1)$$

where χ is the ellipticity of the output polarization state, L is the length of the fibre, and '1', and '2' denote the different fibre lengths. The accuracy of this method is limited by the precision with which the fibre length is reduced.

A more common beat length measurement technique is to use photographs of the Rayleigh, or dipole, scattering in the fibre [4]. Rayleigh scattering techniques are nondestructive and produce good results for beat lengths on the order of centimeters. Using this technique, the beat length manifests itself as a series of light and dark bands on the fibre, as shown in figure 6–2. The bands are a result of the nature of dipole scattering. The radiation field of a dipole is minimum along the dipole axis and maximum perpendicular to it. Since the dipole's axis is oriented in the direction of the electric field [5], which rotates along the birefringent fibre, light and dark lines can be observed by viewing the fibre along the input polarization axis. Bright regions appear where the polarization state is perpendicular to

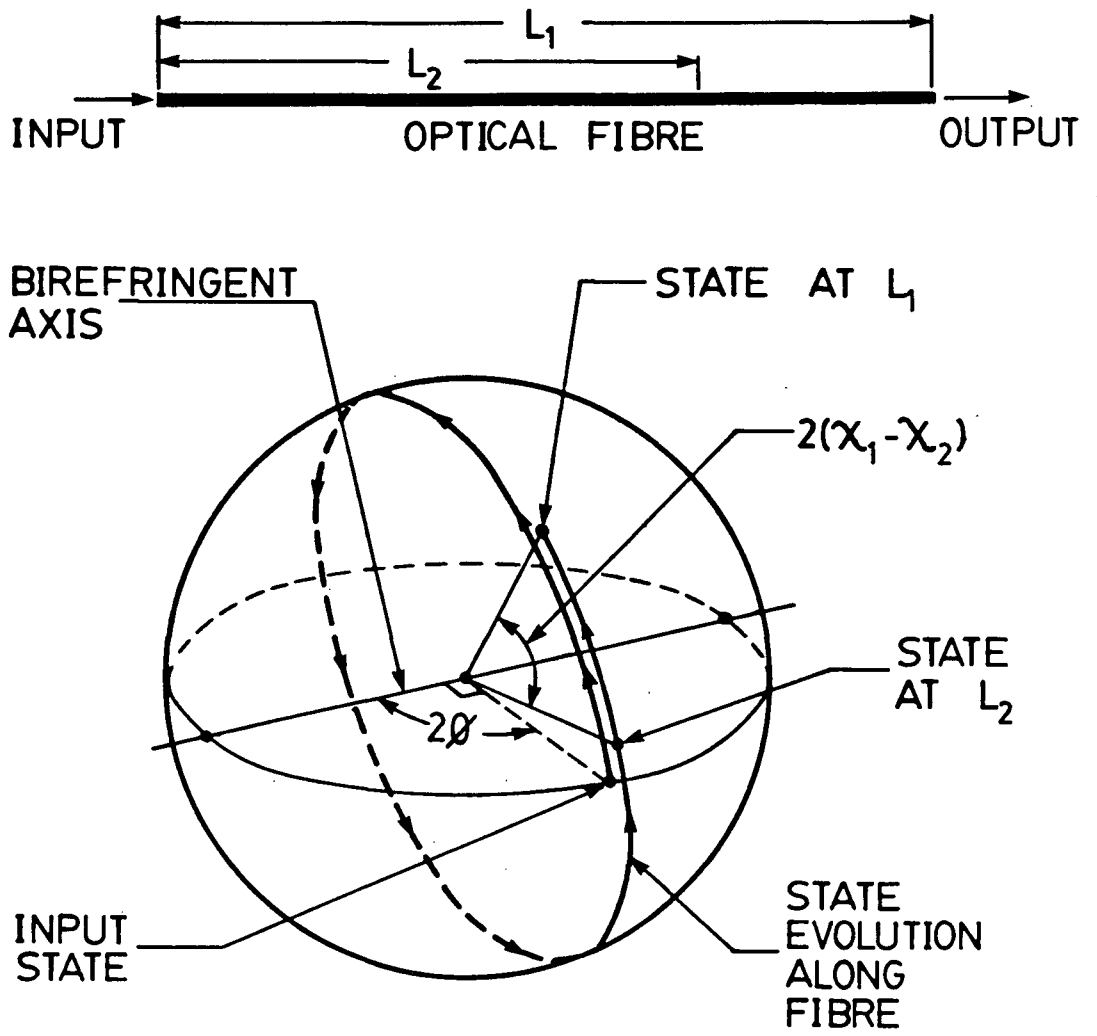

FIGURE 6–1. CUT-BACK METHOD FOR MEASURING BEAT LENGTH
The ellipticity of the polarization state depends on position along the fibre. Note: The state remains on the same orbit on the sphere at all times. In the above figure the paths have been separated for clarity.

the viewing angle while the intervening regions appear darker. This is most easily observed when the two polarization eigenstates are equally excited so that there is a maximum interchange of energy between the two modes.

An alternative method of measuring beat length uses Faraday rotation. This is a nondestructive technique which makes beat length measurements in the millimeter

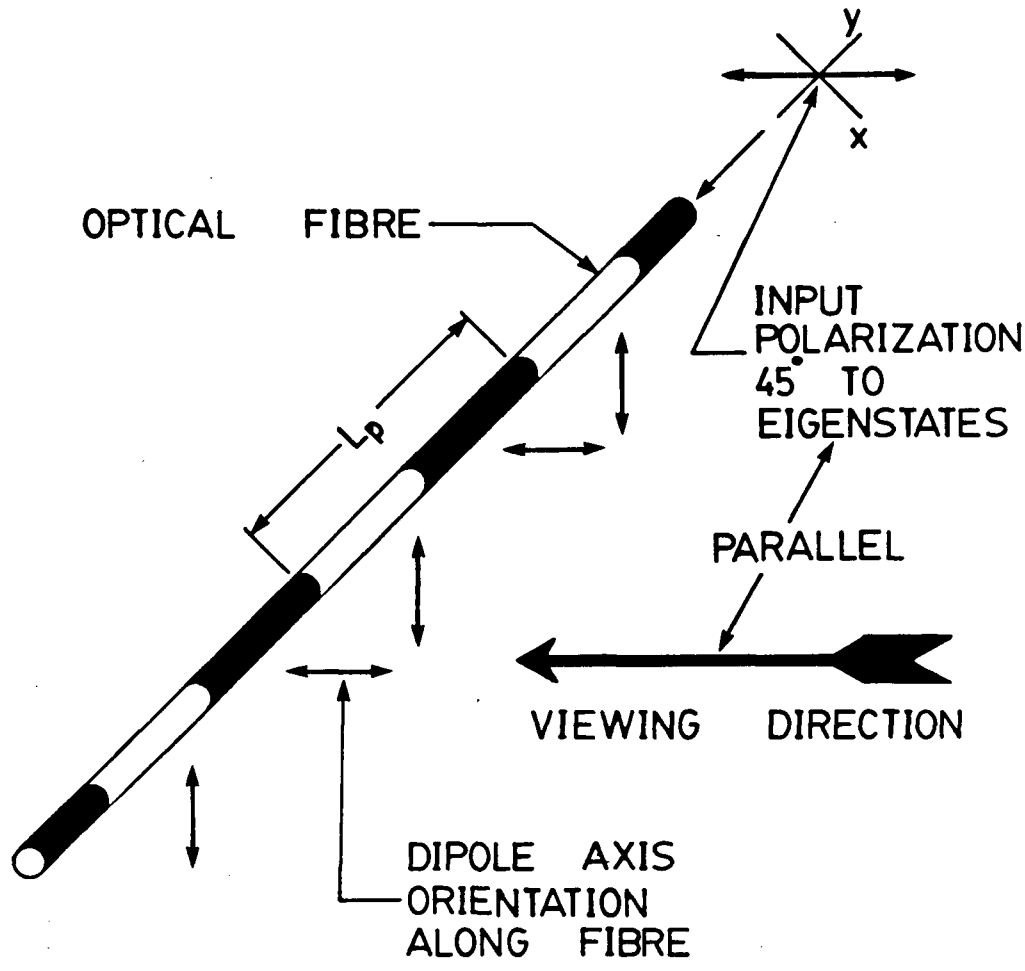

FIGURE 6–2. RAYLEIGH SCATTERING IN A FIBRE
The beat length is the distance between successive dark (or light) bands.

range possible. This technique works by altering the output polarization state with a magnetic field applied parallel to the fibre. The degree to which the output is affected depends on where the magnetic field is applied within a beat, as shown in figure 6–3.

The magnetic field's effect on the output state can be predicted by using the Poincaré sphere. Consider plane polarized light introduced into a birefringent

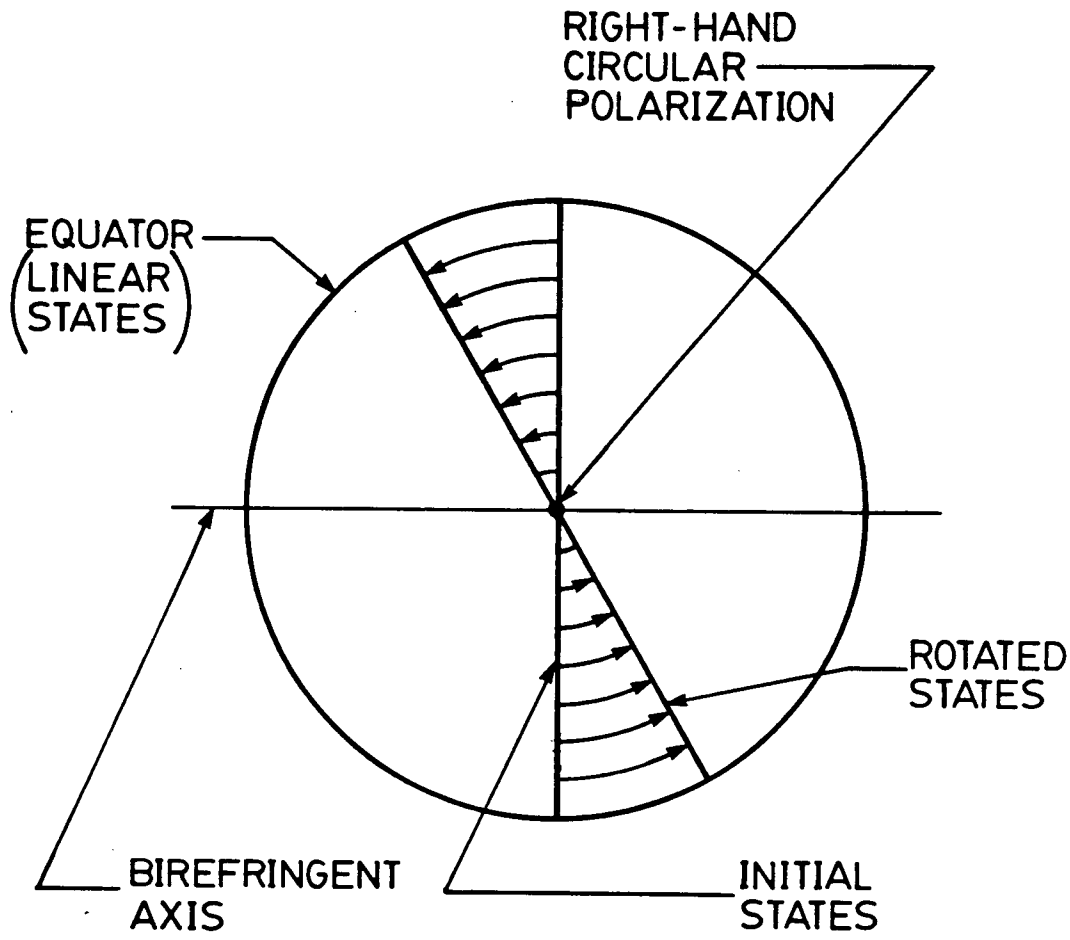

FIGURE 6–3. FARADAY ROTATION OF THE POLARIZATION STATE
The arrowed region is the shift in the polarization states from that of the equally excited polarization states in a birefringent fibre. The rotation is greatest at the equator (linear states) and least at the poles (circular states) of the Poincaré sphere.

fibre in such a way that both polarization eigenstates are equally excited (see appendix A). As the light propagates along the fibre the polarization state rotates on the Poincaré sphere's surface as indicated in figure 6–4. The interaction with the magnetic field Faraday-rotates the state about the poles of the Poincaré sphere. The light then continues along the rest of the fibre rotating on the Poincaré sphere's surface about the same axis as before it interacted with the magnetic field, but in

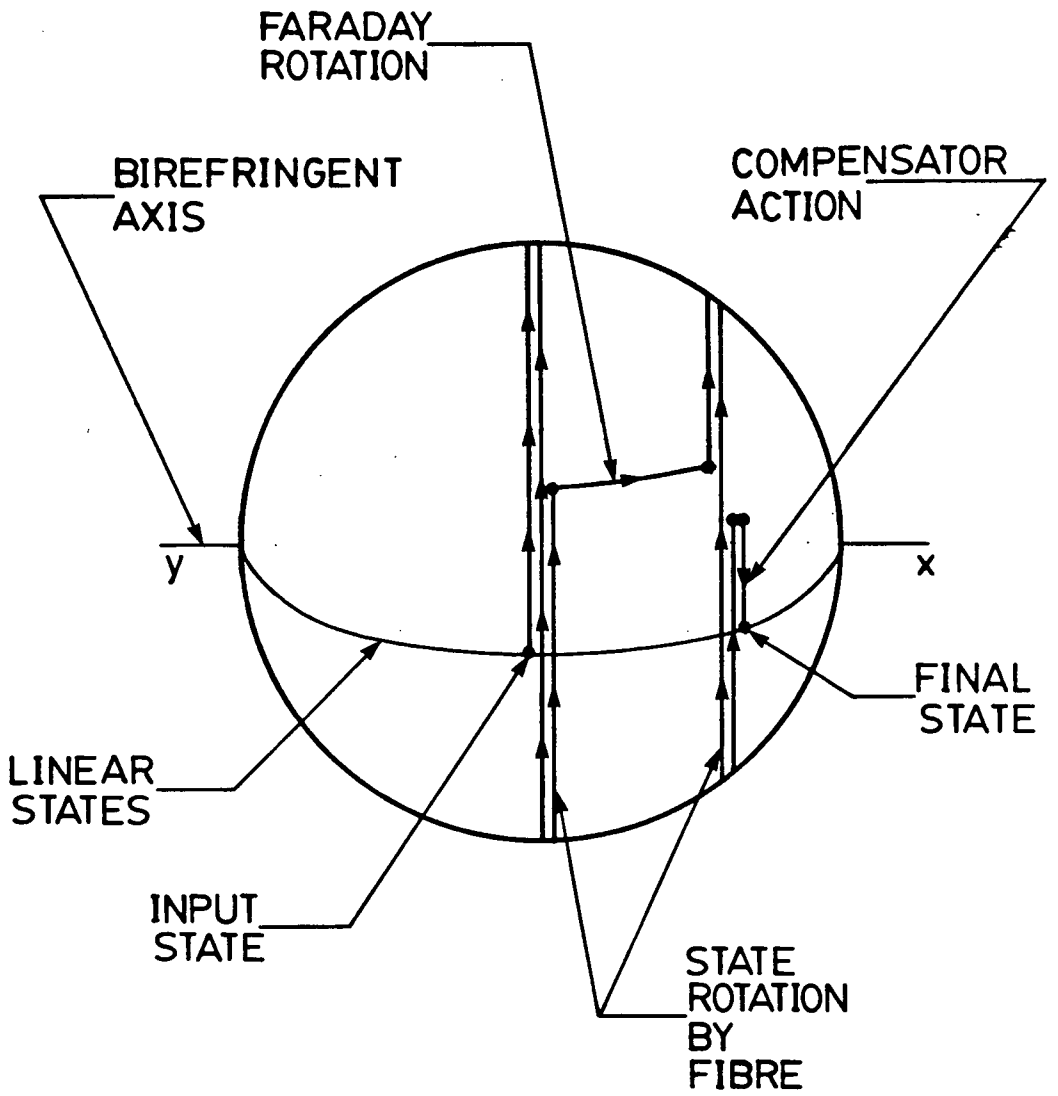

FIGURE 6–4. BEATLENGTH MEASUREMENT BY FARADAY ROTATION
The polarization state development is shown on the Poincaré sphere assuming that the field is applied to a section of fibre which is short compared to the beat length. The states rotate on great circles on the sphere, their paths have been separated for clarity.

a different position. Interactions in regions where the polarization state is circular do not affect the output because of the proximity of the polarization state to the pole (figure 6–3). On the other hand, application of the field in a region where the

output is planar causes the greatest amount of Faraday rotation hence, the output is greatly affected. Therefore, the position of the output state depends on where the magnetic field interaction occurs within a beat.

The state variations can be sensed by passing the output through a Babinet-Soleil compensator (so that the reference state is a linear state) and then a polaroid filter. Since each final state on the Poincaré sphere is a different distance from the transmitted state of the polaroid the output intensity will vary with magnet position [6] [7]. Using this, the beat length is directly measured as the distance the magnet moves along the fibre between maximum intensity outputs.

6.2 EXPERIMENTAL SETUP

The experimental setup for measuring beat length using Faraday rotation is shown in figure 6–5. The following is a description of the major components and their purpose.

- Laser Diode

  The laser diode is a model LDM3-H manufactured by Ortel Corporation, Alhambra, California. It is a multimode laser diode which is capable of emitting 3 mW optical power at 841.2 nm. Its output spectrum is shown in figure 6–6.

- Selfoc Lens

  The Selfoc lens [8] increases the coupling efficiency between the laser diode and the pigtail fiber. The lens was manufactured by Melles Griot, Irvine, California. It is 1.8 mm in diameter and has a numerical aperture of 0.6 and a pitch of 0.25 at 830 nm.

- Pigtail Fibre

  The pigtail fibre is a bow-tie fibre manufactured by York V.S.O.P. Inc., Princeton, New Jersey, the properties of which are listed in table VI–I . The purpose of the pigtail fibre is to transfer polarized light from the laser diode to the test fibre. Though this is not necessary, it is expedient since coupling a fibre

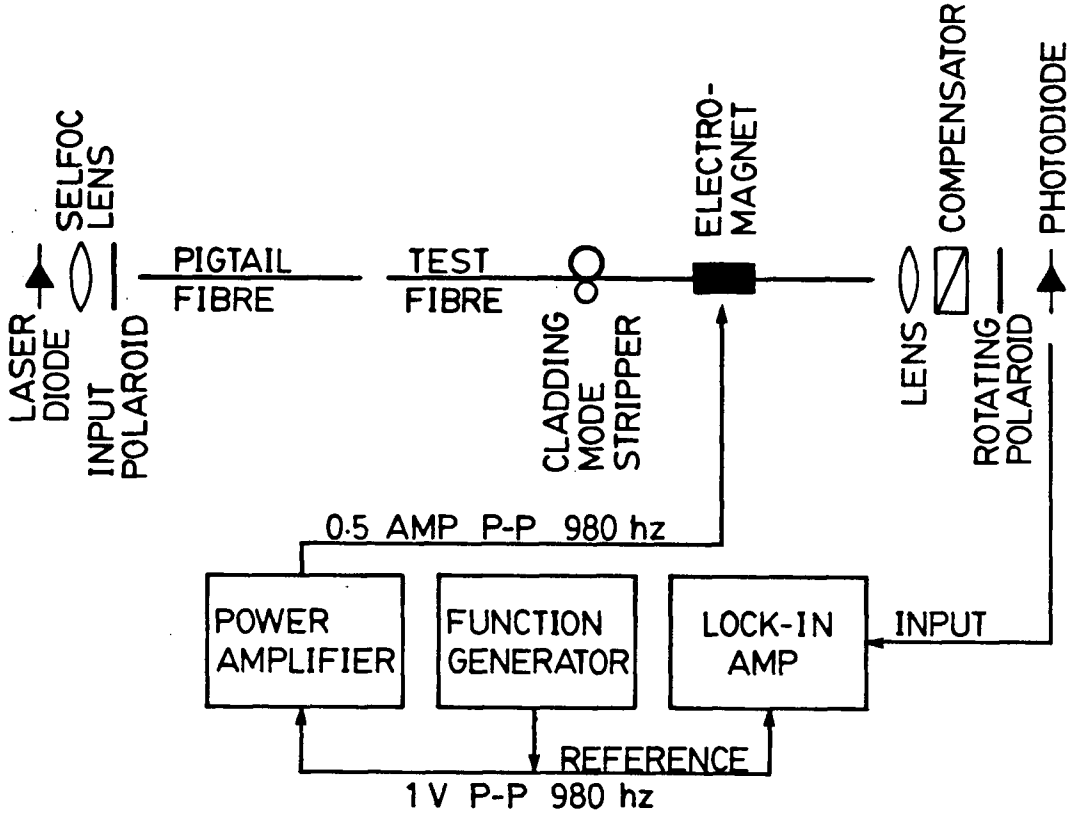

FIGURE 6–5. EXPERIMENTAL SETUP

to another fibre is very easy compared to coupling a fibre to a laser diode (details are in appendix A).

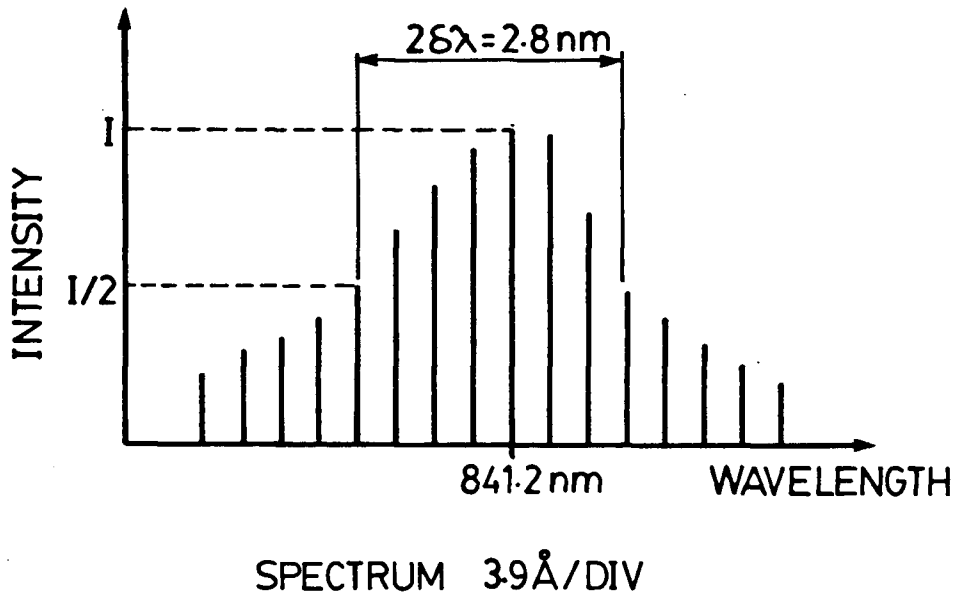

FIGURE 6–6. SPECTRUM OF THE LASER DIODE

Redrawn from data supplied by the manufacturer for the particular device used.

- Babinet-Soleil Compensator

  The Babinet-Soleil compensator is an adjustable birefringent element which is used to convert the output polarization state into a planar state. This conversion maximizes the intensity difference transmitted by the analyzing polaroid as the magnet moves along the fibre.

- Electromagnet

  The electromagnet produces the magnetic field which Faraday rotates the polarization state. It is shown in figure 6–7 along with the magnetic field distributions†. The test fibre is passed through a small hole in the ferrite

---

† The Author thanks A. Labun for his contribution of the electromagnet. Mr. Labun spent many hours designing and building the magnet as part of his Applied Science 459 project [9].

TABLE VI–I BIREFRINGENT FIBRE PROPERTIES

These are the specifications for fibre type HB800 manufactured by York V.S.O.P.

Operating Wavelength	820 nm
Cut-off wavelength	<800 nm
Attenuation	3.5 dB/km
Beatlength at 630 nm	<2 mm (1.3 mm typical)
Fibre Diameter	125 ± 3 μm
Coating Diameter	220 μm (nominal)
Core Diameter†	2–8 μm
$n_{co} - n_{cl}$	0.01 (nominal)

†This range is over all types of highly birefringent fibre available from York V.S.O.P.

core down the center of the magnet. The ferrite core prevents the magnetic field from penetrating into the fibre except where the gap occurs in the core material. The resulting field intensity is 0.5 T which falls to half its value 0.52 mm from the magnet's center when the coil carries a 0.5 amp current. Since the field of a solenoid is directly proportional to current the field strength in Tesla is assumed to be the current in amperes.

- Lock-In Frequency Amplifier

  Since the expected change in signal is small compared to the signal's amplitude a lock-in frequency amplifier is used. This device gives the amplitude of the component of the signal which has the same frequency as the reference signal given to it (for obvious reasons the reference frequency is the same as the modulation frequency of the device causing the effect to be observed). The lock-in amplifier used was a model SR530 made by Stanford Research Systems, Palo Alto, California. It has two 50 dB notch filters at 60 and 120 hz, and a

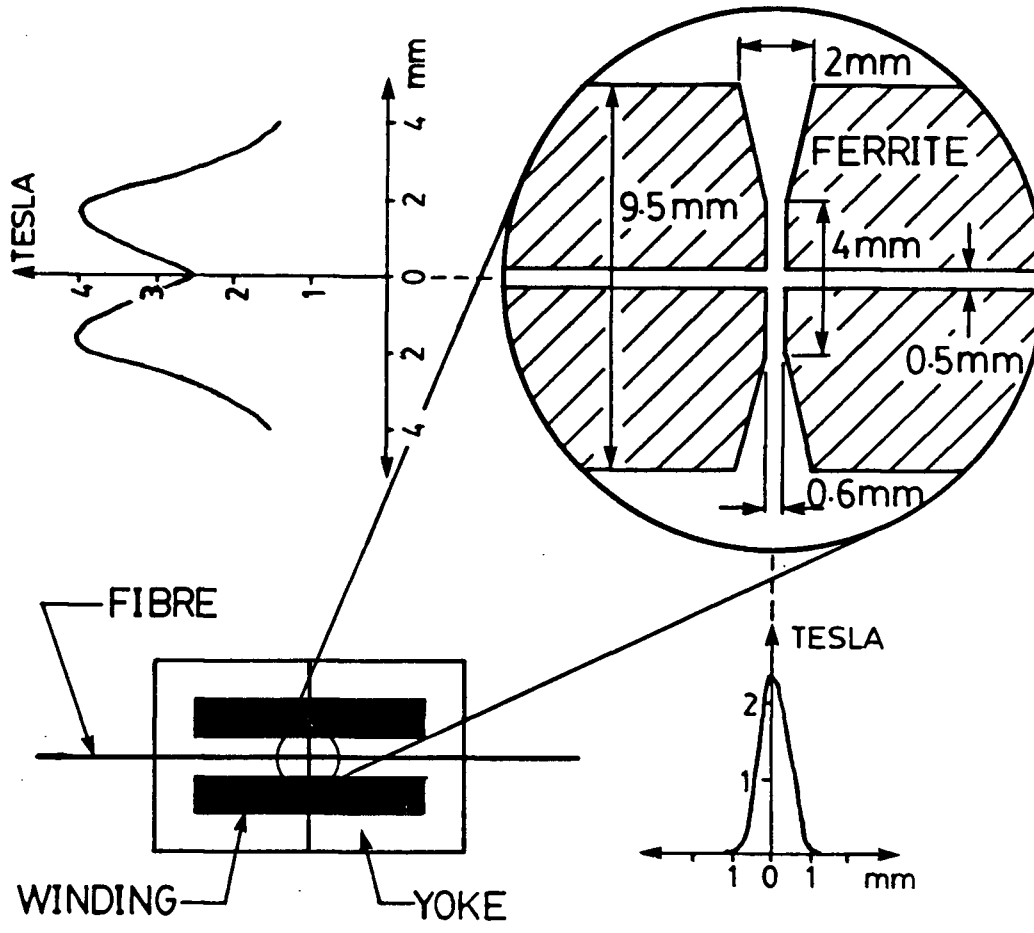

FIGURE 6–7. THE ELECTROMAGNET

The magnet and the field calculations were supplied by A. Labun (see footnote on page 66). A direct measurement of the field could not be performed because of the confined space inside the magnet.

bandpass filter set within 1% of the reference frequency. The noise from the device is rated at 7 nV/$\sqrt{\text{hz}}$ at 1 khz.

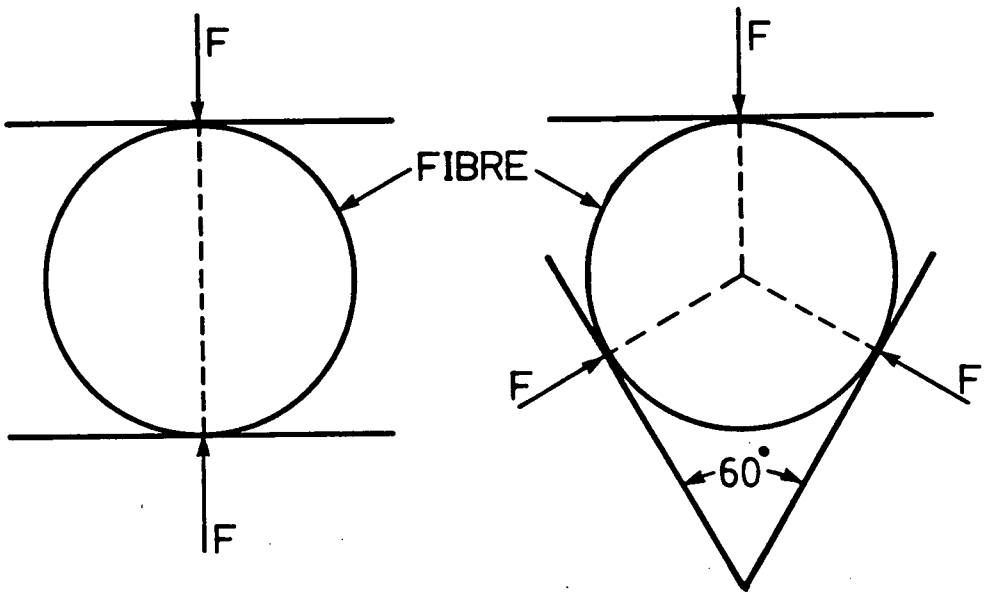

FIGURE 6–8. FIBRE MOUNTS

When a fibre is clamped between two parallel surfaces the overall stress acts in a line through the core. In a 60° groove the overall stress is symmetric about the core.

- Fibre Mountings

In order to perform the experiment the fibres must be held firmly in place without applying stresses which affect the birefringence. When a fibre is clamped between two parallel surfaces a stress is applied to the core. This stress adds vectorially with the internal stresses to give new fast and slow axis, thus, power transfer occurs between the two polarization modes. The effect of the internal stress is reduced by clamping the fibre in a 60° groove [10] as shown in figure 6–8. The groove reduces the effect of the externally applied stress by distributing the force equally about the fibre (the sum is the same in every direction).

- The Photodiode

  The photodiode gives a voltage output proportional to the light intensity it receives. Since the concern here is usually on relative intensities the voltage from the photodiode is often quoted in this work rather than the absolute power.

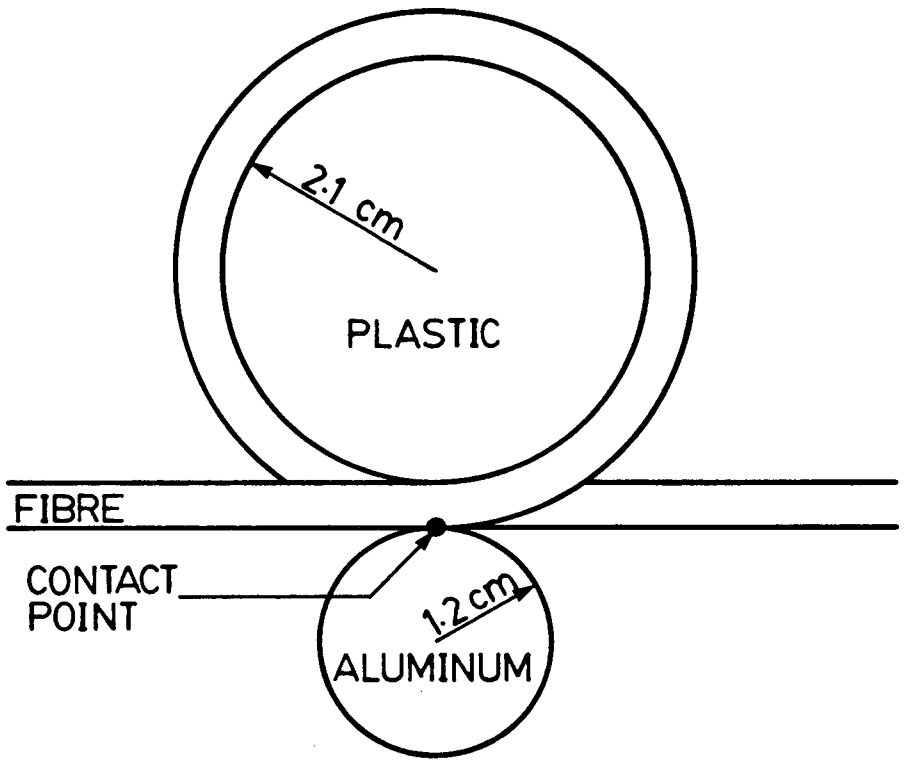

FIGURE 6–9. THE CLADDING MODE STRIPPER

The fibre is wrapped around the plastic disc and brought in contact with a metal disc where the fibre crosses itself.

- The Cladding Mode Stripper

  The cladding mode stripper is used to remove the cladding modes in a fibre. This is done since the cladding modes in a low birefringence fibre do not maintain their polarization state. The device works by allowing the cladding fields to couple into the metal at the point of contact indicated in figure 6–9. The cladding fields thereby experience high ohmic losses. *This device cannot be used on highly birefringent fibre*, to do so would cause the polarization modes to couple resulting in depolarized light (the cladding of a highly birefringent fibre also carries and maintains the polarization state).

6.3 THE EXPERIMENT

The first test fibre used was a type LB800 low birefringence fibre made by York V.S.O.P. This fibre's operating wavelength is 830 nm, and it has a very long beatlength. Since the magnetic field is applied over a region which is short compared to the beat length the Faraday rotation of the polarization state is unaffected by birefringence. Therefore, the polarization state evolution along the fibre will be that depicted in figure 6–4.

During the experiment, plane polarized light was introduced in the fibre. At the output the extinction ratio between the two polarization modes was found to be 97, with the maximum output from the photodiode being 3.5 mV. The magnetic coil was driven with a 0.4 amp current at 980 hz (not a multiple of 60 hz). The magnetic field produced was, therefore, 0.4 T, which if assumed to act over 1 mm would produce a rotation of (using equation (5–10)),

$$\delta\phi = 1.4 \times 10^{-3} \text{ Radians.}$$

Using this rotation with the analyzer at 45° to the plane of polarization yields an expected signal strength of

$$\frac{3.5\text{ mV}}{2}\left(\cos^2\left(\frac{\pi}{4}-\delta\phi\right)-\cos^2\left(\frac{\pi}{4}+\delta\phi\right)\right)=2.5\ \ \mu\text{V}.$$

The reading obtained from the experiment was 2 μV with the noise level at approximately 1 μV.

Having demonstrated the viability of the method on the low birefringence fibre, beat length measurements were attempted on a highly birefringent fibre. A 59 cm sample of York V.S.O.P. HB800 fibre was used, the same one used in the pigtail and the one used in the tapered polarizer.

With only one of the polarization eigenstates excited the extinction ratio was found to be 160 with a maximum output from the photodiode of 559 μV. The cladding mode stripper was removed and the fibre positioned to excite both polarization eigenstates equally (see appendix A). Under this condition the output polarization state is expected to be somewhere on the great circle shown in figure 6–10. This was checked with the compensator removed, leaving only the analyzing polaroid to vary the intensity falling on the photodiode. It was found that rotation of the polaroid did not affect the output of the photodiode. At first it seemed this was due to the light being close to circularly polarized. If this were true the compensator could have been used to transform the circular state into a linear one. Doing this would cause the rotating polaroid to transmit a maximum and a minimum intensity (at 90° to one another). Upon attempting this it was found that the output was unaffected — *a result only possible if the light were unpolarized.*

Knowing that the fibre was depolarizing the light, an attempt was made to measure the depolarization length by using Faraday rotation. The light was polarized along the fibre's fast axis and the magnet was placed as close to the fibre's output end as possible (11.5 cm to magnet center). The intent was to Faraday rotate

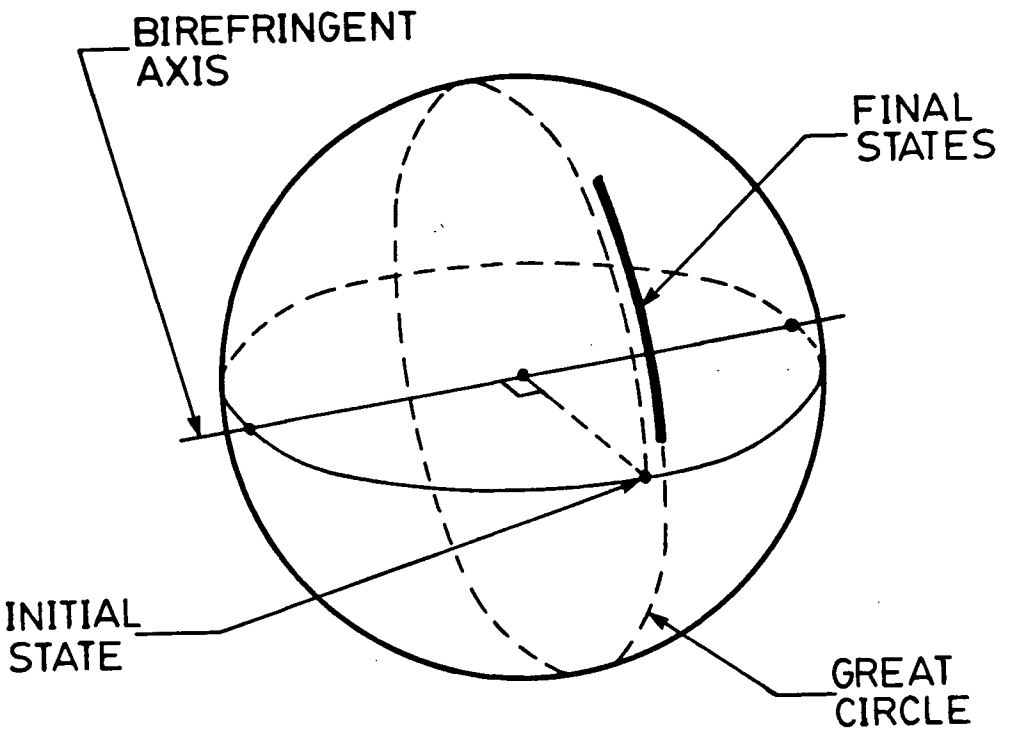

FIGURE 6–10. DEPOLARIZATION OF LIGHT

Depolarization is smearing of the polarization state over the Poincaré sphere's surface. The light is fully depolarized when the smear (energy) is equally distributed over the great circle.

the polarization state , producing an unpolarized component. No output change was detected for magnet positions out to 12.5 cm from the fibre's end (rated beat length is 2 mm) with analyzing polaroid orientations 0°, 45°, and 90° to maximum power output. This implies that the depolarization length is less than 11.5 cm.

6.4 CONCLUSIONS

Depolarization of light in highly birefringent fibres prevents beat length measurements using the equipment described above.

Depolarization is caused by the birefringence varying with wavelength [11]. Each wavelength of light has a different beat length thus, their polarization states spread out over the Poincaré sphere's surface, as shown in figure 6–10. The spreading over the surface causes the light to become depolarized, the speed with which this occurs defines a depolarization length.

According to Rashleigh [12] the depolarization length of a highly birefringent fibre is given by

$$\ell_d = \frac{1}{2\delta\mathrm{v}(dB/dk)}, \tag{6–2}$$

where $B = \beta_x - \beta_y$ is the birefringence and $2\delta\mathrm{v}$ is the bandwidth of the source defined as

$$\delta\mathrm{v} = \frac{\pi\delta\lambda}{2\ln(2)\lambda^2}, \tag{6–3}$$

where λ is the peak wavelength ($\lambda = 2\pi/k$) and $\delta\lambda$ is the bandwidth. The quantity, ℓ_d in equation (6–2) is the distance along the fibre for the extremes of the bandwidth, $\lambda \pm \delta\lambda/2$, to gain a relative phase shift of 2π (one rotation on the Poincaré sphere). For fibres with a large stress birefringence [13]

$$\frac{dB}{dk} \sim \frac{B}{k}.$$

Using the above two equations in equation (6–1) and the relation between birefringence and beat length, $B = 2\pi/L_p$, yields,

$$\ell_d = \frac{\ln(2)\lambda L_p}{\pi\delta\lambda}. \tag{6–4}$$

The specifications (figure 6–6) for the laser diode are $\lambda = 841.2$ nm, and $\delta\lambda \approx 1.4$ nm. Using this data and assuming the beat length is 2 mm equation (6–4) predicts a depolarization length of 26.5 cm. This value is longer than the length found by experiment. The experimental finding may be shorter for three reasons:

1. The signal strength may not have been strong enough to be detected (power levels were approximately 1/6 of that in the low birefringence experiment).
2. Even after 10 cm the spreading of the polarization state is probably large enough that the signal from Faraday rotation would be undetectable with the given equipment.
3. The actual beat length at 840 nm is likely less than 2 mm. The beat length measurement was performed by the manufacturer at 633 nm giving a typical beat length as 1.3 mm with 2 mm the maximum.

Referring to equation (6–4) the depolarization length may be increased by:

1. increasing the laser's wavelength,
2. decreasing the laser's bandwidth, or
3. increasing the beat length.

Since beat length measurements are to be performed on this particular fibre at the application wavelength neither the beat length nor the laser wavelength can be changed. The only alternative left is to change the bandwidth. This can be done through purchase of a single mode laser diode ($\delta\lambda \sim 0.01$ nm) [14] but the cost of doing so is prohibitive at this time†.

In conclusion, the short depolarization length prohibits beat length measurements on highly birefringent fibers using the equipment described above.

---

† Most manufacturers rate their fibres using He-Ne lasers. This may be a result of low cost for a single-mode laser with a large power output.

REFERENCES

[1] Kaminow, Ivan P. "Polarization in Optical Fibers," *IEEE Journal of Quantum Electronics*, **17**, (1981), p.15–22.

[2] Rashleigh, S.C., W.K. Burns, and R.P. Moeller. "Polarization Holding in Birefringent Single-Mode Fibers," *Optics Letters*, **1**, (1982), p.40–42.

[3] Rashleigh, S.C. "Wavelength Dependence of Birefringence in Highly Birefringent Fibers," *Optics Letters*, **7**, (1982), p.294–296.

[4] [1].

[5] Snyder, Allen W., and John D. Love. *Optical Waveguide Theory*, (New York: Chapman and Hall, 1983), p.461.

[6] Papp, A., and H. Harms. "Faraday Effect in Glass Fibers," *Journal of Magnetism and Magnetic Materials*, **2**, (1976), p.287–291.

[7] Harms, H., A. Papp, and K. Kempter. "Magnetooptical Properties of Index-Gradient Optical Fibers," *Applied Optics*, **15**, (1976), p.799–801.

[8] Hentschel, Christian. *Fiber Optics Handbook*, (Federal Republic of Germany: Hewlett Packard, 1983), p.125–126.

[9] Labun, A. "Polarization Beat Length Measurement on Highly Birefringent Optical Fibres Using Faraday Rotation," *APSC 459: University of British Columbia*(April 1985).

[10] Kumar, A., and R. Ulrich, "Birefringence of Optical Fiber Pressed into a V Groove," *Optics Letters*, **6**, (1981), p.644–646.

[11] [3].

[12] Rashleigh, Scott C. "Origins and Control of Polarization Effects in Single-Mode Fibers," *Journal of Lightwave Technology*, **1**, (1983), p.312–331.

[12] ibid.

[13] [8], p.127.

CHAPTER 7–POLARIZER THEORY

Currently, many polarization dependent optical fibre devices are being developed, such as gyroscopes, interferometers, and, as described in chapter 1, current sensors. Every application requires a polarized input and an analyzer at the output. The input light is easily polarized by inserting a polaroid between the laser and the fibre (Appendix A). The output may be analyzed by using polaroids in conjunction with bulk components, such as lenses, beam splitters, and Wollaston prisms. In focusing the light through the components some power is lost. Also, destabilization of the polarization signals may occcur when component alignments are altered by shocks and other violent events which could be encountered if the equipment is used, as intended, in the field. These problems are alleviated through the use of in-line polarizers rather than bulk components.

The description of the various in-line polarizers is presented in this chapter along with the principles of operation.

7.1 BIREFRINGENT CRYSTAL POLARIZER

One of the first in-line polarizers was a birefringent crystal polarizer proposed by Bergh et. al [1]. The polarizer is formed by bringing a birefringent crystal into contact with a section of fibre whose cladding has been polished flat and close to the core as shown in figure 7–1. The evanescent field in the cladding excites fields in the crystal. When the crystal index is above the cladding's, the evanescent field excites an outward travelling wave, causing power loss. When the crystal index is

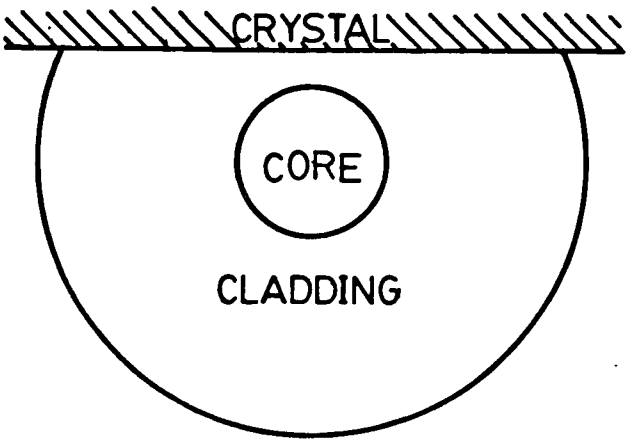

FIGURE 7–1. BIREFRINGENT CRYSTAL POLARIZER

A birefringent crystal is brought into contact with a fibre with the crystal axis oriented in such a way so as to suppress one of the polarization eigenstates.

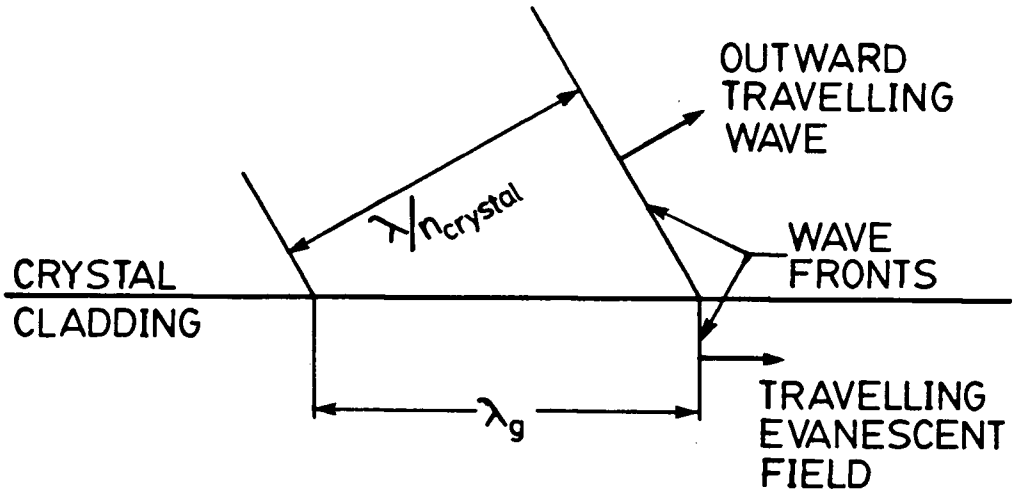

FIGURE 7–2. RAY BEHAVIOR IN A CRYSTAL POLARIZER

The cladding field excites a field in the crystal. For guide wavelengths longer than the natural wavelength in the crystal ($\lambda/n_{crystal}$) an outward travelling wave is excited.

lower than the cladding's an evanescent field is excited in the crystal so no power is lost.

Continuity of the field across the boundary guarantees that the distance between wavefronts along the boundary is the guide wavelength, λ_g of section 3.2. The speed of light cannot be exceeded hence, the maximum wavelength allowed in the crystal is $\lambda/n_{crystal}$. The guide wavelength is also limited by the speed of light. In the cladding, for guided modes, the guide wavelength is limited to values below λ/n_{cl}. When the crystal index is less than the cladding index, the wavelength in the cladding is less than the maximum wavelength allowed in the crystal, hence, the field in the crystal is evanescent. For a crystal index greater than the cladding index the guide wavelength exceeds the maximum wavelength in the crystal, hence an outward propagating wave is excited in the crystal, as shown in figure 7–2. Polarization is achieved by choosing a birefringent crystal and orienting its axes so that one polarization mode sees a crystal index greater than the cladding's and the other sees one which is less. In doing so, one polarization mode experiences high attenuation while the other continues unimpeded along the fibre thus, the light becomes polarized (extinction ratios as high as 60 dB have been reported [2]).

7.2 METALLIC COATING POLARIZER

Another polarizer which is similar to the birefringent crystal polarizer, is formed by replacing the crystal in figure 7–1 with a metallic coating [3]. This polarizer has been demonstrated to have a polarization ratio as high as 45 dB [4]. The electric field parallel to the metallic surface excites the metal's surface electrons. The electrons move in the metal, suffering ohmic losses, hence the parallel field is attenuated. The perpendicular component does not excite any electrons and, hence, is not impeded. The attenuation difference polarizes the light perpendicular to the boundary.

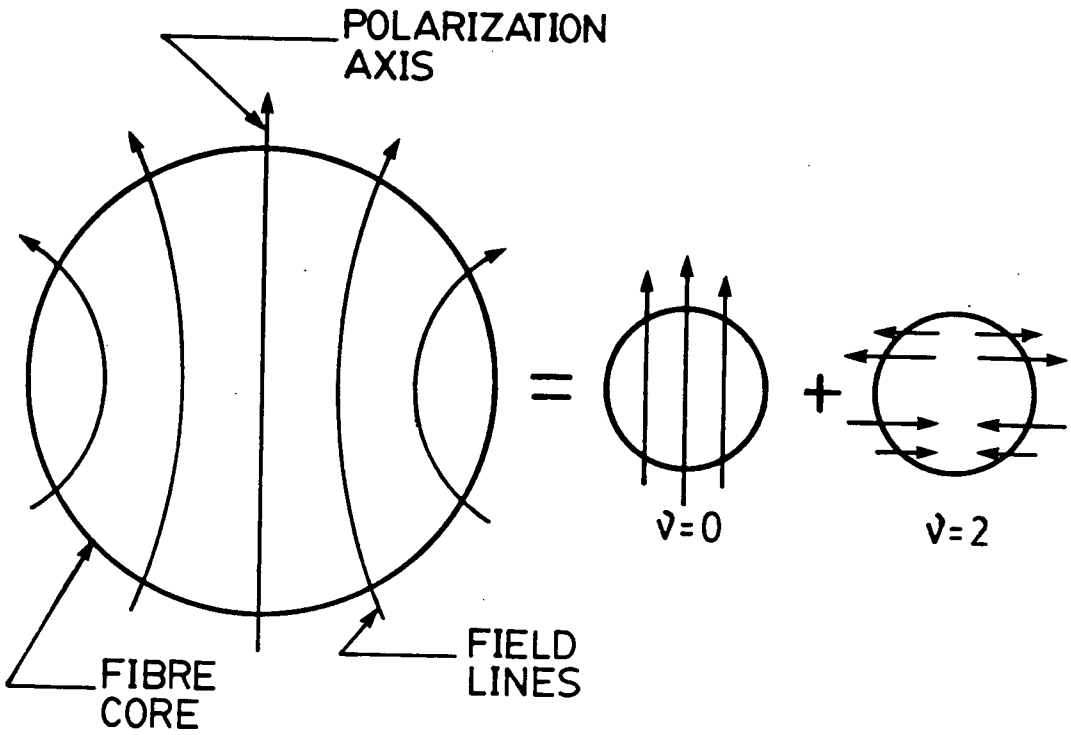

FIGURE 7–3. FIELD LINES OF A POLARIZATION MODE

The curvature of the field has been exagerated. The field is predominantly a planar mode ($\nu = 0$) with a small contribution from higher order modes (predominantly $\nu = 2$).

7.3 COIL POLARIZERS

In any single mode fibre two orthogonal polarization modes exist (section 3.4). The fields of the polarization modes are not actually planar but are bent as shown in figure 7–3. [5]. The reason for the field curvature comes from Maxwell's equation, $\nabla \cdot \vec{H} = 0$, which states that the magnetic field lines must form closed loops†. The magnetic field is symmetric about the polarization axis running through the

† This condition was not invoked in solving Maxwell's equations for the fibre. This does not appreciably affect the field solutions since most of the power is polarized along one axis. Experiments have shown that there is a 70 dB difference between the polarization mode's components [6].

centre of the fibre in the transverse plane, hence, in order for the magnetic field lines to form closed loops the field must bend towards the outer edges of the fibre. The curved field is a superposition of two different polarization modes, one is the fundamental mode ($\nu = 0$) and the other is a higher order mode ($\nu = 2$) polarized orthogonally to it. Therefore, the polarization state has both x and y components.

Both the crystal and metallic coating polarizers attenuate the light along one axis hence, both of the fibre's polarization modes are attenuated. Since the modes have field components along both axes it is impossible to fully suppress one polarization mode without also attenuating the other. This limits the effectiveness of the birefringent crystal and the metallic coating polarizers.

Increased effectiveness is accomplished through increasing the leaky mode loss. A mode becomes leaky when power in the component perpendicular to the axis of polarization is allowed to escape from the fibre.

Birefringent fibres already exhibit this property, one of the polarization modes leaks more than the other [7]. In a birefringent fibre the refractive index difference between the core and the cladding for each polarization axis is approximately equivalent [8]. Assuming that the y polarized mode is leaky and that the x polarized mode is the more strongly guided mode, the core index for the x polarization is higher than that for y as indicated in figure 7–4. The difference between the core and cladding indices keeps each polarization mode guided along the fibre but, the small difference between y's core index and x's cladding index causes the y polarization to lose power.

The y polarization mode has a small x component which travels with the y component. Therefore, the effective core index the x component experiences is n_{co}^{y} and, since its associated evanescent field is polarized in the x direction, the cladding index is n_{cl}^{x}. The difference between n_{co}^{y} and n_{cl}^{x} keeps this component of the field guided. The difference between the two indices is low, hence the V value

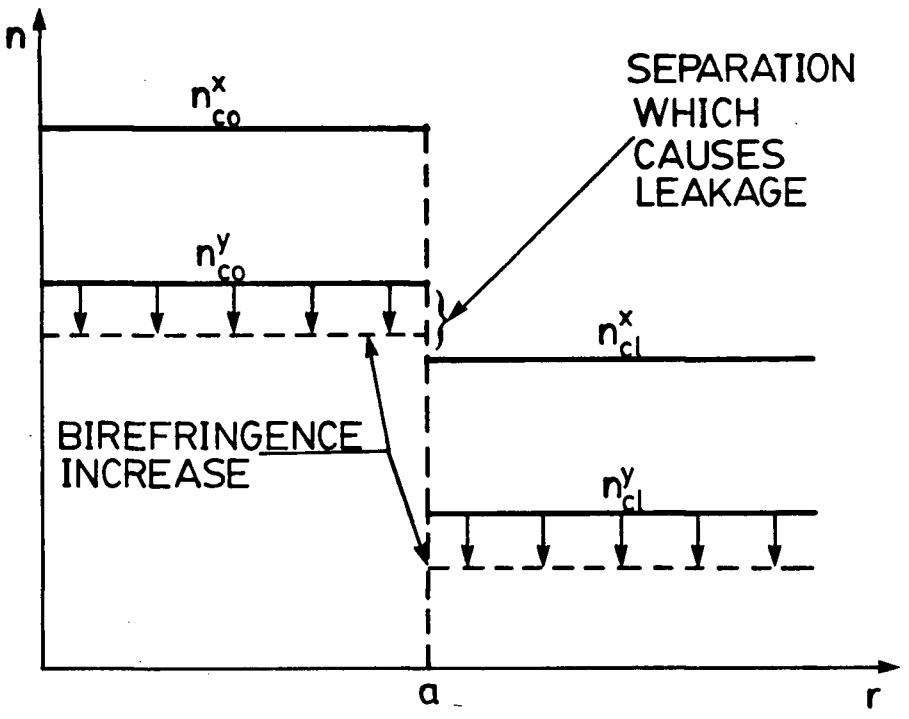

FIGURE 7–4. INDEX PROFILE OF A BIREFRINGENT FIBRE

The y polarized mode is assumed to be leaky and the x polarized mode is assumed to be the more strongly guided mode. The n's are the refractive indices experienced by the indicated polarization. An increase in birefringence shifts n^y_{co} and n^y_{cl} downward an equal amount.

for the x component of the y polarization is low. The low V value means that the x component propagates well below cutoff (it is a high order mode in a single mode fibre). Therefore, this component of the mode experiences high attenuation causing the polarization mode to lose power [9].

This effect can be increased by introducing an extra birefringence in the fibre to decrease the difference between n^y_{co} and n^x_{cl} (make V smaller) as indicated in figure 7–4. The birefringence can be raised through bending the fibre [10]. Bending or coiling the fibre exerts a tensile stress on the core parallel to the radius of curvature of the bend. This stress adds vectorially with the internal stress on the core to

change the birefringence (see section 2.2). The birefringence is raised when the radius of curvature coincides with the fibre's fast axis and is decreased when the radius of curvature coincides with the fibre's slow axis [11]. Raising the birefringence causes the weakly guided mode to become more leaky making coiled birefringent fibre polarizers possible. The attenuation and the extinction ratio are adjusted through choice of wavelength and bending radius (extinction ratios as high as 62 dB have been reported [12]).

7.4 TAPERED POLARIZERS

For the coiled polarizer it has been found that both the extinction ratio and the attenuation increase with wavelength. This indicates that the polarizing ability of the fibre increases with decreasing fibre parameter, V. This was first noted by Villarruel et. al. [13] who suggested that a polarizer could be made by locally reducing the fibre parameter through a decrease in core size (form a biconical taper). Reducing the fibre parameter causes more of the power to travel in the cladding (section 3.4) until the light is no longer guided by the core but by the cladding. The point at which this occurs is considered to be where the fibre parameter is unity [14] (from figure 3–9 only 22% of the power is in the core when $V = 1$). As the light travels over the section where $V \leq 1$ the fundamental mode couples to higher order modes. Birefringent fibres are single mode type but, higher order modes can propagate without loss over the tapered section because of the larger diameter of the guiding structure (it is the tapered cladding diameter) and because of the increased difference in refractive index between the cladding index and the external medium. Essentially the structure is a multimode fibre with the entire fibre as the core and the external medium as the cladding. As the fibre returns to its original size the light becomes guided by the core again hence, the power that is still in the fundamental mode is recaptured by the fibre and propagates along it. Other modes

are not captured by the fibre since they would propagate in cutoff thus, the power they carry is lost.

The tapered polarizer relies on the coupling to be different for each polarization.

The coupling coefficient between modes j and l has been found to be (equation (4–42))

$$C_{jl} = \frac{k}{4(\beta_j - \beta_l)} \sqrt{\frac{\epsilon_0}{\mu_0}} \int_{A_\infty} \hat{e}_j^* \cdot \hat{e}_l \frac{\partial n^2}{\partial z} dA.$$

Snyder [15] has shown that the coupling in a gradual taper is predominantly with the mode described by the second solution of the eigenvalue equation (3–39) with $\nu = 0$. The coupling strength is very sensitive to small differences between the propagation constants of the two coupling modes $(\beta_j - \beta_l)$. In a highly birefringent fibre the difference in propagation constants is markedly different for the two polarization modes. Recall that the cutoffs are determined by V which is approximately the same for each polarization since the difference between the core and cladding indices is the same for each. However, the propagation constants are proportional to refractive index which is different along each axis in a birefringent fibre. Therefore, one polarization mode propagates much closer to cutoff than the other. The polarization mode which is closer to cut-off (fast mode) transfers far more power into the higher order modes than the other mode does because the propagation constants of the higher order modes are just above the fundamental mode's cutoff. This difference in power transfer means that the taper recaptures more light from one mode than the other, yielding polarized light.

Further increases in the taper's polarizing ability have been observed by matching the external refractive index to the cladding index [16] [17] [18]. The polarization increases because the structure is closer to being a step index fibre with an infinite cladding. In this case, when the mode is no longer guided by the core it radiates away due to the lack of a guiding structure (couples to radiation modes).

Again, this polarizes the light in a birefringent fibre due to one of the modes being closer to cut-off than the other.

It is, therefore, feasible to polarize light in a tapered section of a highly birefringent fibre with an external medium which is index matched to the cladding. The building and testing of such tapered in line polarizers is the main objective of this thesis.

7.5 MODE COUPLING IN A TAPER

The following is an examination of the coupling that occurs in a taper.

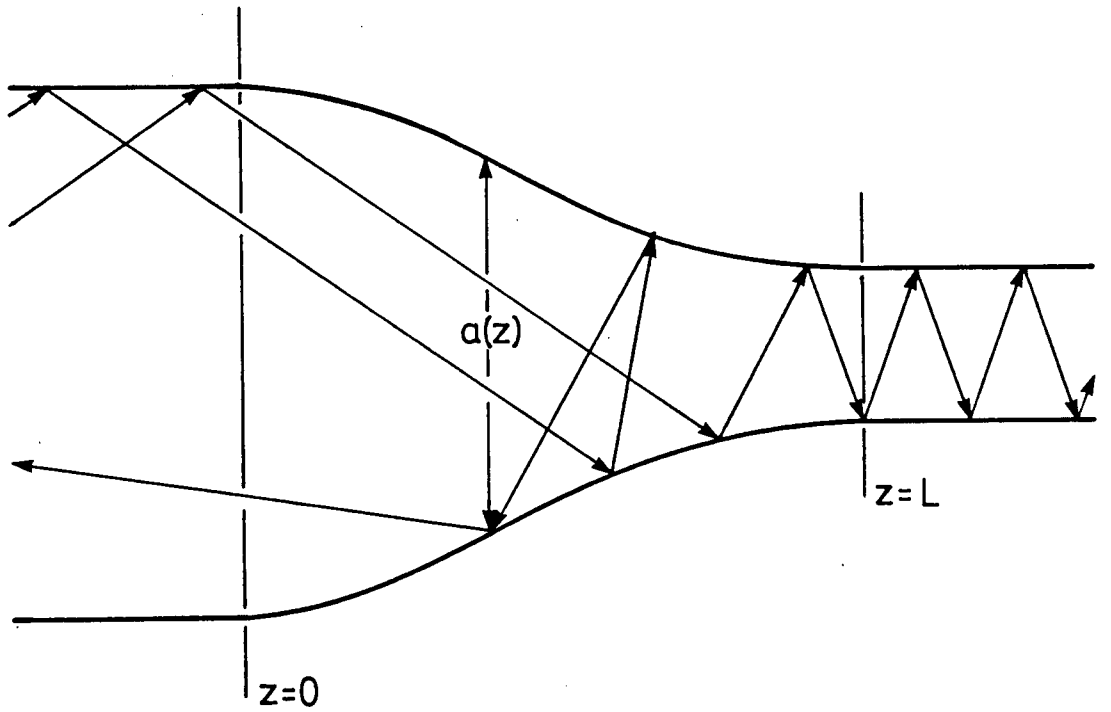

FIGURE 7–5. RAY PATHS IN A TAPER

The angle of the interface redirects the rays in the taper.

For a qualitative explanation of the coupling mechanism consider a ray reflecting off the core–cladding interface, as shown in figure 7–5. In the region of change the reflected ray's angle with the fibre axis will be different from the incident ray's angle. Since each mode travels at a different angle this indicates mode coupling has occurred.

This effect can be quantified by considering a step index fibre with slowly varying guide geometry. The expression for the refractive index in such a fibre is [19]

$$n^2(r,z) = n_{co}^2[1 - 2\Delta\mathcal{H}(r - a(z))], \tag{7–1}$$

where $a(z)$is the core size at point z, and $\mathcal{H}$ is the unit step function defined as

$$\begin{aligned} \mathcal{H}(x) &= 1 \quad \text{for} \quad x > 0 \\ &= 0 \quad \text{for} \quad x < 0. \end{aligned}$$

Substituting the refractive index profile into the coupling coefficient equation (equation (4–42)) gives the coupling coefficient for a step index fibre,

$$C_{jl} = \frac{kn_{co}^2\Delta}{4(\beta_j - \beta_l)}\sqrt{\frac{\epsilon_0}{\mu_0}}\frac{da^2}{dz}\int_0^{2\pi}(\hat{e}_j \cdot \hat{e}_l)_{r=a(z)}d\phi, \tag{7–2}$$

where the $\hat{e}$'s are the normalized local mode fields given by equation (4–20) and j and l denote different fields in the same region of the fibre†. The dependence on the derivative of a^2 strongly influences the coupling strength. The strong coupling is attributed to the steeper slope of the interface causing greater differences between incident and reflected angles.

---

† This does not denote the mode on each side of a junction, but the amount of interchange that occurs at point z (the result is undefined for j=l).

Since the fibre modes couple with radiation modes as well as bound modes power losses occur. The loss calculation requires the amplitude and phase coefficients, b_j. These coefficients are found by using a perturbation analysis on the coupling equations. Assuming the fibre geometry varies slowly with z the coupling is weak, hence the right hand side of equation (4–39) is assumed small. This yields the first order solution for b_l,

$$b_l(z) = b_l(0)\exp\left(i\int_0^z \beta_l(z)dz\right). \tag{7–3}$$

Taking this solution and substituting it back into the right hand side of the coupling equation gives the second order solution [20] for coupling to another mode,

$$b_{\pm j}(z) = \pm b_l(0)\left[\exp\left(\pm i\int_0^z \beta_j(z)dz\right)\right]\int_0^z C_{\pm jl}(z)\exp(i\delta\beta z)dz, \tag{7–4}$$

where $\delta\beta$ is the average difference in propagation constants between the coupled modes,

$$\delta\beta = \frac{1}{z}\int_0^z \Big(\beta_l(z) \mp \beta_j(z)\Big)dz. \tag{7–5}$$

The propagation constant for a radiation mode is a function of the cladding parameter, Q, and is independent of position along the fibre, z. Therefore, for radiation mode coupling the above equations are of the form

$$b_j(Q) = \left(b_l(0)\exp(i\beta_j(Q)z)\int_0^z C_{jl}(Q,z)\exp(i\delta\beta z)dz\right)\Bigg|_{z=L}, \tag{7–6}$$

and

$$\delta\beta = \frac{1}{z}\int_0^z \beta_l(z)dz - \beta(Q) \approx \beta_l(z) - \beta(Q). \tag{7–7}$$

The above approximation is valid since β_j is approximately constant (the difference between the lower bound, kn_{cl}, and its upper bound, kn_{co}, is very small). Integrating equation (7–6) twice by parts assuming $\delta\beta$ approximately constant in z yields

$$\frac{b_j(Q)}{b_l(0)} = \frac{iC_{jl}(0)}{\delta\beta(0)} - \frac{iC_{jl}(L)\exp(i\delta\beta L)}{\delta\beta(L)} + \frac{\exp(i\delta\beta L)}{\delta\beta(L)}\frac{d}{dz}\left(\frac{C_{jl}}{\delta\beta}\right)\Big|_L - \frac{1}{\delta\beta(0)}\frac{d}{dz}\left(\frac{C_{jl}}{\delta\beta}\right)\Big|_0 - \int_0^L \exp(i\delta\beta z)\frac{d}{dz}\left(\frac{1}{\delta\beta}\frac{d}{dz}\left(\frac{C_{jl}}{\delta\beta}\right)\right)dz. \tag{7–8}$$

At this point it is expedient to pursue this analysis on a tapered fibre, as shown in figure 7–5. Assuming the core radius is constant at both the input and the output of the tapered section gives $C_{jl}(0) = C_{jl}(L) = 0$†. Therefore the first two terms in the above equation are negligible. Taking the taper length, L, far larger than the beat length, $2\pi/\delta\beta$, (i.e. $L\delta\beta >> 1$) (assumes that the interaction length is not short) further simplifies the expression for $b_j(Q)$. Using (7–5) one finds the derivative of $1/\delta\beta$ is of order $1/L\delta\beta$ since C_{jl} varies slowly compared to $1/\delta\beta$. Therefore, the integral is of order $|1/L\delta\beta|^2$ (the exponential part varies far faster than the derivative part) and the remaining two terms are of order $|1/L\delta\beta|$. Since $L\delta\beta >> 1$ the integral will be small compared to the remaining two terms. Finally, if the radius change is large the modes at the input will be more strongly guided than those at the output. Therefore, the propagation constant at the output will be much closer to cutoff than at the input, thus

$$|\delta\beta(0)| >> |\delta\beta(L)|.$$

---

† This can be verified using equation (7–2) since $(da^2/dz) = 0$. It is also expected since no mode coupling takes place in an ideal, straight fibre.

The value of b_j is then approximately

$$b_j = \frac{\exp(i\delta\beta L)}{\delta\beta(L)} \frac{d}{dz}\left(\frac{C_{jl}}{\delta\beta}\right)\Big|_L.$$

Substituting this into the equation for power in a radiation mode, (4–20), and using (7–5) yields [21]

$$P_j = \int_0^{akn_{cl}} \left|\left(\frac{L}{[\delta\beta(L)]^2}\left(\frac{dC_{jl}}{dz}\right)\Big|_L\right)\right|^2 dQ. \qquad (7-9)$$

Noting that the coupling coefficient depends on the taper's slope it is easy to see that the radiated power is affected by the curvature of the interface. The power radiated is also sensitive to the difference in propagation constants between the guided and the radiation mode, $\delta\beta$. In a birefringent fibre one polarization mode lies closer to cutoff than the other hence, it couples to radiation modes more effectively. This causes one mode to lose more power than the other , yielding polarized light.

REFERENCES

[1] Bergh, R.A., H.C. Lefevre, and H.J. Shaw. "Single-Mode Fiber-Optic Polarizer," *Optics Letters*, **5**, (1980), p.479–481.

[2] ibid.

[3] Eickhoff, W. "In-Line Fibre-Optic Polariser," *Electronics Letters*, **16**, (1980), p.762–764.

[4] Gruchmann, D., K. Petermann, L. Staudigel, and E. Weidel. "Fibre-Optic Polarizers with High Extinction Ratio," *Proceedings of the Ninth European Conference on Optical Communications*, Geneva, Switzerland, (October 23–26, 1983), p.305–308.

[5] Varnham, M.P., D.N. Payne, and J.D. Love. "Fundamental Limits to the Transmission of Linearly Polarised Light by Birefringent Optical Fibres," *Electronics Letters*, **20**, (1984), p.55–56.

[6] ibid.

[7] Varnham, M.P., D.N. Payne, R.D. Birch, and E.J. Tarbox. "Single-Polarization Operation of Highly Birefringent Bow-Tie Optical Fibres," *Electronics Letters*, **19**, (1983), p.246–247.

[8] Birch, R.D., M.P. Varnham, D.N. Payne, and K. Okamoto. "Fabrication of a Stress-Guiding Optical Fibre," *Electronics Letters*, **19**, (1983), p.866–867.

[9] Snyder, A.W., and F. Rühl. "New Single-Mode Single-Polarisation Optical Fibre," *Electronics Letters*, **19**, (1983), p.185–186.

[10] Ulrich, R., S.C. Rashleigh, and W. Eickhoff. "Bending-Induced Birefringence In Single-Mode Fibres," *Optics Letters*, **5**, (1980), p.273–275.

[11] Varnham, M.P., D.N. Payne, R.D. Birch, and E.J. Tarbox. "Bend Behavior of Polarising Optical Fibres," *Electronics Letters*, **19**, (1983), p.679–680.

[12] Varnham, M.P., D.N. Payne, A.J. Barlow, and E.J. Tarbox. "Coiled-Birefringent-Fiber Polarizers," *Optics Letters*, **9**, (1984), p.306–307.

[13] Villarruel, Carl A., M. Abebe, William K. Burns, and R.P. Moeller. "In-Line Birefringent Fiber Polarizer," *Proceedings of the Optical Fibre Conference*, New Orleans, (January 23–25, 1984), p.14.

[14] Cassidy, David T., Derwyn C. Johnson, and Kenneth O. Hill. "Wavelength-Dependent Transmission of Monomode Optical Fiber Tapers," *Applied Optics*, **24**, (1985), p.945–950.

[15] Snyder, Allen W., "Coupling of Modes on a Tapered Dielectric Cylinder," *IEEE Transactions on Microwave Theory and Techniques*, **18**, (1970), p.383–392.

[16] Lacroix, Suzanne, Richard J. Black, Christian Veilleux, and Jean Lapierre. "Tapered Single-Mode Fibers: External Refractive-Index Dependence," *Applied Optics*, **25**, (1986), p.2468–2469.

[17] de Fornel, F., M.P. Varnham, and D.N. Payne. "Finite Cladding Effects in Highly Birefringent Fibre Taper- Polarisers," *Electronics Letters*, **20**, (1984), p.398–399.

[18] Varnham, M.P., F. de Fornel, D.N. Payne, C.M. Ragdale, A.J. Barlow, and E.J. Tarbox. "Comparison Between Coil and Taper Fibre-Polisers," *Proceedings of the Society of Photo-Optical Instrumentation Engineers*, **514**, (1984), p.329–332.

[19] Snyder, Allen W., and John D. Love. *Optical Waveguide Theory*, (New York: Chapman and Hall, 1983), p.557.

[20] ibid., p.556.

[21] ibid., p.563.

CHAPTER 8–TAPER FABRICATION

This thesis was initiated in order to produce tapered polarizers for use in optical fibre current transducers being developed by B.C. Hydro. The theoretical background has been covered in the preceding sections. The theory was presented to give an understanding of light propagation in optical fibres. With this understanding, the mechanisms by which fibre devices polarize light were evaluated. The method best suited to the current sensor application was chosen to be the in-line tapered polarizer.

Tapered polarizers offer the possibility of high extinction ratios, ease of manufacture, and compact packaging. Tapered highly birefringent fibres have been demonstrated to be very efficient polarizers [1], and their dependence on the external refractive index has been noted [2]. To date, most researchers have enhanced the taper's polarizing ability through immersion in an index matching oil [3] [4].

Instead of oil another possible method of obtaining an index matched external medium is by collapsing a fused quartz tube onto the tapered section. The quartz tube has the same index of refraction as the cladding and its thermal expansion is similar to the fibre's since both the tube and the cladding are fused quartz. Similar work has been done by Jedrzejewski et. al. [5] for making a tapered beam expander on a singlemode fibre. The tapered beam expander was clad in Vycor†. Vycor

† Vycor is a high silicate glass made by Corning.

has a lower index of refraction than silica hence, it behaves like a cladding on the taper, keeping the light guided. The construction of the tapered beam expander is similar to that of the tapered polarizer. The beam expander is a tapered multimode fibre clad in vycor and the polarizer is a tapered birefringent fibre clad in quartz. What makes the polarizer different from the beam expander is the emphasis on polarization state rather than transmittance. The exterior medium of a tapered polarizer is applied not to keep the modes guided, as in the tapered beam expander, but to make it easier for one polarization mode to escape, thus producing polarized light.

The effects of cladding a tapered polarizer in quartz tubes has not been investigated until now. The following is an account of the work performed in an attempt to apply quartz tubing to tapered polarizers in order to enhance their performance.

8.1 THE TEST BENCH

Tapered fibre polarizers were made by heating and stretching pieces of highly birefringent fibre to form biconical tapers. This was performed on a vertical test bench in order to minimize bending of the tapered section. If this had been performed horizontally the weight of the taper itself would have caused the structure to sag, introducing a bend, which would have affected performance. The test bench and equipment are shown in figure 8–1. Most of the equipment is the same as that used in the beat length experiment. Descriptions of the equipment are found in section 6.2. Some added information and notes are given below.

- Input Polaroid

  Even though the polarizing action of the taper on unpolarized light could be detected at the output an input polaroid is still required. The input polaroid is necessary because the laser diode emits weakly polarized light. By introducing the polaroid the results are independent of the polarization state emitted by the diode.

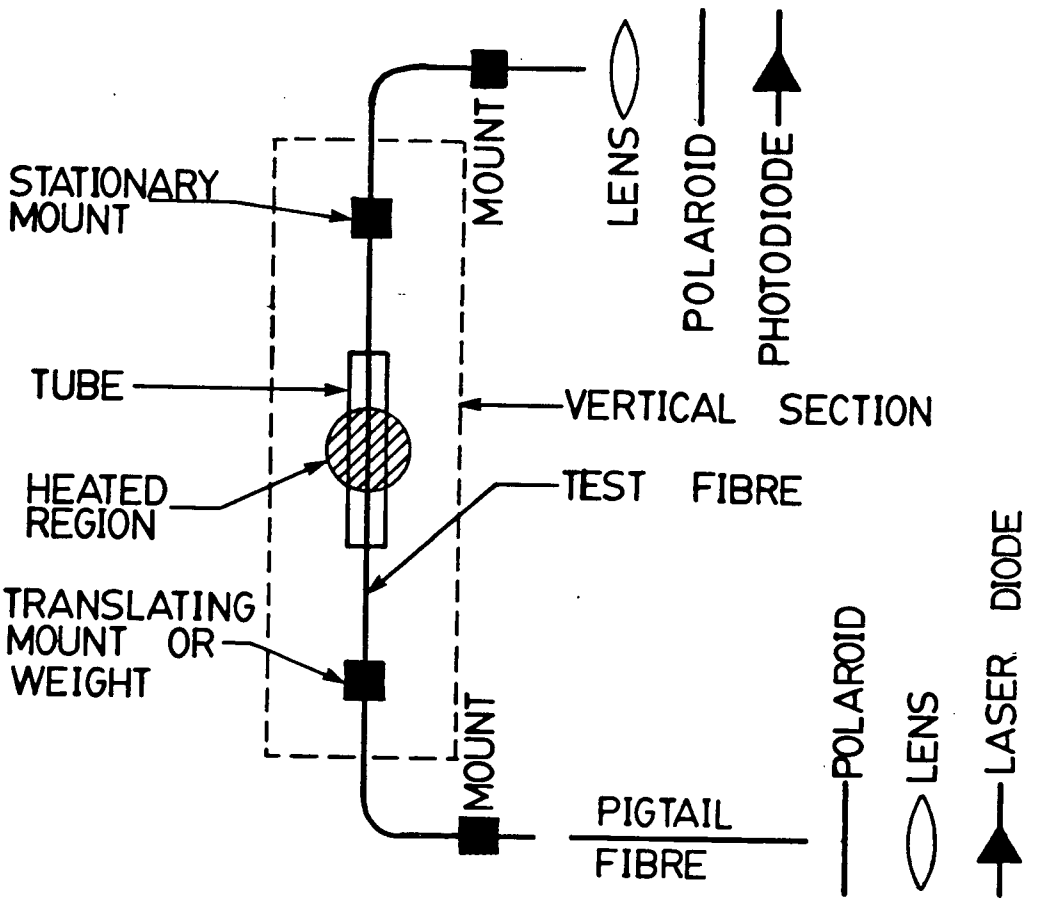

FIGURE 8–1. THE TEST BENCH

- Test Fibres

  For the tapered polarizer the fibre used is the same as that used in the beat length experiments (York V.S.O.P., highly birefringent fibre with a 2mm beat-length as described in table VI-I). As already mentioned this fibre has a short depolarization length. This does not affect the experiment since the taper itself is a polarizer. Light is introduced into the fibre in a way which excites both polarization eigenstates equally (appendix A). The light quickly becomes depolarized in the fibre (section 6.4). The effect of the taper on the depolarized

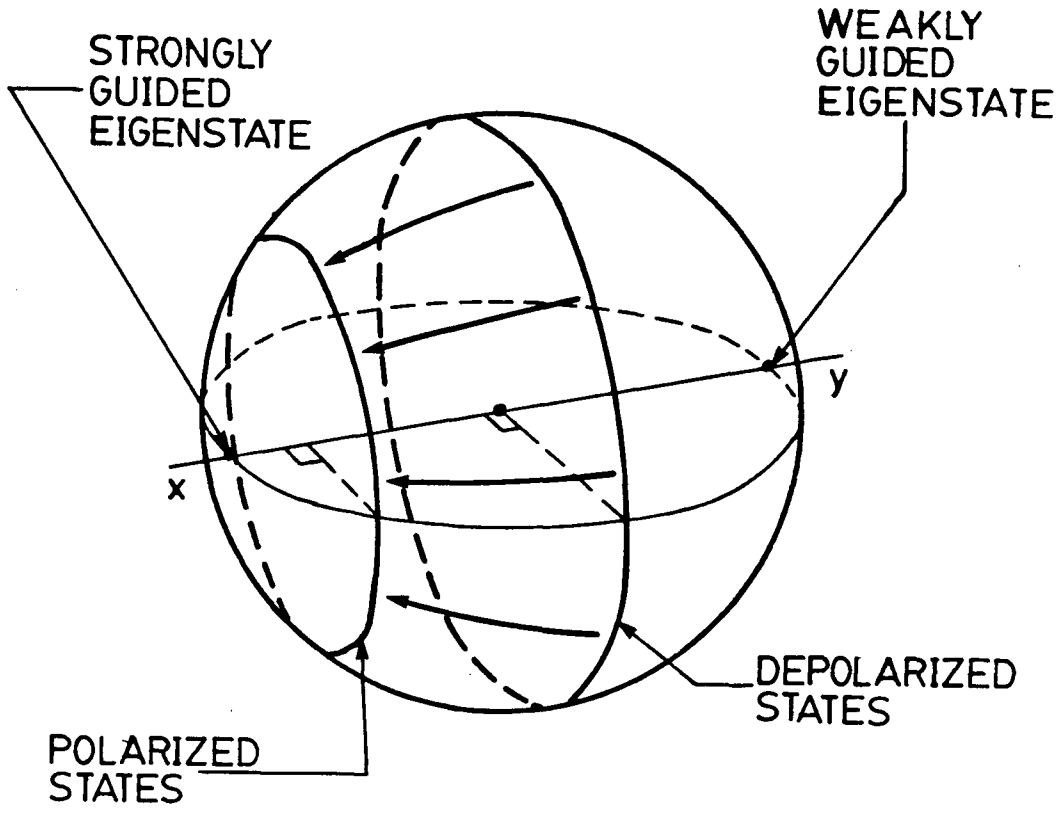

FIGURE 8–2. POLARIZATION OF DEPOLARIZED LIGHT

The depolarized light in the fibre occupies a ring on the Poincaré sphere which passes through the poles and the linear polarization states at 45° to the eigenstates. The polarizing taper moves this ring towards the strongly guided eigenstate.

light is a shift in the ring of states the light occupies on the Poincaré sphere towards the fibre's strongly guided eigenstate (x polarized mode) as shown in figure 8–2. The birefringence then rotates these states about the axis through the eigenstates thus, the new ring of states is maintained along the fibre. At the output the distance on the Poincaré sphere from the ring to the x eigenstate is shorter than to the y eigenstate hence, a rotating polaroid would

transmit more power when aligned with the x eigenstate than when aligned with y. This means that the taper's polarizing ability can be evaluated.

The test fibre is not always a piece of highly birefringent fibre. The test fibre is often a piece of multimode fibre. The melting characteristics of multimode fibre is not the same as for birefringent fibre however, a multimode fibre is a good test piece for technique development and practice. The larger core diameter allows this fibre to transmit more light and the softening point is more closely matched to silica than the birefringent fibre and there are no internal stresses in the fibre so it is not as easily shattered. These properties make the multimode fibre easier to work with but, more importantly, multimode fibre is far cheaper than birefringent fibre (a few dollars a metre versus $15.00 U.S. for birefringent fibre).

TABLE VIII–I PROPERTIES OF FUSED QUARTZ

Refractive Index	1.4585
Softening Point (C)	1600
Annealing Point (C)	1084
Thermal Expansion (10^{-7}/C)	5.5

- Quartz Tubes

The quartz tube is collapsed onto the fibre in order to index match the external medium to the fibre's cladding, which is also fused quartz. The properties of fused quartz are listed in table VIII–I . The capillary tubes used have a 0.3 mm inside diameter and a 0.4 mm outside diameter. They were obtained from Vitro Dynamics Inc., Rockaway, New Jersey.

- Heat Sources

  In order to taper the fibre an intense heat source is required. Three† heat sources were considered:

  1. An induction furnace:

     An induction furnace was used by Jedrzejewski et. al. in manufacturing tapered beam expanders [6]. This device offers a very symmetric heat distribution due to the fibre being heated inside a graphite block. The induction furnace was not used in this work since it was felt that while the graphite block cools the fibre taper would elongate further and the birefringence would change making it difficult to maintain and monitor the polarization.

  2. An electric arc:

     Electric arcs are often used for fusion splicing two fibres together [7] [8]. Since its use has been proven and a unit was available this method was tried as discussed in the next section.

  3. Torches:

     Various gas torches are available. The type most commonly used in fibre manufacture is oxy-hydrogen, which is the cleanest burning and produces very high tempertures. Owing to the author's inability to obtain such a torch the use of butane-air and oxy-propane torches was pursued the results of which are presented in later sections.

---

† A fourth method may be to use radiative heating from an arc lamp but this was not considered until after the experiments had been performed.

- Stretching the Fibre

  In order to form the taper the fibre must be stretched. Since maintaining the alignments at both the input and the output are crucial extra fibre mounts must be introduced to isolate the region to be stretched. One of the mounts holds the fibre steady while the other translates to stretch the fibre. The translating stage may be replaced by a suspended weight. The weight is of the order of only a few grams otherwise the fibre will stretch too rapidly and break (in fibre manufacture the tension on the fibre is equivalent to a fraction of a gram [9]).

8.2 TAPERING WITH AN ELECTRIC ARC

Initial attempts at tapering a fibre were done using an electric arc. The electric arc was seen as a viable heat source for this work since it has proven itself of use in arc welding fibres.

Arc heating a fibre begins by placing the fibre between two electrodes. An alternating voltage is applied to the electrodes to form an arc. The arc is localized over only a couple millimeters of fibre hence, heat is applied over a small region. The amount of heat applied is adjusted by varying the applied voltage (for the equipment used, the voltage could be varied from 0 to 100 V with breakdown occurring above 45 V when the electrodes were 0.5 mm apart). A taper is formed by pulling the fibre downward hence, the top end of the taper remains fixed in the arc while the bottom end travels downward out of the arc resulting in the shape shown in figure 8–3. The expected shape is an abrupt taper at the top and a more gradual taper at the bottom.

The first step was to adjust the arc so that the fibre would soften just enough to be stretched†. This was done by suspending bare pieces of multimode fibre in

---

† The 'softening point' of a glass describes the temperture at which its viscosity

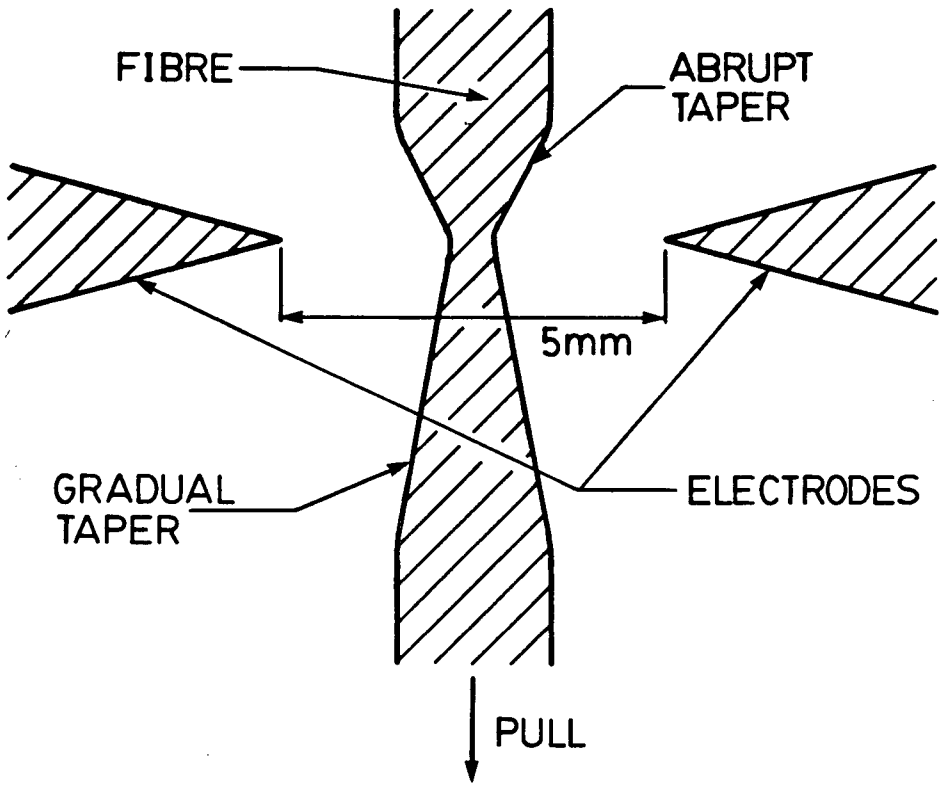

FIGURE 8–3. ELECTRIC ARC HEATING OF A FIBRE

The figure is not to scale. The difference between the abrupt and gradual tapers has been exaggerated.

the arc with a small clip on the end for weight (approximately 5 grams). Power was applied to the electrodes to observe the tapering process. This was repeated at many different voltages, with similar results for each trial — the fibre tapered rapidly and broke.

---

is $10^{6.5}$ to 10^{7} Pa·s [10]. It is a vague term since what distinguishes a glass from any other material is the lack of a defined melting point (as a glass is heated it becomes a less viscous liquid [11]).

On account of the difficulty in slowing this down enough to control the tapering process the suspended weight was abandoned and a translating mount was used in its place. The viability of this method was checked by stretching the fibre in steps. The arc voltage was set to 60 V and the fibre was stretched a small amount. This was repeated several times , turning the arc on while stretching the fibre and off when stretching stopped. Surprisingly, the resulting taper looked reasonably symmetric. The fibre did not have a stepped structure despite the uneven pulling rate and the arc being turned on and off. The taper's smoothness can be attributed to the high surface tension of its constituent glass.

By necessity, this method was used throughout the rest of the work for the following reason:

A property of fused quartz is that when heated it glows brilliantly. When forming a taper, heat is applied to the fibre causing it to glow (it is mostly fused quartz). Some of the emitted light is launched back into the fibre towards the laser. This light couples into the laser, increasing its optical output. This not only destabilizes the optical signals but it also shortens the laser's lifespan. Therefore, it is necessary to halt the test in order to record the polarization properties of the taper. Since visual inspection showed that the taper profile was unaffected by irregularities in pulling rate and heat application, halting and restarting the experiment is not expected to adversly affect fibre properties.

The above method was then used to reduce the transmission of a multimode fibre by 50%. A fibre was mounted on the test bench with the section to be tapered stripped of its cladding (approximately 2 cm above and below). The initial reading from the lock-in frequency amplifier was 1.245 mV which was reduced to 0.695 mV by tapering the fibre with a 60 V arc. While heating the fibre the taper vibrated in the arc, lowering the transmitted level to 0.4 mV.

The ability to reduce the transmission by a specified amount by tapering the fibre looked promising but the violence with which the fibre was thrust about by

the arc was a concern. The vibration lowered the transmission level and there was danger of fatiguing the taper.

The solution to this problem lay in the task at hand. The glass tube that was to be collapsed around the taper would also protect it. The hope was that when heated with the arc the glass tube would collapse onto the fibre. The collapsed tube would shield the fibre as well as give added strength to the structure so that vibrations would be reduced while tapering.

There are three ways to encase a fibre inside a tube as shown in figure 8–4. The first method is to place a tube over the stripped section of fibre and glue both ends in place using Norland Optical Adhesive #81 (an ultraviolet curing cement which is hard and clear). Gluing both ends guarantees that both the fibre and the tube will be stretched equally. Unfortunatly, it is difficult to heat the structure enough to form the taper. The problem experienced is due to debris on the inside of the tube (bits of glass, pieces of the fibre's plastic coating, and some glue). The arc heats both the tube and the debris on the inside wall. Some of the debris burns while the rest vapourizes and travels away from the heated region. As the vapour enters cooler regions of the tube it condenses on the inside wall. Since the tube is sealed the material never escapes so the process repeats itself carrying much of the heat away from the section to be tapered. (In trials a 95 V arc was applied for 5 minutes. The only effect being the formation of a black residue on the inner wall).

A modification of this method showed more promise. Glue was applied at the bottom of the tube and the top was left open so that the debris could escape. The arc was turned on and left on until the tube stopped glowing red and became clear in the region to be tapered (the debris was burned away). The top of the fibre was then glued, the arc was turned back on and the tapering process began. Though it is easier to form a taper using this process residual debris left in the tube cools the taper.

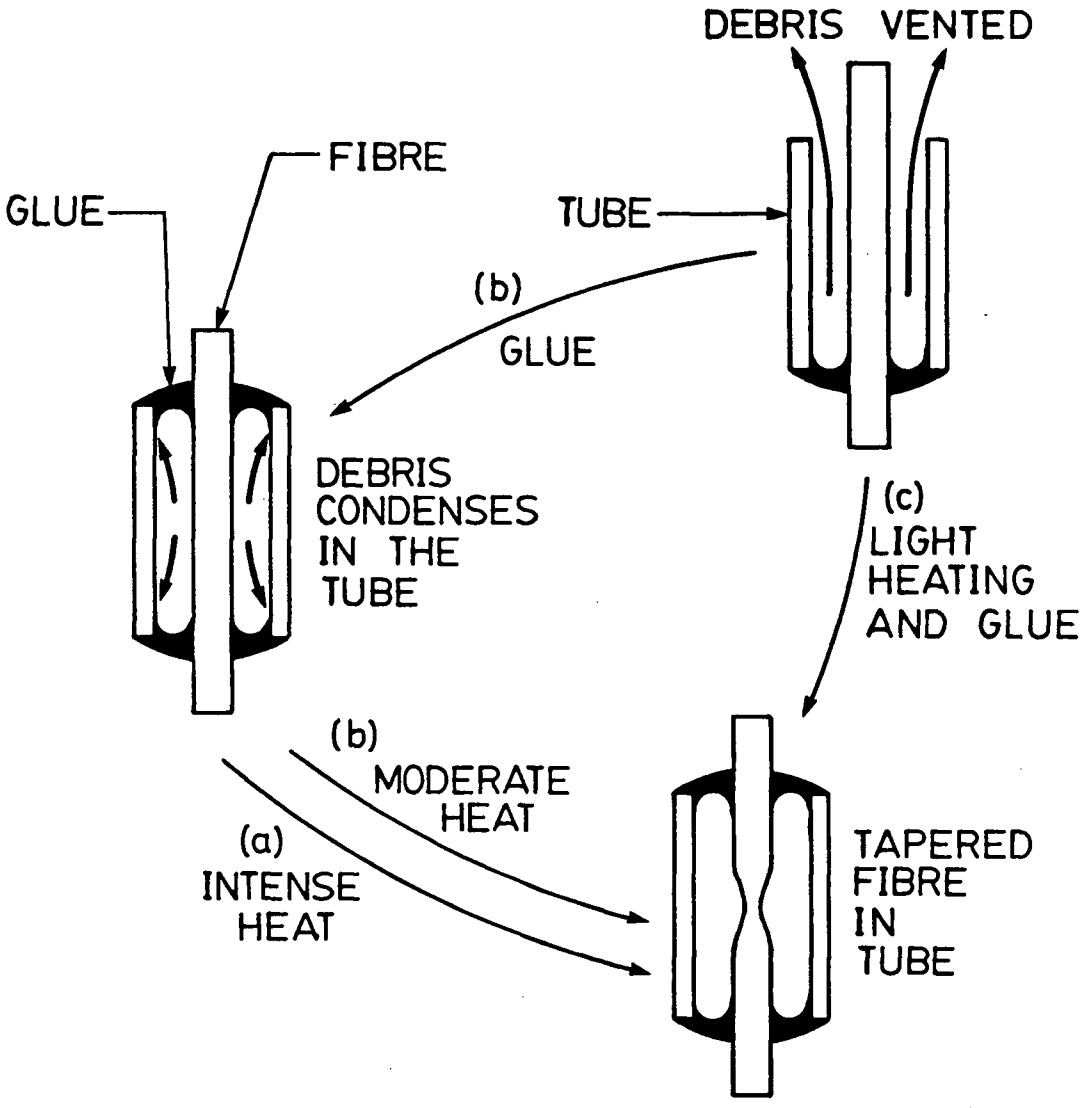

FIGURE 8–4. FIBRE-TUBE APPLICATION

One method is to glue both ends, then taper the fibre (a). Another is to glue one end of the tube then heat to clear the debris, then glue the other end and form the taper (b). The final method is to glue one end of the tube, taper the fibre, then glue the other end (c).

This problem was alleviated by not applying glue to the top of the tube until

the tapering process was complete. By leaving the tube open the debris was vented away throughout the process. Using this method, the transmittance was easily reduced by 50%.

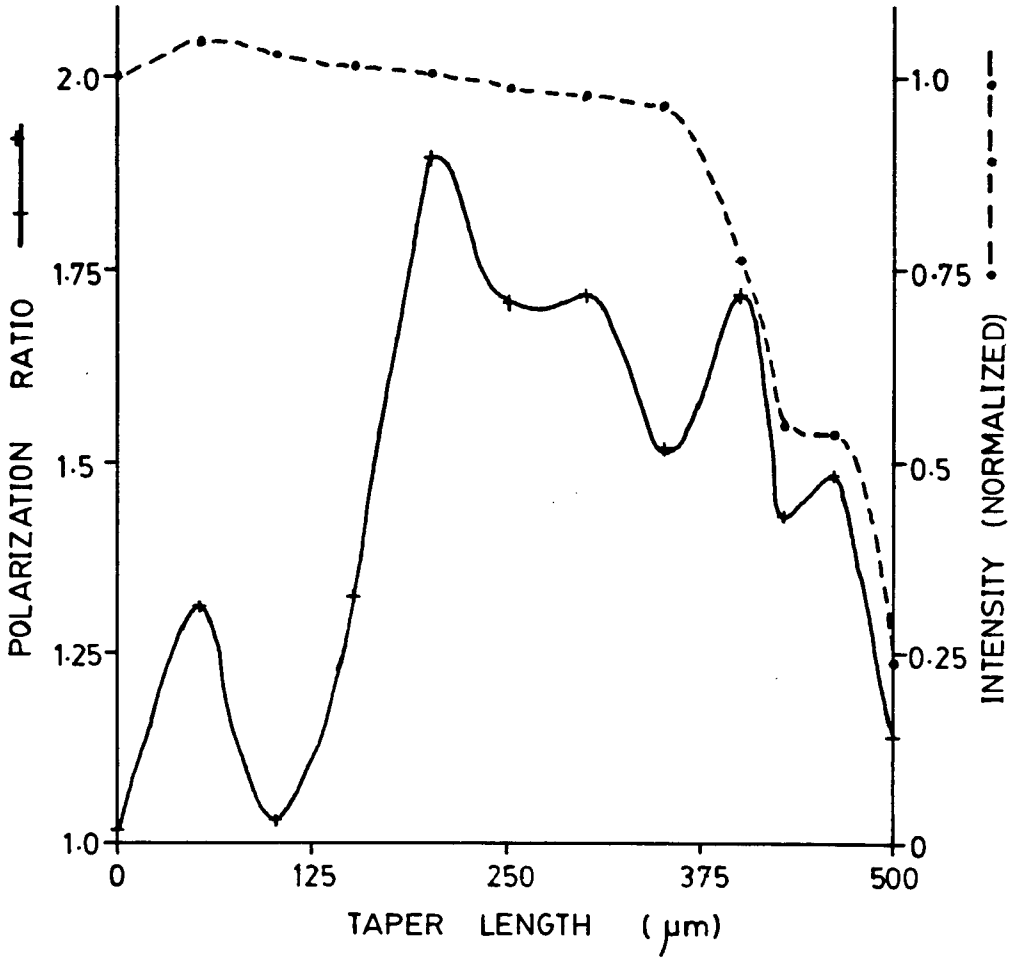

FIGURE 8–5. BIREFRINGENT TAPER — JULY 17

Note that the taper length increases during the experiment so that data for a given taper length can only be taken once, and no repeat measurement is possible. (Once tapering is restarted one cannot go back and retake a measurement.)

The next step was to make a tapered polarizer. A piece of highly birefringent fibre was inserted into a fused quartz capillary tube, one end of the tube was glued, and then the fibre was tapered. The results of the first sample are shown in figure 8–5. The transmission curve is reasonably smooth while the polarization ratio oscillates wildly. The smoothness of the transmission curve tends to indicate that the tapering process was good but the roughness of the polarization ratio shows that the polarization modes were exchanging power rather than being attenuated. The mode coupling could have been due to bending of the taper by vibration in the arc and/or pressure from the walls of the tube (which did not collapse onto the fibre though it did contact the tapered region).

Subsequent trials were performed with far more care and attention to consistent pulling rates and maintaining a straight taper, the result of which is shown in figure 8–6. The fibre definitely showed polarizing ability (polarization ratio of 1.6), but the total power throughput was extremely low (dropped by 86%).

The power loss can be attributed to the taper being too abrupt causing stronger coupling to other modes. The polarization ratio is lower than expected which also may be due to the stronger coupling or possibly to the lack of an index matched external medium (again, the tube did not collapse onto the fibre).

Owing to the above results, this method was deemed inadequate however, it did teach the following:

1. At least one end of the tube must be kept open so that debris inside the tube can escape. If it cannot escape, the debris condenses on the inside of the tube, cooling the fibre so much that it cannot be tapered.
2. The taper should be gradual. This will keep losses to a minimum and allow more control of the tapering process.
3. The tapering process can be interrupted without adversely affecting the fibre shape or performance.

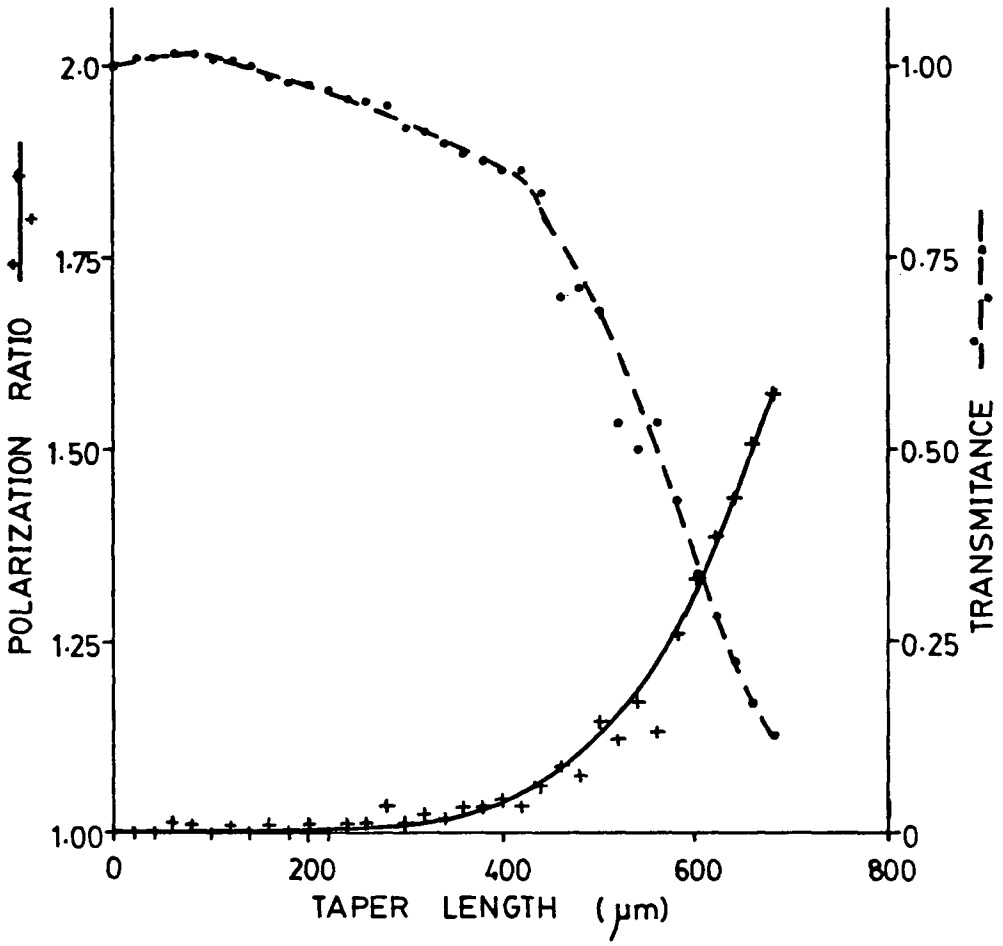

FIGURE 8-6. BIREFRINGENT TAPER — JULY 23

4. Though the fibre does taper the tube does not. The tube is left unaffected by the arc. This could be a result of several things. First, the fibre may be pulled more than the tube so only the fibre will taper. The effect could also be due to the fibre having a lower softening point than the tube (lower viscosity so easier to stretch).

5. It has been verified that the fibre taper does polarize the transmitted light. The task now is to enhance this effect.

8.3 TAPERING WITH A BUTANE TORCH

Since the electric arc did not produce enough heat over a large area of the fibre to form a gradual taper a butane torch was tried. The torch used was a Radio Shack miniature butane soldering torch. This uses replaceable butane cylinders and develops a temperature of 1370 C in a flame approximately 7 mm in diameter and 15 mm long.

For the first tapers, multimode fibre was used. The butane torch allowed longer tapers to be made (up to 18 mm) and the quartz tube collapsed towards the fibre (though the tube and fibre did not bond). The only problem encountered was that the flame did not develop enough heat to burn the debris out of the tube. This situation was countered by clearing the tube with the electric arc prior to tapering. The results for one of the tapers is shown in figure 8–7. It is evident that the longer taper length desired is more likely to be realized by using the butane torch than by using the electric arc. After tapering and gluing, this particular sample was bumped several times with the end of a pencil with no perceptible change in transmission. Therefore, it seems as if a robust tapered polarizer can be made.

Attempts were made to manufacture some highly birefringent tapered polarizers. A typical result is given in figure 8–8. The polarization ratio was just below 2.0 and the resulting curves are reasonably smooth.

The rise in polarization ratio over that obtained through electric arc heating is due to the taper being more gradual. It was also encouraging to see the tube beginning to collapse onto the fibre. The fact that the tube did not completely collapse onto the fibre indicates that it is not being heated enough to do so. It also indicates that the softening point of the fibre may be much lower than that of fused quartz.

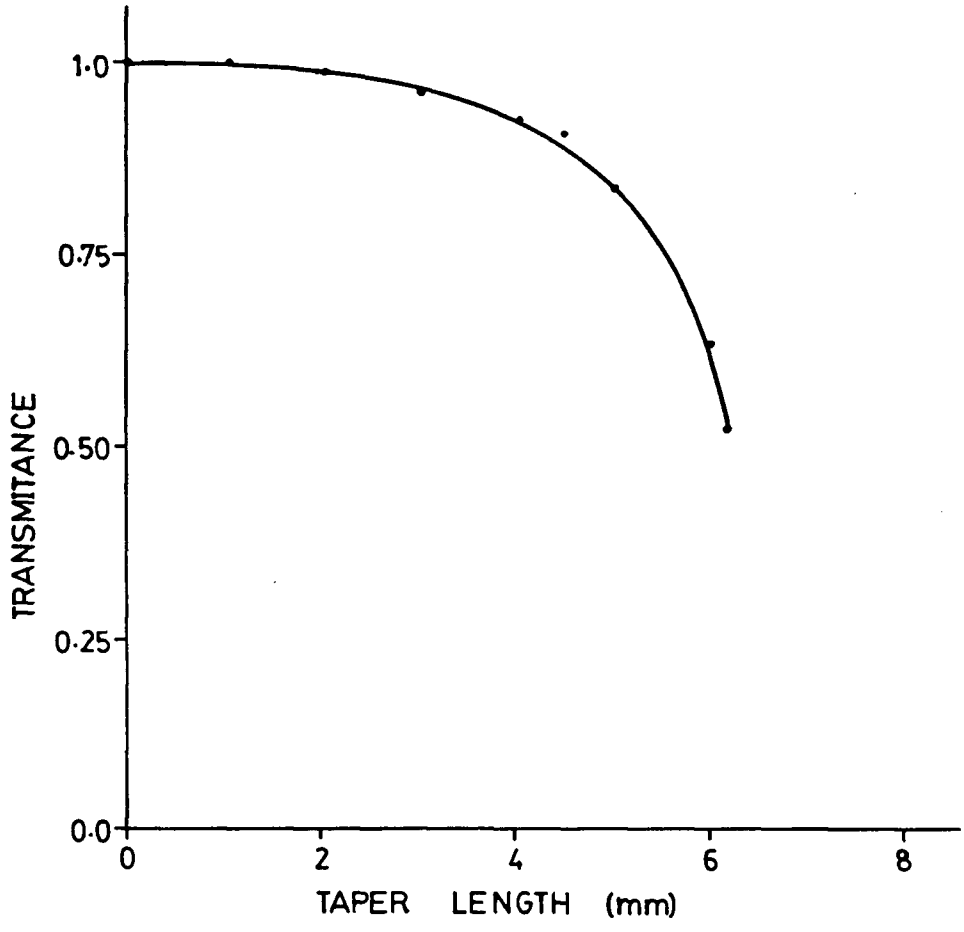

FIGURE 8–7. MULTIMODE FIBRE TAPER — AUGUST 15

Large portions of the birefringent fibre are borosilicate glass (stress lobes). The softening point of borosilicate is 850 C while that of quartz is 1600 C. The presence of low softening point material in the fibre allows the fibre to be stretched and tapered at lower temperatures than that required to collapse the quartz tube. Therefore, it may be possible to collapse the tube onto the fibre by using a hotter flame.

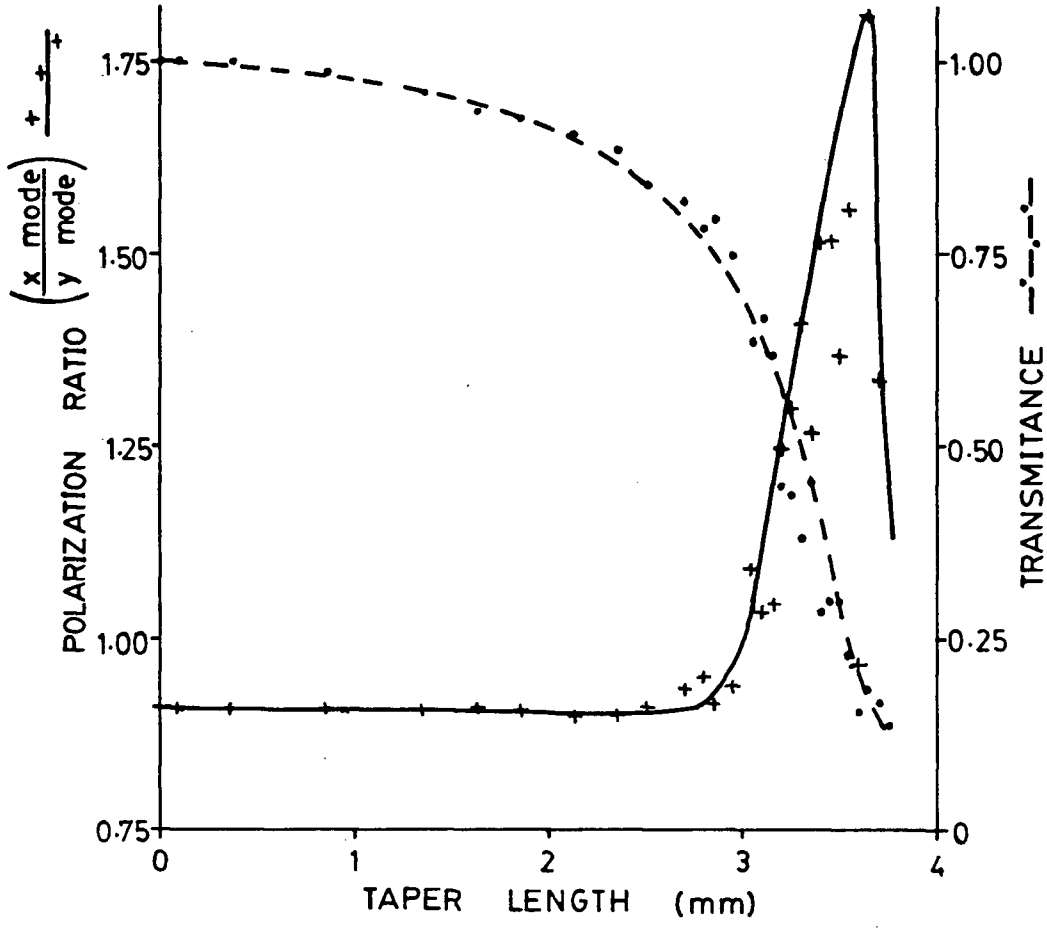

FIGURE 8–8. BIREFRINGENT FIBRE TAPER — SAMPLE G

8.4 TAPERING BY USING AN OXY-PROPANE TORCH

More heat can be applied by using an oxy-propane torch (flame temperatures in excess of 5000 C are obtainable). The one obtained was a 'Little Torch' manufactured by Smith Equipment. This is a small jeweler's torch. It comes with interchangeable sapphire tips, the smallest of which produces a pin-head size flame

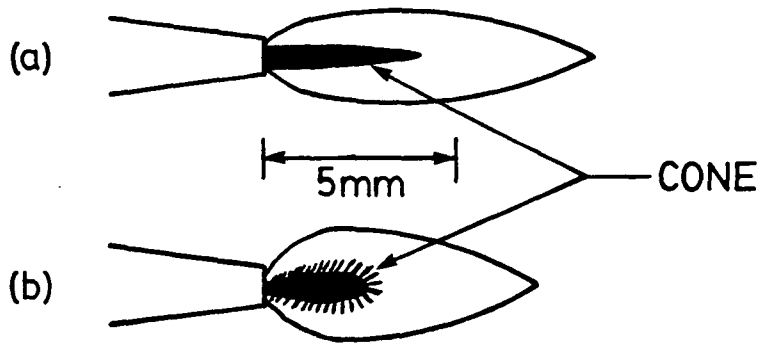

FIGURE 8–9. OXY-PROPANE TORCH FLAME SHAPES

The above flames are produced by using tip #3. The flame is small and gentle in each case. The focused flame (a) has, as the name suggests, a well focused cone. By adjusting the oxygen content so that the yellow part of the flame just disappears a diffuse flame (b) is obtained.

and the largest tip yields a flame a few inches long and the diameter of a pencil. The tip used for most of the work was tip #3, which produced flames as depicted in figure 8–9.

The first task was to try to bond the tube to the fibre. A short piece of multimode fibre was inserted into a capillary tube and mounted on the test bench. It was found that the torch produced enough heat to clear the debris from the tube. The fibre was then tapered during which the quartz tube collapsed onto the fibre. On examination of the fibre structure it was noted that the fibre was stuck to the inside wall. This resulted in the fibre bending at the entrance to the collapsed region, as shown in figure 8–10. This problem was solved by gently tapering the tube preceding the collapsed region. This narrowed the path forces the fibre to straighten out.

The fibre-tube bond was also tested. The taper was bent at angles up to 90° without breaking and allowed to spring back to its original shape. If the tube had

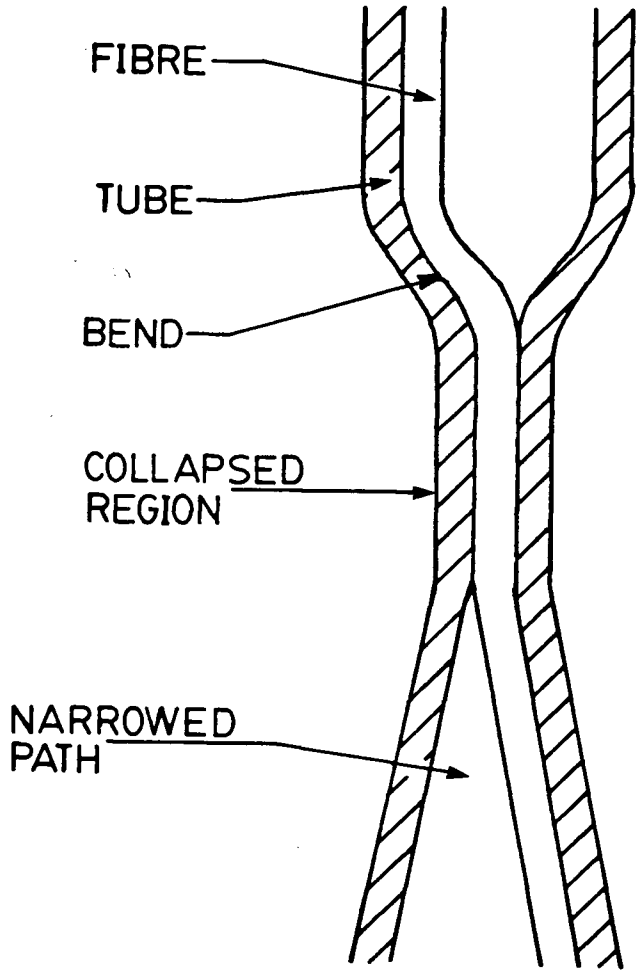

FIGURE 8–10. ENTRANCE OF FIBRE INTO THE COLLAPSED REGION
The fibre sticks to the fibre wall causing a bend in the fibre unless the area preceding the collapsed region is also gently tapered providing a narrow path.

not been bonded to the fibre it would have behaved like a thin tube and shattered. Another test was to break the taper at its waist and examine the broken end under a microscope. There was no discernible difference between the fibre material and the quartz tube, further, it looked like one complete structure therefore, the tube and fibre were bonded.

Subsequent tapers were made in the same manner but, the fibre and tube did not always bond together. Later tests showed that they bonded only when the structure was heated enough to glow white hot. This indicates that high heat is required for applying the external cladding.

Collapsing the tube introduces kinks and bends in the structure but these can be straightened by heating and pulling the fibre. The bends are due to different thermal expansions of the materials, one side of the tube collapsing before the other, and pressure from the flame. During the collapse the heat must be applied evenly otherwise bubbles are trapped between the fibre and the tube. The bubbles prevent the tube and fibre from contacting and, more importantly, are sites where the fibre often breaks (possibly high stress areas).

Putting all of this together, the following procedure for tapering a fibre should be adopted:

1. A 0.3 mm internal diameter by 0.4 mm outside diameter fused quartz capillary is placed over a section of uncoated fibre. This is then mounted on the test bench.
2. Debris is cleared from the tube by applying a diffuse flame. The heat makes the debris glow red. The tube is clear when the red glow disappears and the tube looks clear.
3. The tube is then bonded to the fibre using a focused flame. The flame is moved slowly along the tube making the tube glow white (this is extremely bright so protective glasses must be worn).
4. The fibre path is then eased along the entrance to the collapsed region. This is done by applying heat just above and below the collapsed region while pulling on the fibre so that the tube develops a gentle taper, as shown in figure 8–10. This is done with barely enough heat to make the structure glow dull white. At the same time and in the same manner, the bends and twists which developed in the collapsed region are straightened out.

5. A bubble free area of the collapsed region is chosen for the taper. The taper is formed by slowly moving a diffuse flame up and down the region to be tapered while pulling on the fibre. The amount of heat applied is just enough to make the tube glow white.

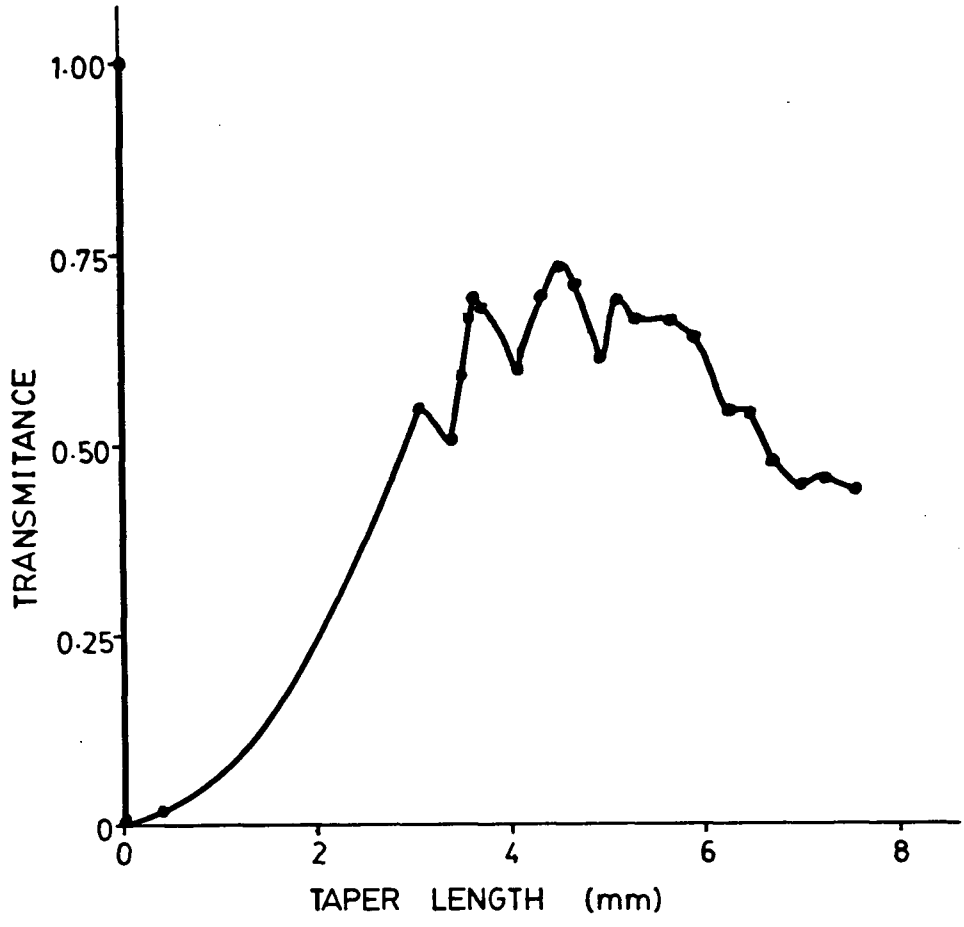

FIGURE 8–11. MULTIMODE FIBRE — MARCH 6

Using this method, a transmission test was attempted on a multimode fibre, the result of which is shown in figure 8–11. The sharp transmission drop between the untapered fibre (taper length 0 mm) and the very short taper length (just above 0 mm) corresponds to the collapse of the tube onto the fibre. The following output rise is the straightening of the collapsed region and the easing of the fibre path. The bumps on the rest of the curve are most likely due to bends developing in the tapered section of the taper.

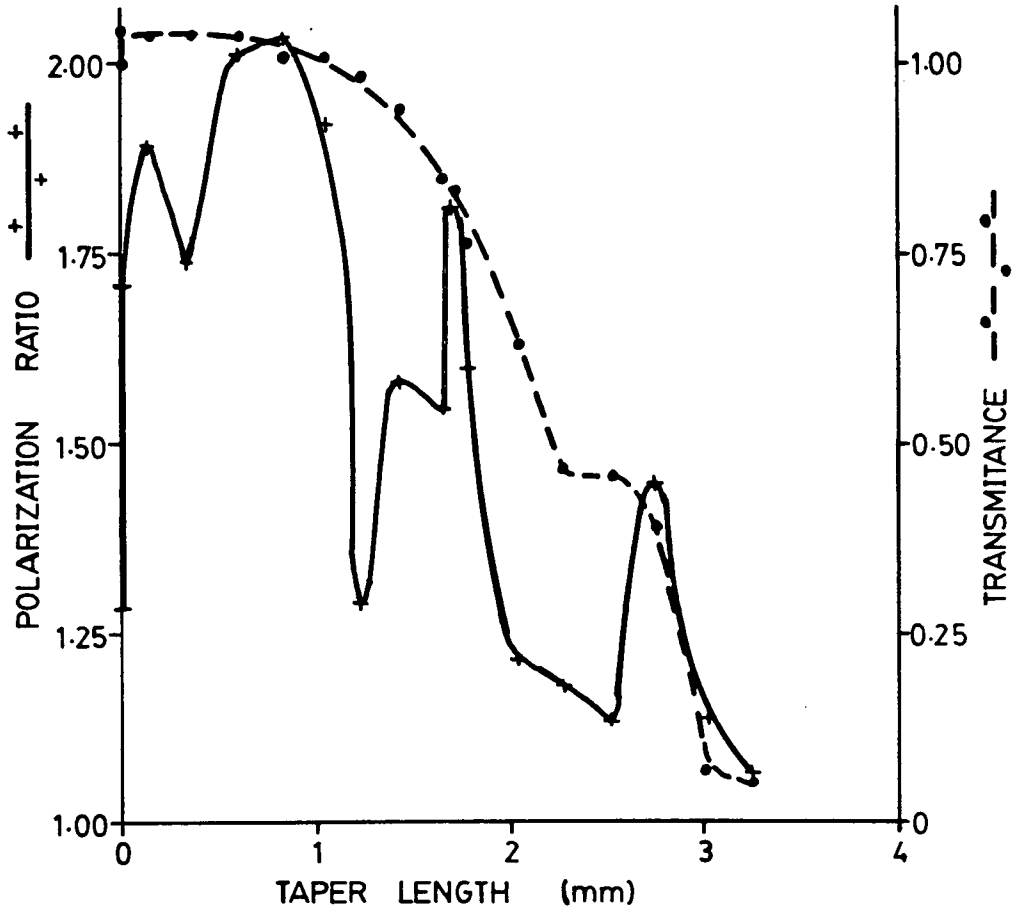

FIGURE 8–12. BIREFRINGENT TAPER — MARCH 12

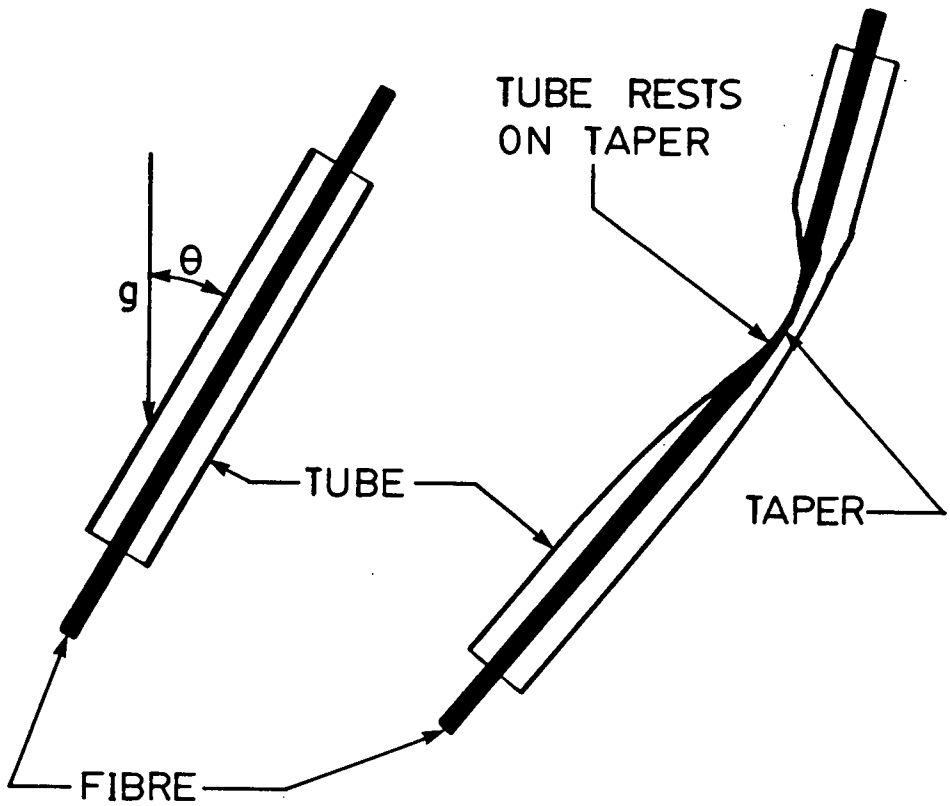

FIGURE 8–13. TAPER MISALIGNMENT WITH THE VERTICAL

Since the effects of the fibre bending in the tube needed investigation an attempt was made to taper the fibre without collapsing the tube onto it. The hope was to make as straight a taper as possible for comparison purposes. The fibre still had to be protected by a capillary tube otherwise the flame pressure would push on the taper causing a bend. The result of the test is shown in figure 8–12. Though the maximum polarization ratio is high there seems to be no repeatability to the experiment. The wild oscillations in the polarization ratio and the smoothness of the transmission indicates that the polarization effect observed is not due to the tapering of the fibre but to coupling between the polarization states. The possible explanations for this are as follows:

1. The fibre and tube may not be vertical, hence the tube will rest on the taper and, possibly, on heating will introduce a bend, as shown in figure 8–13. This applies stress on the fibre which causes the polarization modes to couple.
2. The pulling rate may be too fast which would keep the fibre in tension, causing internal stress and/or fatiguing the fibre. Small cracks that may develop are removed by annealing the fibre, which occurs on subsequent fibre heatings.
3. The pulling rate may be too slow allowing the fibre to stretch and develop extra length between the mounts giving the possibility of bends existing in the fibre.

This problem was solved by replacing the translating mount by a suspended weight. By attaching a light weight to the bottom of the fibre the structure is always vertical and the pulling rate is self determined by the heat applied and the mass of the weight.

The weight cannot be attached to the fibre since heating the structure causes the fibre to taper rapidly before the tube begins to collapse. Attaching the weight to the tube also poses a problem. During the collapse stage the structure tapers rapidly without the tube and fibre bonding (in one trial a taper was formed which was 114 mm long and hair thin, yet the fibre and the tube were not in contact). The alternative is to collapse the tube onto the fibre with no weight on the fibre and then apply the weight but this results in a severely bent taper which is nearly impossible to straighten. With no weight on the fibre the bending forces and flame pressure are enough to lift the fibre up so very sharp bends can form. The solution is to keep the weight on the fibre and support it during the collapsing stage. In doing this, the fibre cannot bend upward to form sharp bends since it cannot lift the weight.

Many birefringent fibres were stretched using the above method. They showed drops in transmission by a factor of over 100 and there seemed no control on polarization properties. When these tapers were examined sharp kinks were found in

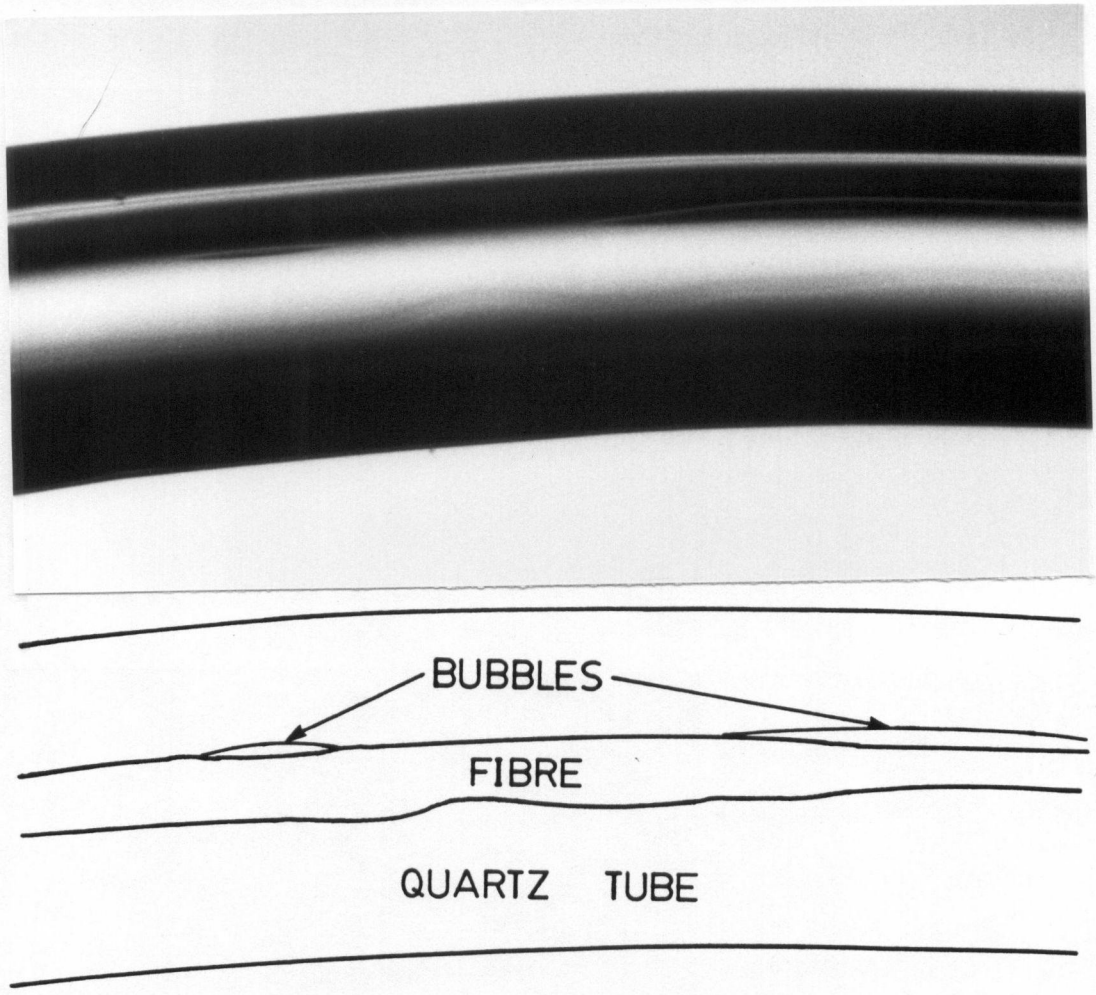

FIGURE 8–14. FIBRE BENDS INSIDE COLAPSED TUBE
The variations in fibre diameter can be observed along the fibre.

the collapsed region of the fibre as show in figure 8–14. The bends were prevalent in the region where collapsing began. These bends are responsible for both high losses and the polarization effects seen in previous samples.

These bends are a result of the different softening points of the tube and the fibre. When the tube is stiffer than the fibre (has a higher softening point) the taper shape is determined by the collapsed tube. If a glass with a lower softening

point were used the collapsed tube would be expected to follow the tapered fibre. This would result in a straighter taper than previously obtained.

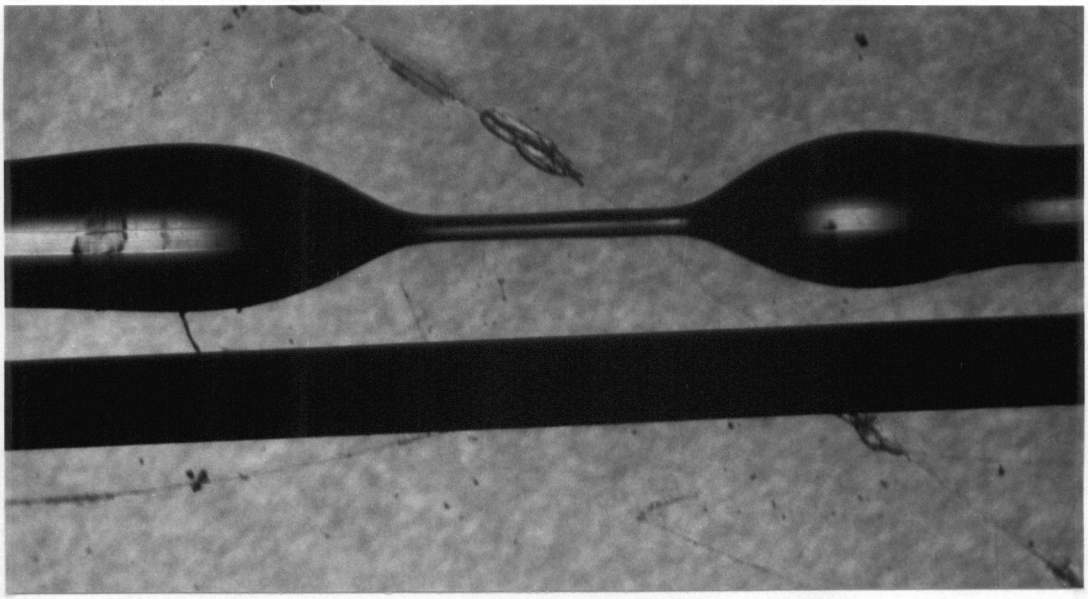

FIGURE 8–15. BOROSILICATE TUBE APPLICATION TO A FIBRE

The fibre is left bare as the tube material balls up on both sides of the heated region. The above is shown against a 0.5 mm pencil lead.

To check this, borosilicate tubing was collapsed onto the tapered fibres. The tubes used had a 0.5 mm inside diameter and a 0.9 mm outside diameter. In the first test, a tube was placed over the fibre and heated. The tube collapsed onto the fibre and 'balled up', as shown in figure 8–15, leaving the fibre bare where the taper is to be formed.

The 'balling' of the tube occurs at too low a temperature to taper the fibre so the taper must be made prior to collapsing the tube onto the fibre. The result of doing so is shown in figure 8–16. The resulting tapers were very straight inside the collapsed tube but, often the sample would break. The breakage may be a result of internal stresses developing due to the thermal expansion of borosilicate being about twice that of the cladding material (fused quartz). In one trial, a bare

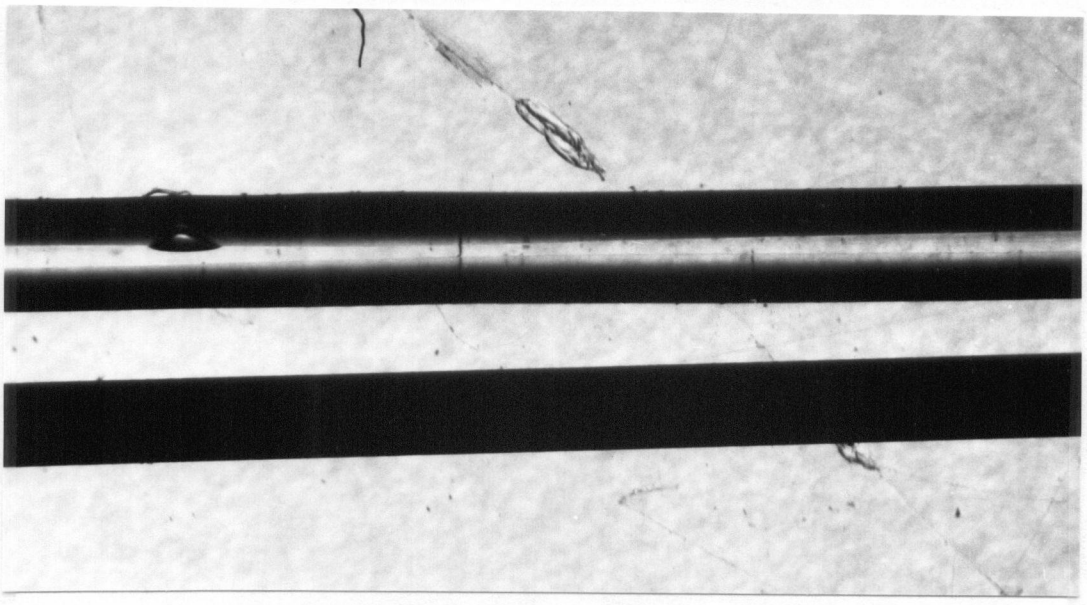

FIGURE 8–16. FIBRE INSIDE A COLLAPSED BOROSILICATE TUBE
The tapered fibre is straight and encased in the centre of the collapsed tube. In the above picture, the fibre is in the bright section in the tube. A 0.5 mm pencil lead is shown for reference.

tapered fibre demonstrated a polarization ratio of 2.22. A tube was collapsed onto the taper raising the polarization ratio to 2.66. It is uncertain whether the rise in polarization ratio can be attributed to the refractive index of the borosilicate tubing or to internal stresses. Despite this uncertainty, this experiment using borosilicate tubes is not to be discounted since it does not introduce any bends in the taper.

An attempt was made to study the effects the stresses and bends were having on the fibre. This was done by making a tapered highly birefringent fibre and immersing it in an index matched solution. The tapers were made vertically without any protective tubing. So that the taper would be handled as little as possible, the tapering was performed inside of the test basin in the vertical position as shown in figure 8–17. Once the taper is made the entire optic bench is rotated to the horizontal position so that the basin can be filled with an index matching fluid.

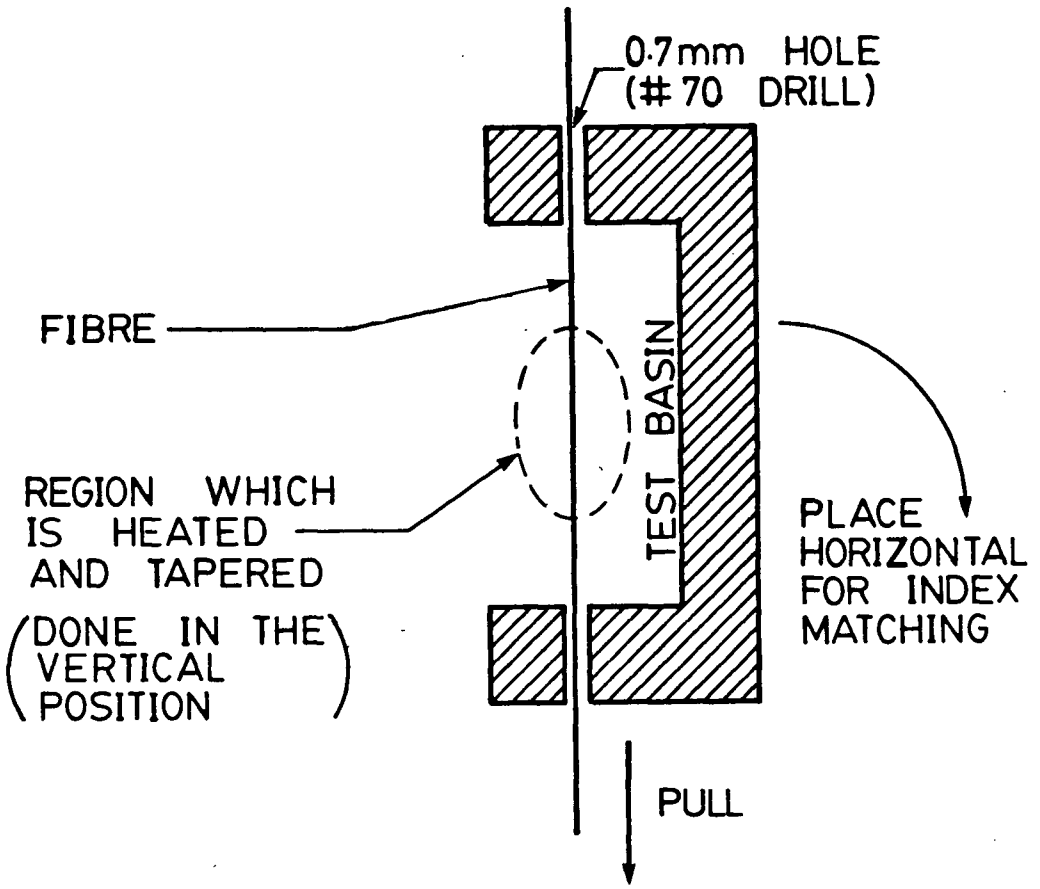

FIGURE 8–17. TAPERING IN A TEST BASIN

The basin can be filled with index matching fluids when placed in the horizontal position. Tapering occurs with the fibre and basin vertical, as shown.

For the test, a highly birefringent fibre was tapered to produce a polarization ratio of 2.89. The bench was then placed horizontally and the polarization ratio was remeasured. The polarization ratio had dropped to 2.65, probably due to the fibre flexing under its own weight. The fibre was then covered in water ($n_{\text{water}} = 1.33$). Glycerol ($n_{glycerol} = 1.47$) was added 2 drops at a time to raise the refractive index of the solution. The effect on polarization was noted, the results of which are shown

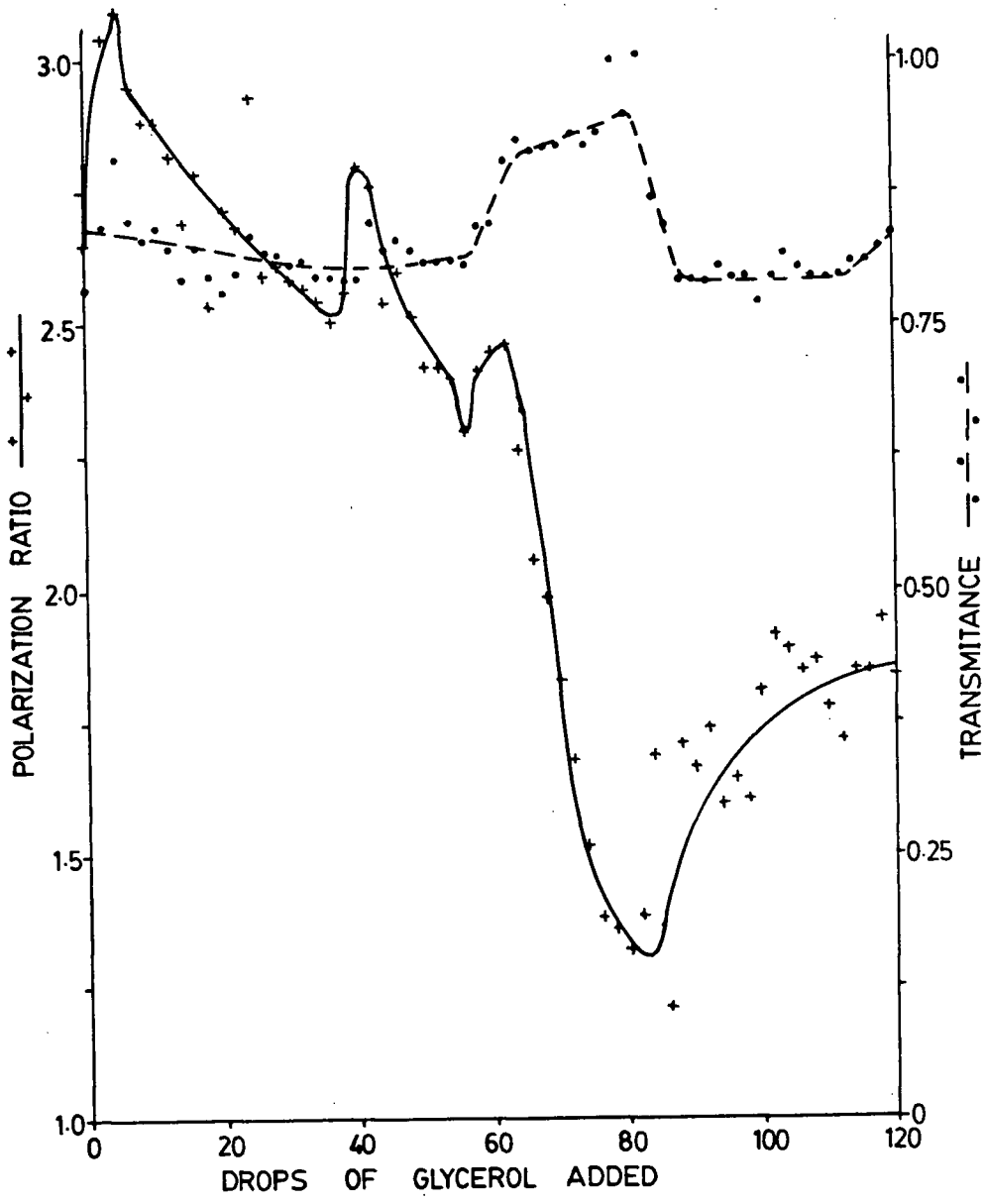

FIGURE 8–18. INDEX MATCHING WITH WATER AND GLYCEROL
The transmittance has been normalized against the maximum output rather than the initial input.

in figure 8–18. The polarization ratio was altered to values as low as 1.21 and as

high as 3.18. This was not as high as hoped for two reasons:

1. The taper length and shape may not be optimum for this wavelength.
2. The concentration of glycerol and water may not match silica ($n = 1.458$) that closely. It was also noted that the drops of glycerol could be detected as they sat on the taper before being mixed into the solution (output would decline by as much as 10%). This decrease is most likely due to a slight bend in the taper though its existence could not be detected visually.

The losses detected in the slight bends in index matching with glycerol and water indicates that the major problem encountered in trying to produce a polarizing taper is bending of the fibre in the quartz tubing.

REFERENCES

[1] Varnham, M.P., F. de Fornel, D.N. Payne, C.M. Ragdale, A.J. Barlow, and E.J. Tarbox. "Comparison Between Coil and Taper Fibre-Polarisers," *Proceedings of the Society of Photo-Optical Instrumentation Engineers*, **514**, (1984), p.329–332.

[2] Lacroix, Suzanne, Richard J. Black, Christian Veilleux, and Jean Lapierre. "Tapered Single-Mode Fibers: External Refractive-Index Dependence," *Applied Optics*, **25**, (1986), p.2468–2469.

[3] de Fornel, F., M.P. Varnham, and D.N. Payne. "Finite Cladding Effects in Highly Birefringent Fibre Taper-Polarisers," *Electronics Letters*, **20**, (1984), p.398–399.

[4] [1].

[5] Jedrzejewski, K.P., F. Martinez, J.D. Hussey, and F.P. Payne. "Tapered-Beam Expander for Single-Mode Optical-Fibre Gap Devices," *Electronics Letters*, **22**, (1986), p.105–106.

[6] ibid.

[7] Hentschel, Christian. *Fiber Optics Handbook* , (Federal Republic of Germany: Hewlett Packard, 1983), p.130.

[8] Kapron, F.P., John C. Dyment, Jan Conradi, and Carl W. Anderson. *Fiber Optic Communications*, (Bell Northern Research, 1979), section 5.4.

[9] Manfré, G. "Forces Acting in the Continuous Drawing of Glass Fibres," *Glass Technology*, **10**, (1969), p.99–106.

[10] McLellan, George W., and Errol B. Shand editors. *Glass Engineering Handbook*, (New York: McGraw-Hill Book Company, 1984), p. 2-5.

[11] ibid. p.1-3.

CHAPTER 9–DISCUSSION AND CONCLUSIONS

This thesis is concerned with the production of in line polarizers for optical fibres. It reviews the pertinent theory of propagation of polarized light in optical fibres and it attempts to demonstrate that a tapered section of birefringent fibre with a quartz cladding can be used as an in line polarizer for optical fibre applications. The work differed from known tapered beam expanders with vycor cladding [1] in the following three ways:

1. The Vycor has a lower index of refraction than the silica cladding ($\delta n = 0.004$) so the fibre modes remain guided in the taper (the taper acts as the core while the Vycor acts as the cladding). The purpose of cladding the tapered polarizer in quartz is not to keep the modes guided but to allow them to radiate away more easily.
2. The concern in the beam expander is on spot size and intensity rather than polarization state.
3. The fibre used in the tapered beam expander is a single mode fibre which is predominantly fused quartz. The tapered polarizer's fibre is also a single mode fibre but, it is highly birefringent and, though most of it is fused quartz, large portions are composed of borosilicate glass. This can cause a difference because the softening point of borosilicate is less than 850 C while that of fused quartz is 1600 C.

To the best knowledge of the author, there has been no attempt to clad a tapered polarizer in quartz.

Several methods of producing fibres were evaluated and tried and many tapers were produced and tested. The following summarizes the author's assessment of the potential for manufacturing tapered optical fibre polarizers based on the simplest techniques available. It presents his major contributions to this area of research.

Regardless of method, it was found that the following must be observed when applying a fused quartz tube to a tapered polarizer:

1. The ends of the quartz tube must be left open throughout the tapering process. By leaving the ends open, the gases produced by debris burning inside the tube are allowed to escape. When the gases cannot escape they condense inside the tube, either to be revaporized, giving rise to convection currents in the tube, or burning further to form a black residue. The convection currents and the residue keep the fibre cool, preventing it from getting hot enough to taper.
2. Collapsing the tube onto the fibre requires high temperatures (oxy-propane provides enough heat). High temperatures are necessary to soften the quartz tube enough to collapse onto the fibre. Intense heating lowers the viscosity of the tube so that surface tension becomes the dominant force, causing the tube to collapse onto the fibre.
3. The taper must be kept very straight otherwise internal stresses develop causing the polarization modes to exchange energy with each other. The best way to do this is to suspend a weight from the structure to keep the fibre straight as it tapers.

The cause of most problems encountered in applying the quartz tube to the fibre is the difference in the softening temperature (known as the softening point) between them. The effective softening point of the fibre is lower than the tube as evidenced by the inability to collapse the tube onto the fibre and form the taper at the same time. One example is the 114 mm long taper in which the tube had not collapsed onto the fibre. Also, when using the electric arc, the fibre tapered

but the quartz tube remained unaffected. The effective softening point of the fibre is lower because large portions of the fibre are borosilicate glass (the stress lobes) which have a lower softening point than quartz (less than 850 C versus 1600 C). The lower softening point gives rise to the following problems:

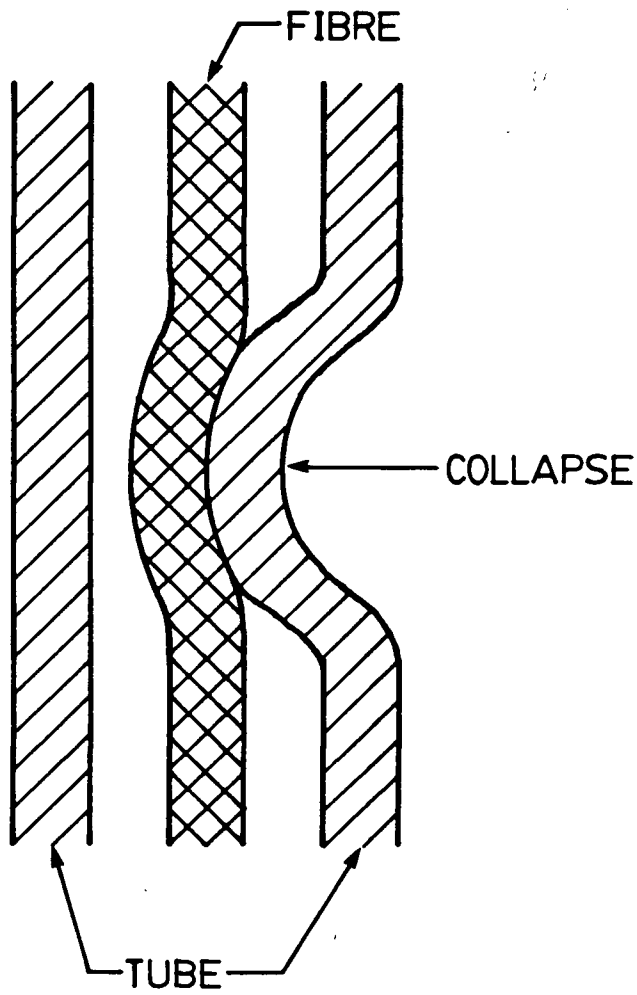

FIGURE 9–1. COLLAPSING TUBE BENDING A FIBRE

1. The collapsing tube wall exerts pressure on the fibre which forces a bend to develop causing the polarization modes to couple. If the fibre were under high tension the inward collapse of the tube would be halted and only a small bend would develop in the fibre†. However, when the fibre is heated, tension causes the fibre to stretch inelastically. Therefore, as the tube presses inward the fibre stretches and deforms to mate with the wall of the tube as shown in figure 9–1.

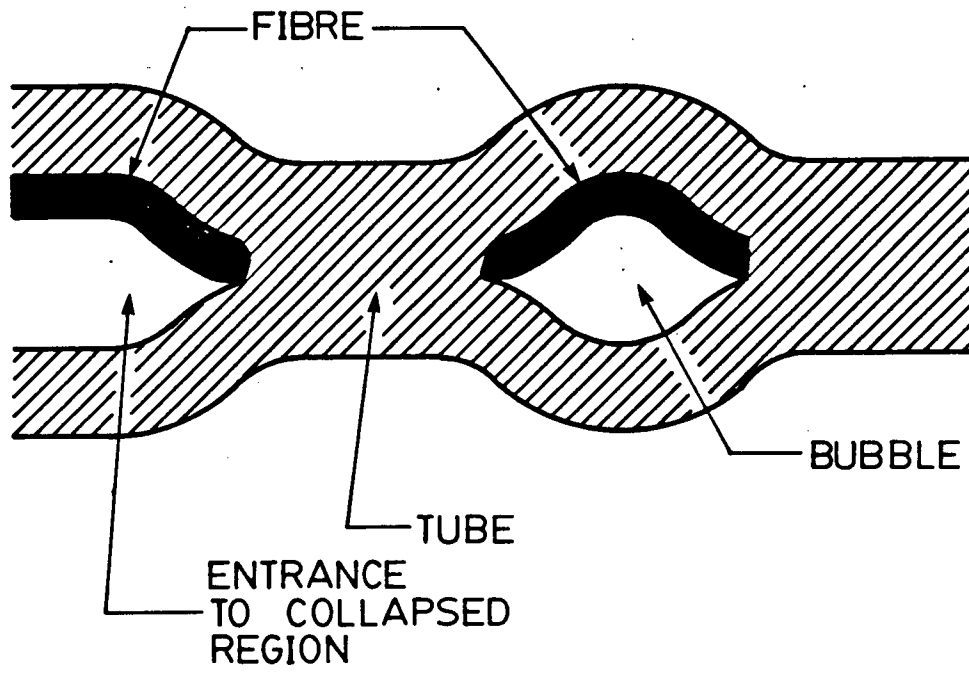

FIGURE 9–2. FIBRE BENDING IN BUBBLES

---

† This is analogous to a weight (the collapsing tube wall) being suspended from the centre of a horizontal string (the fibre).

2. The lower softening point of the fibre causes the fibre to weakly bond to the tube wall (there is sufficient heat for the two glasses to bond). This bond causes the fibre to follow the tube wall inside bubbles and at the entrance to the collapsed region as shown in figure 9–2. The bends introduced by this bond again cause power losses and mode coupling.

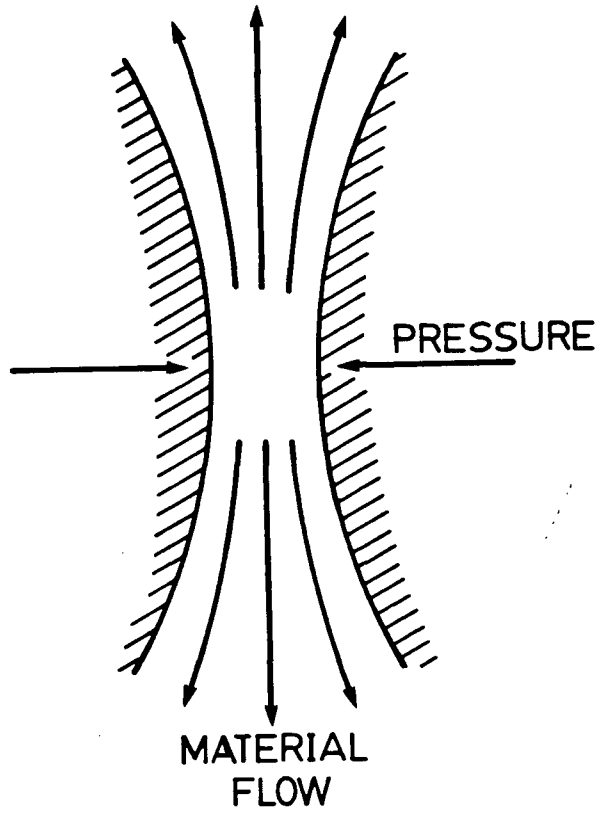

FIGURE 9–3. FIBRE IN THE COLLAPSED REGION OF THE TUBE
During the collapse stage the tube walls press in on the fibre causing the fibre material to deform and flow.

3. In the collapsed region the fibre cross section may be irregularly shaped. The lower softening point of the fibre makes it more prone to flowing and deforming than the quartz tube. When the collapsed region is heated the surface

tension of the quartz presses inward squeezing the fibre out of the region thus, locally changing the fibre diameter as shown in figure 9–3. When heated in a nonuniform fashion, the fibre diameter will vary causing strong mode coupling to occur (similar to the taper of section 7.5). This results in higher losses and affects the polarization performance. This squeezing effect can also deform the fibre's stress lobes, which would affect the birefringence, making the fibre more prone to polarization mode coupling. Unfortunatly, the birefringence could not be checked due to the short depolarization length of the fibre (chapter 6).

Once the tube has collapsed on the fibre the internal stresses developed by the tube are far larger than that in the fibre. Internal stresses develop and are affected by the following:

1. Differences in thermal expansion between the various materials.
2. How the various parts bond: Rigid bonds tend to raise the stress level whereas elastic bonds alleviate and take up some of stress themselves.
3. The geometry of the structure. The stress is zero at interfaces with air (no stress can be transferred between the air and the glass). This means that where bends and bubbles form in the collapsed region high stresses develop which alter the birefringence and cause mode coupling.

The above problems arise from uneven heat and flame pressure. The flame pressure and application of heat on one side of the tube causes the heated side to collapse onto the fibre faster than the opposite side of the tube. This introduces a bend in the fibre. Flame jitter and uneven application of the heat along the fibre result in bubbles forming and varying degrees of fibre squeezing taking place, which also affect birefringence.

The above problems may not affect power throughput but they will affect polarization state as can be seen in figure 8.5 where the transmission remains constant while polarization state varies. Therefore, non-birefringent fibre tapers, such

as the tapered beam expander, may not suffer adverse affects when clad in quartz. However, internal stresses and deformation of the fibre by the quartz tube cause strong coupling between polarization states in a tapered polarizer.

It may be possible to alleviate most of the problems by using a tube material which has a lower softening point than the fibre. The tapers made by this process are quite straight but there are two problems:

1. The expansion of fused quartz is very low, a tubing material would have to be found which has a low thermal expansion. (The thermal expansion of fused quartz is 5.5×10^{-7}/C and that of borosilicate is 10×10^{-7}/C). Differences in thermal expansion cause large stresses to develop as the fibre cools. The large stresses may not appreciably affect the transmission characteristics since tube application is symmetric about the fibre hence, the stress is also symmetric. The large stresses that do develop make it easier to break the fibre in handling.
2. Finding a glass with same index of refraction but with a lower softening point than fused quartz. The refractive index of quartz is lower than most available glasses making it difficult to find a substitute.

An alternative way to solve the problem is to remove all perturbations and asymmetries in the applied heat so that the tube collapses symmetrically onto the fibre. This may be possible by using an induction furnace. An induction furnace provides a symmetric and intense heat but long cooling times make its use awkward. As the fibre cools the birefringence changes causing the polarization properties to change. Since birefringence is temperature dependent the final properties cannot be predicted from measured properties while the fibre is hot. Therefore, the fibre must be allowed to cool to the same temperature each time it is stretched so that a reliable comparison of its properties can be made. Waiting for the furnace to cool is impractical because of the long cooling and heating times associated with induction furnaces (the furnace develops heat inside a graphite block surrounding the fibre). If the induction furnace is to be used effectively, a monochromator is necessary.

The effective solution is to prepare a taper in the induction furnace, then analyze the wavelength dependence of its properties using the monochromator. The most optimum operating wavelength can then be chosen†. This differs from the method researched: a wavelength of operation was chosen (850 nm) and the taper profile was altered to optimize performance whereas, with the monochromator a taper is made and the optimum wavelength is chosen. Chosing the wavelength is simpler since the analysis finds the optimum every time, whereas in changing the taper profile to suit the wavelength it is possible to overshoot the optimum point. Once overshot it cannot be undone (a fibre cannot be detapered).

In conclusion, tapered polarizer performance cannot be enhanced by using a torch or an electric arc to collapse a fused quartz tube onto the taper. The task is formidable since uneven heat application causes the tube and fibre to deform, stressing the taper. The stress alters the birefringence of the fibre giving rise to mode coupling and losses. It may still be possible to increase polarizer performance by finding a better material than quartz for the cladding or, an induction furnace or radiative heating by a high intensity arc lamp could perhaps be used to heat the fibre symmetrically.

REFERENCES

[1] Jedrzejewski, K.P. F.Martinez, J.D. Minelly, C.D. Hussey, and F.P. Payne. "Tapered-Beam Expander for Single-Mode Optical-Fibre Gap Devices," *Electronics Letters*, **22**, (1986), p.105–106.

---

† In industrial production this means that many polarizers must be made in order to select the few that have the desired wavelength response.

APPENDIX A–FIBRE ALIGNMENT

This appendix contains a description of the preparation and alignment of optical fibres for an experiment. Polishing apparatus and techniques are described along with the details on aligning the optical fibres.

A.1 FIBRE POLISHING

Before fibre alignment commences the ends of the fibres must be polished in order to improve their optical properties. A roughened end face can highly attenuate the light passing through it due to reflections off the surface irregularities. Polishing the ends is even more crucial for polarization dependent applications, such as the tapered polarizer. Small blemishes allow most of the incident optical energy, to pass virtually unimpeded, but the blemishes refract the light causing depolarization.

A smooth finish is achieved by doing the following:

1. The end of the fibre is dipped in methyl-chloride in order to dissolve the protective coating. This works for the acrylate coating on fibres made by York V.S.O.P. but others may require the use of sulfuric acid.
2. The fibre is then inserted in a long sleeve which has a hole down its center just large enough to accommodate the fibre, as shown in figure A–1. The fibre is 'glued' with the end protruding 1 mm out the end of the sleeve. The glue is water soluble wax which is removed by washing in water.

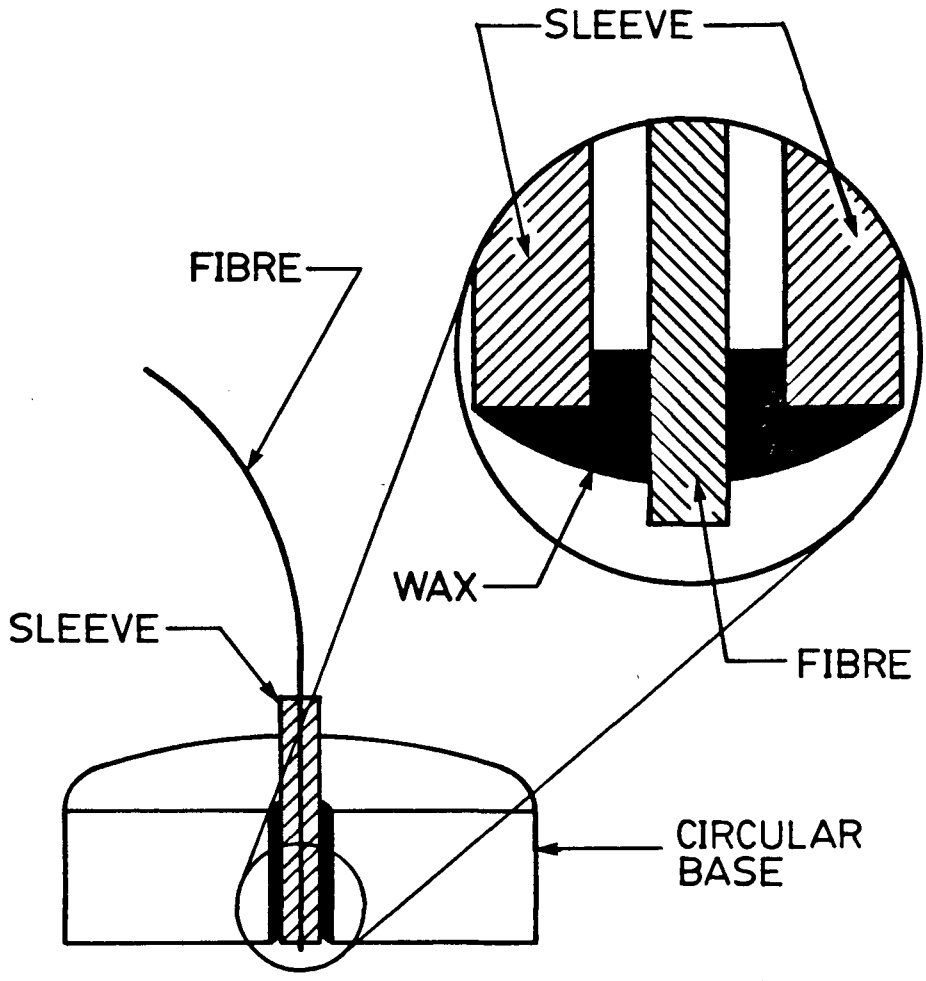

FIGURE A–1. FIBRE POLISHING APPARATUS

3. The sleeve is inserted into a close fitting hole in a circular base. The bottom face of the circular base is machined flat and perpendicular to the hole so that the fibre is held at right angles to the polishing surface.
4. The base is placed on a piece of fine sand paper mounted on a smooth, clean surface. The fibre is polished by moving the base in a circular motion with

gentle pressure on the sleeve. For best results start with a coarse paper and progress to a finer paper (the papers used were 15, 3, and 0.3 grit). When changing papers the fibre is wiped gently with a piece of gauze to remove any large pieces of grit which may mar the finish.

5. Once the fibre is polished the fibre is removed from the sleeve by washing in water.

A.2 LASER-FIBRE ALIGNMENT

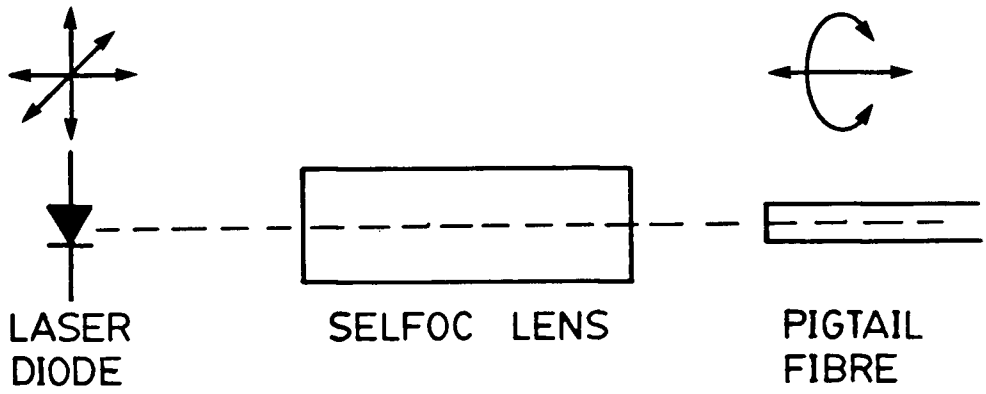

FIGURE A–2. LASER-LENS POSITIONING
The laser, lens, and fibre are placed in a line. The allowed alignment motions are indicated by arrows.

With a polished fibre in hand work can proceed to setting up the laser and pigtail fibre on the optical fibre test bench. This is accomplished by doing the following:

1. The lens is glued in place using ultraviolet curing glue (Norland Optical adhesive #61 was used).

2. The laser is placed behind the lens on a three axis stage and the fibre is then set on the other side of the lens on a translating mount as shown in figure A–2.
3. The position of maximum intensity is found through moving the fibre in a line towards or away from the lens and through translation of the laser in the plane transverse to the fibre-lens-laser axis (laser-lens distance is kept fixed).
4. The maximum is recorded and the laser is moved towards (or away) from the lens. Then the maximum is found again as described in step 3.
5. The iterative process continues until the absolute maximum is found. The fibre and the lens are now aligned.

A.3 EXCITING THE POLARIZATION EIGENSTATES

Having found the position for maximum throughput the fibre can be glued in place. However, for polarization dependent systems the fibre birefringent axis must also be aligned.

For the pigtail fibre a linear output state is guaranteed by exciting one of the polarization eigenstates. This is accomplished through rotation of the fibre about its central axis as explained below.

1. The fibre is aligned for maximum throughput as described above, with the exception that a polaroid is mounted between the lens and the fibre. The alignment is performed with the polaroid in place because refraction within the polaroid changes the light's path length and, therefore, shifts the focal point.
2. The fast axis is then found through analysis of the output polarization state. The analyzing polaroid is rotated and the maximum and minimum intensities transmitted are recorded. This is really a measure of the ellipticity of the state using the extinction ratio (max/min).
3. The fibre input is rotated and the reading is taken again. This process continues until the maximum extinction ratio (polarization ratio) is found. At

the absolute maximum only the polarization eigenstate of the fibre is excited. This eigenstate is indistinguishable from the other eigenstate at 90°. Rotation of the input by 45° excites both eigenstates equally giving an extinction ratio close to unity. Once the fibre is aligned the fibre may be glued in place using ultraviolet curing glue.

A.4 FIBRE-FIBRE COUPLING

Coupling a fibre to another fibre is similar to coupling a laser to a fibre with two exceptions:

1. There is no lens to improve coupling efficiency.
2. One of the fibres is fixed in place while the other is mounted on a three axis stage and is allowed to rotate about its axis (the test fibre is held stationary so that the experimental conditions are constant). The alignment for maximum power is performed through movement of the one fibre only, hence, this is not an iterative process like the laser-fibre alignment but is done in one step. The alignment for exciting the polarization modes is done in the same manner as before.

LIST OF VARIABLES

a The length of the major axis of an ellipse.

a The radius of the core.

a_j The amplitude of mode j.

A The cross sectional area of the fibre core.

b The length of the minor axis of an ellipse.

b_j The amplitude and phase coefficient of a mode.

$\mathcal{B}$ The birefringence ($\mathcal{B} = |\beta_x - \beta_y| = 2\pi/L_p$).

c The speed of light in vacuum (2.998×10^8 m/s).

C_{jl} The coupling coefficient between modes j and l.

$\vec{\mathrm{D}}$ The dielectric field.

$\hat{e}_j$ The normalized electric field mode j.

$\vec{e}_j$ The electric field mode j.

$\vec{\mathrm{E}}$ The electric field.

$\vec{\mathrm{E}}_N$ The electric field perpendicular to the direction of travel.

$\vec{\mathrm{E}}_T$ The electric field transverse to the direction of travel.

E_i The amplitude of the incident electric field.

E_r The amplitude of the reflected electric field.

E_t The amplitude of the transmitted electric field.

$\mathcal{E}$ The extinction ratio.

f The frequency in hertz.

$\vec{G}$ is the function $\vec{\mathrm{E}}_1 \times \vec{\mathrm{H}}_2^* + \vec{\mathrm{E}}_2^* \times \vec{\mathrm{H}}_1$.

$\hat{h}_j$ The normalized magnetic field mode j.

$\vec{h}_j$ The magnetic field mode j.

$\vec{\mathrm{H}}$ The magnetic field.

$H_\nu^{(1)}$ Hankel function of the first kind of integer order ν.

$\mathcal{H}$ The unit step function.

J_ν Bessel function of integer order ν.

$\vec{\mathrm{J}}$ The current density.

k The wave number in free space ($k = 2\pi/\lambda$).

K_ν Modified Bessel function of integer order ν.

ℓ_d The depolarization length.

L Taper length.

L_p Beat length.

n Refractive index of the medium.

n_{cl} Refractive index of the cladding.

n_{co} Refractive index of the core.

P Power.

Q Imaginary form of the cladding parameter ($Q = iW$).

r_d Beam displacement from fibre centre.

R_0 Bending radius.

$\vec{\mathrm{S}}$ The Poynting vector.

S_j The power in mode j.

t Time.

T Transmittance.

U The core parameter ($a\sqrt{k^2 n_{co}^2 - \beta^2}$).

$\tilde{V}$ The Verdet constant.

V The waveguide parameter ($ak\sqrt{n_{co}^2 - n_{cl}^2}$).

W The cladding parameter ($a\sqrt{\beta^2 - k^2 n_{cl}^2}$).

α Power attenuation coefficient.

β The propagation constant (angular spatial frequency).

γ The attenuation coefficient in the cladding.

$\delta\beta$ The average difference between the propagation constants of two coupled modes.

$\delta\lambda$ The bandwidth of the source.

δz The beam displacement on reflection.

$\delta\phi$ The phase shift between two modes.

Δ The profile height parameter ($2\Delta = 1 - (n_{cl}/n_{co})^2$).

ϵ The permitivity of the material.

ϵ_0 The permitivity of free space (8.854×10^{-12} coulomb^2/N$-$m^2).

ς The angle the polarization state rotates through about an axis through a Poincaré sphere.

η The ratio of power in the core to total power.

θ_c The critcal angle as defined by Snell's law: $\cos\theta_c = n_{cl}/n_{co}$.

θ_{co} The angle a ray makes with the fibre axis in the core.

θ_{cl} The angle a ray makes with the fibre axis in the cladding.

λ The wavelength in free space.

λ_g The guide wavelength.

λ_{co} The wavelength in the core (λ/n_{co}).

μ_0 The permeability of free space ($4\pi \times 10^{-7}$ weber/amp $-$ m).

ν The mode number.

ρ Spot size of a beam.

Φ The phase shift on reflection.

χ The ellipticity of polarized light ($\chi = \pm \arctan(a/b)$).

ω Angular frequency ($\omega = 2\pi f$).

ϑ The angle an applied magnetic field makes with the direction of propagation.

BIBLIOGRAPHY

[1] Abramowitz, Milton, and Irene A. Stegun. *Handbook of Mathematical Functions*, (New York: Dover Publications Inc., 1964).

[2] Baldwin, George C. *An Introduction to Nonlinear Optics*, (New York: Plenum Press, 1969).

[3] Bergh, R.A., et. al. "Single-Mode Fiber-Optic Polarizer," *Optics Letters*, **5**, (1980), p.479–481.

[4] Birch, R.D., et. al. "Fabrication of Polarisation-Maintaining Fibres Using Gas-Phase Etching," *Electronics Letters*, **18**, (1982), p.1036–1038.

[5] Birch, R.D., et. al. "Fabrication of a Stress-Guiding Optical Fibre," *Electronics Letters*, **19**, (1983), p.866–867.

[6] Bowdler, G.W. *Measurements In High-voltage Test Circuits*, (New York: Pergamon Press Inc., 1973).

[7] Cassidy, David T., et. al. "Wavelength-Dependent Transmission of Monomode Optical Fiber Tapers," *Applied Optics*, **24**, (1985), p.945–950.

[8] Eickhoff, W. "In-Line Fibre-Optic Polariser," *Electronics Letters*, **16**, (1980), p.762–764.

[9] de Fornel, F., et. al. "Finite Cladding Effects in Highly Birefringent Fibre Taper-Polarisers," *Electronics Letters*, **20**, (1984), p.398–399.

[10] Giallorenzi, Thomas G., et. al. "Optical Fiber Sensor Technology," *IEEE Journal of Quantum Electronics*, **18**, (1982), p.626–665.

[11] Giallorenzi, Thomas G., et. al. "Optical-Fiber Sensors Challenge the Competition," *IEEE Spectrum*, **23**, (Sept. 1986), p.44–49.

[12] Goos, Von F., and H. Hänchen. "Ein neuer und fundamentaler Versuch zur Totalreflexion," *Annalen der Physik*, **1**, (1947), p.333–346.

[13] Gruchmann, D., et. al. "Fibre-Optic Polarizers with High Extinction Ratio," *Proceedings of the Ninth European Conference on Optical Communications*, Geneva, Switzerland, (October 23–26, 1983), p.305–308.

[14] Harms, H., et. al. "Magnetooptical Properties of Index-Gradient Optical Fibers," *Applied Optics*, **15**, (1976), p.799–801.

[15] Hentschel, Christian. *Fiber Optics Handbook* , (Federal Republic of Germany: Hewlett Packard, 1983).

[16] Jacobs, Ira. "Lightwave Communications Passes its First Test," *Bell Laboratories Record*, **54**, (1976), p.290–297.

[17] Jedrzejewski, K.P., et. al. "Tapered-Beam Expander for Single-Mode Optical-Fibre Gap Devices," *Electronics Letters*, **22**, (1986), p.105–106.

[18] Johnson, Mark. "Poincaré Sphere Representation of Birefringent Networks," *Applied Optics*, **20**, (1981), p.2075–2080.

[19] Jordan, Edward C., and Keith G. Balmain. *Electromagnetic Waves and Radiating Systems*, (New Jersey:Prentice-Hall Inc., 1968).

[20] Kaminow, Ivan P. "Polarization in Optical Fibers," *IEEE Journal of Quantum Electronics*, **17**, (1981), p.15–22.

[21] Kaminow, I.P., and V. Ramaswamy. "Single-Polarization Optical Fibers: Slab Model," *Applied Physics Letters*, **34**, (1979), p.268–270.

[22] Kapron, Felix P., et. al. "Birefringence in Dielectric Optical Waveguides," *IEEE Journal of Quantum Electronics*, **8**, (1972), p.222–225.

[23] Kapron, Felix P., et. al. *Fiber Optic Communications*, (Bell Northern Research, 1979).

[24] Katsuyama, T., et. al. "Low-Loss Single Polarisation Fibres," *Electronics Letters*, **17**, (1981), p.473.

[25] Kumar, A., and R. Ulrich, "Birefringence of Optical Fiber Pressed into a V Groove," *Optics Letters*, **6**, (1981), p.644–646.

[26] Kumar, A., et. al. "Birefringence Calculations in Elliptical-Core Optical Fibres," *Electronics Letters*, **20**, (1984), p.112–113.

[27] Lacroix, Suzanne, et. al. "Tapered Single-Mode Fibers: External Refractive-Index Dependence," *Applied Optics*, **25**, (1986), p.2468–2469.

[28] Lotsch, Helmut K.V. "Reflection and Refraction of a Beam of Light at a Plane Interface," *Journal of the Optical Society of America*, **58**, (1968), p.551–561.

[29] Manfré, G. "Forces Acting in the Continuous Drawing of Glass Fibres," *Glass Technology*, **10**, (1969), p.99–106.

[30] McLellan, George W., and Errol B. Shand, eds. *Glass Engineering Handbook*, (New York: McGraw-Hill Book Company, 1984).

[31] McMahon, Donald H., et. al. "Fiber-Optic Transducers," *IEEE Spectrum*, **18**, (Dec. 1981), p.24–29.

[32] Miller, Stewart E., and Alan G. Chynoweth. *Optical Fiber Telecommunications*, (New York: Academic Press, 1979).

[33] Papp, A., and H. Harms. "Faraday Effect in Glass Fibers," *Journal of Magnetism and Magnetic Materials*, **2**, (1976), p.287–291.

[34] Payne, David N., et. al. "Development of Low- and High-Birefringence Optical Fibers," *IEEE Journal of Quantum Electronics*, **18**, 1982, p.477–487.

[35] Payne, D.N., et. al. "Characterization of Specialty Fibres and Components," *Technical Digest: Symposium On Optical Fiber Measurements*, Boulder Colorado, (Sept. 9–10, 1986), p.107–113.

[36] Ramachandran, G.N., and S. Ramaseshan. *Handbuch der Physik XXV/1*, S. Flügge ed., (Berlin: Springer-Verlag, 1961).

[37] Rashleigh, S.C. "Wavelength Dependence of Birefringence in Highly Birefringent Fibers," *Optics Letters*, **7**, (1982), p.294–296.

[38] Rashleigh, Scott C. "Origins and Control of Polarization Effects in Single-Mode Fibers," *Journal of Lightwave Technology*, **1**, (1983), p.312–331.

[39] Rashleigh, S.C., et. al. "Polarization Holding in Birefringent Single-Mode Fibers," *Optics Letters*, **1**, (1982), p.40–42.

[40] Rich, T.C., and D.A. Pinnow. "Total Optical Attenuation in Bulk Fused Silica," *Applied Physics Letters*, **20**, (1972), p.264–266.

[41] Rigterink, M.D. "Materials Systems and Fiber Fabrication Processes in the U.S.A.," *Topical Meeting on Optical Fiber Transmission*, (January 7–9, 1975), Williamsburg, Virginia.

[42] Saito, S., et. al. "The Laser Current Transformer for EHV Power Transmission Lines," *IEEE Journal of Quantum Electronics*, **2**, (1966), p.255–259.

[43] Saito, Shigebumi, et. al. "Development of the Laser Current Transformer for Extra-High-Voltage Power Transmission Lines," *IEEE Journal of Quantum Electronics*, **3**, (1967), p.589–597.

[44] Snyder, Allen W., "Coupling of Modes on a Tapered Dielectric Cylinder," *IEEE Transactions on Microwave Theory and Techniques*, **18**, (1970), p.383–392.

[45] Snyder, Allen W. "Mode Propagation in a Nonuniform Cylindrical Medium," *IEEE Transactions on Microwave Theory and Techniques*, **19**, (1971), p.402–403.

[46] Snyder, Allen W. "Continuous Mode Spectrum of a circular Dielectric Rod," *IEEE Transactions on Microwave Theory and Techniques*, **19**, (1971), p.720–727.

[47] Snyder, Allen W., and John D. Love. "Goos-Hänchen Shift," *Applied Optics*, **15**, (1976), p.236–238.

[48] Snyder, Allen W., and John D. Love. *Optical Waveguide Theory*, (New York: Chapman and Hall, 1983).

[49] Snyder, A.W., and F. Rühl. "New Single-Mode Single-Polarisation Optical Fibre," *Electronics Letters*, **19**, (1983), p.185–186.

[50] Tasker, G. William, and William G. French. "Low-Loss Optical Waveguides with Pure Fused SiO_2 Cores," *Proceedings of the IEEE*, (1974), p.1281–1282.

[51] Uchida, T., et. al. "A Light-Focusing Fiber Guide," *IEEE Journal of Quantum Electronics*, (1969), p.331.

[52] Ulrich, R., et. al. "Bending-Induced Birefringence In Single-Mode Fibres," *Optics Letters*, **5**, (1980), p.273–275.

[53] Van Uitert, L.G., et. al. "Borosilicate Glasses for Optical Waveguides," *Material Research Bulletin*, **8**, (1973), p.469–476.

[54] Varnham, M.P., et. al. "Comparison Between Coil and Taper Fibre-Polisers," *Proceedings of the Society of Photo-Optical Instrumentation Engineers*, **514**, (1984), p.329–332.

[55] Varnham, M.P., et. al. "Coiled-Birefringent-Fiber Polarizers," *Optics Letters*, **9**, (1984), p.306–307.

[56] Varnham, M.P., rt. al. "Single-Polarisation Operation of Highly Birefringent Bow-Tie Optical Fibres," *Electronics Letters*, **19**, (1983), p.246–247.

[57] Varnham, M.P., et. al. "Bend Behavior of Polarising Optical Fibres," *Electronics Letters*, **19**, (1983), p.679–680.

[58] Varnham, Malcolm P., et. al. " Analytic Solution for the Birefringence Produced by Thermal Stress in Polarization-Maintaining Optical Fibers," *Journal of Lightwave Technology*, **1**, (1983), p.332–339.

[59] Varnham, M.P., rt. al. "Fundamental Limits to the Transmission of Linearly Polarised Light by Birefringent Optical Fibres," *Electronics Letters*, **20**, (1984), p.55–56.

[60] Villarruel, Carl A., et. al. "In-Line Birefringent Fiber Polarizer," *Proceedings of the Optical Fiber Conference*, New Orleans, (January 23–25, 1984), p.14.